UNIVERSIDADE
BEIRA INTERIOR

Optimal Sizing of Renewable Energy Communities: A Multi-Objective Optimization Approach

Carlos Pedro Tavares Freire Marques

Dissertação para obtenção do Grau de Mestre em
Engenharia Eletromecânica
2º ciclo de estudos

Orientador: Professor Doutor José Álvaro Nunes Pombo

janeiro de 2024

Declaração de Integridade

Eu, Carlos Pedro Tavares Freire Marques, que abaixo assino, estudante com o número de inscrição M12142 de/o Engenharia Eletromecânica da Faculdade de Engenharia, declaro ter desenvolvido o presente trabalho e elaborado o presente texto em total consonância com o **Código de Integridades da Universidade da Beira Interior**.

Mais concretamente afirmo não ter incorrido em qualquer das variedades de Fraude Académica, e que aqui declaro conhecer, que em particular atendi à exigida referenciação de frases, extratos, imagens e outras formas de trabalho intelectual, e assumindo assim na íntegra as responsabilidades da autoria.

Universidade da Beira Interior, Covilhã 31/01/2024

Assinado por: **Carlos Pedro Tavares Freire Marques**
Num. de Identificação: 30417326
Data: 2024.01.31 03:32:14+00'00'

Dedicatory

To my parents, for the years of continuous unconditional support, effort, and patience.

Acknowledgements

My biggest acknowledgment goes to my advisor and supervisor of the manuscript, Prof. Dr. José Álvaro Nunes Pombo, for the availability since day one, and all the guidance and help given for the possible development of this dissertation, without which it could not have been possible. I would also like to thank him for all the knowledge, experience and advices shared during this period, which allowed me to grow both professionally and personally.

To the laboratory personnel for their support and friendliness from day one. A special thanks to João Faria, for all the support, availability and encouragement he gave me in the difficulties of this project.

To the colleagues and friends I made during the academic career, especially Bruno Eusébio, Daniel Balacó, Daniel Nunes, Gonçalo Almeida, Miguel Cruz, Pedro Pereira and Rodrigo Antunes for their companionship, support and mutual aid during the academic stages.

To my family for the advices, help, and for being a constant source of support and encouragement.

To everyone who directly or indirectly contributed to the completion of this dissertation.

Resumo

As comunidades de energia renovável (RECs) ganharam popularidade como uma nova forma de reduzir as emissões de carbono e promover a independência energética. No entanto, a determinação do dimensionamento ótimo de cada unidade de produção e armazenamento nas RECs impõe desafios devido a objetivos contraditórios, tais como a minimização dos custos e a maximização da produção de energia. Numa tentativa de abordar esta questão de forma otimizada, este documento propõe um novo algoritmo de otimização multiobjectivo (MOA) denominado por Multi-Objective Arithmetic & Differential Evolution Optimization (MOADEO). No entanto, para determinar o dimensionamento ótimo de cada unidade de produção e de armazenamento em RECs, este trabalho recorre a um outro algoritmo de otimização multiobjectivo já existente e amplamente utilizado na literatura, chamado Multi-Objective Particle Swarm Optimization (MOPSO), com múltiplos enxames. Esta abordagem com múltiplos enxames visa promover uma maior diversidade de soluções, assegurando simultaneamente uma boa pluralidade de soluções não dominantes que definem a fronteira de Pareto. Para avaliar a eficácia e a fiabilidade desta abordagem, foram avaliados quatro estudos de caso com diferentes estratégias de gestão de energia (EMSs) baseadas em operações reais, com o objetivo de reproduzir os desafios práticos encontrados em RECs reais. Os resultados demonstram a eficácia da abordagem proposta na determinação do dimensionamento ótimo das unidades de produção e armazenamento, abordando ao mesmo tempo vários objetivos contraditórios, incluindo a viabilidade económica e a flexibilidade, especificamente o custo nivelado da energia (LCOE), o rácio de autoconsumo (SCR) e o rácio de autossuficiência (SSR). Os resultados fornecem também informações importantes que esclarecem quais as EMSs mais adequadas para este tipo de comunidades.

Palavras-chave

comunidade de energia renovável (REC); estratégia de gestão de energia (EMS); algoritmo de otimização multi-objetivo (MOA); multi enxame MOPSO; sistemas de armazenamento de energia (ESSs); partilha de armazenamento de energia

Abstract

Renewable energy communities (RECs) have gained popularity as a new mean of reducing carbon emissions and enhancing energy independence. However, determining the optimal sizing for each production and storage unit within RECs poses challenges due to conflicting objectives, such as minimizing costs while maximizing energy production. In an attempt to optimally address this issue, this paper proposes a new multi-objective optimization algorithm (MOA) denoted Multi-Objective Arithmetic & Differential Evolution Optimization (MOADEO). Nevertheless, to determine the optimal sizing of each of the production and storage units in RECs, this paper employs an existent and widely used MOA present in the literature, named Multi-Objective Particle Swarm Optimization (MOPSO), with multiple swarms. This multiple swarms approach aims to foster a broader diversity of solutions while concurrently ensuring a good plurality of nondominant solutions that define the Pareto Front. To evaluate the effectiveness and reliability of this approach, four case studies with different energy management strategies (EMSs) focused on real-world operations were evaluated, aiming to replicate the practical challenges encountered in actual RECs. The results demonstrate the effectiveness of the proposed approach in determining the optimal size of production and storage units, while simultaneously addressing multiple conflicting objectives, including economic and flexibility viability, specifically Levelized Cost of Energy (LCOE), Self-Consumption Ratio (SCR) and Self-Sufficiency Ratio (SSR). The findings also provide valuable insights that clarify which EMSs are most suitable for this type of communities.

Keywords

renewable energy community (REC); energy management strategy (EMS); multi-objective optimization algorithm (MOA); multi-swarm MOPSO; energy storage systems (ESSs); energy storage sharing

Table of Contents

List of Figures

List of Tables

List of Acronyms

ADMM	Alternating Direction Method of Multipliers
ALO	Ant Lion Optimizer
ANN	Artificial Neural Network
AOA	Arithmetic Optimization Algorithm
BESS	Battery Energy Storage System
BWO	Black Widow Optimization
CEC	Citizen Energy Communities
COP21	Conference Of Parties 21
DE	Differential Evolution
DOE	Department of Energy
EC	Energy Community
EDP	Engineering Design Problem
EMS	Energy Management Strategy
ESS	Energy Storage System
EU	European Union
FL	Fuzzy Logic
FPA	Flower Pollination Algorithm
GA	Genetic Algorithm
GHA	Grasshopper Optimization Algorithm
GHG	Greenhouse Gas
GLS	Guided Local Search
GWO	Grey Wolf Optimizer
HES	Hybrid Energy Systems
ILS	Iterated Local Search
KiBaM	Kinetic Battery Model
LM	Levenberg-Marquardt method
MaOPs	Many-objective Optimization Problems
MIDACO	Mixed Integer Distributed Ant Colony Optimization
MOA	Multi-objective Optimization Algorithm
MOADEO	Multi-Objective Arithmetic & Differential Evolution Optimization
MAOA	Multi-Objective Arithmetic Optimization Algorithm
MOFPA	Multi-Objective Flower Pollination Algorithm
MOLA	Multi-Objective Lichtenberg Algorithm

MOO	Multi-objective Optimization
MOP	Multi-objective Optimization Problem
MOPSO	Multi-Objective Particle Swarm Optimization
MPPT	Maximum Power Point Tracking
MSMEs	Micro, Small and Medium-sized Enterprises
NEEG	Net Energy Exchanged with the Grid
NPV	Net Present Value
NRM	Newton Raphson Method
NSGA-II	Non-dominated Sorting Genetic Algorithm
NSWOA	Non-Dominated Sorting Whale Optimization Algorithm
OEDI	Open Energy Data Initiative
PNEC 2030	National Energy and Climate Plan 2030
PSO	Particle Swarm Optimization
PV	Photovoltaic
RDF	Closed Distribution Networks
REC	Renewable Energy Community
RES	Renewable Energy Sources
RNC2050	2050 Carbon Neutrality Roadmap
SA	Simulated Annealing
SA-EHO	Self-Adaptive Elephant Herd Optimization
SEN	National Electrical System
SOC_{max}	Upper limit of State of Charge
SOC_{min}	Lower limit of State of Charge
SOO	Single-objective Optimization
SOP	Single-objective Optimization Problem
STC	Standard Test Conditions
STD	Standard Deviation
TMY3	Typical Meteorological Year version 3
TMY	Typical Meteorological Year
TRR	Trust Region-Reflective method
TS	Tabu Search
UPAC	Self-Consumption Production Unit
VCG	Vickrey–Clark–Groves
WOA	Whale Optimization Algorithm

List of Symbols

a	Maximum value of the objective function
A	Energy deficit that must be imported to satisfy the load demand
b	Minimum value of the objective function
$best$	Best solution
b_{beam}	Thickness of the beam
B	Surplus energy produced
c	Capacity ratio of the battery
c_1	Cognitive acceleration coefficient
c_2	Social acceleration coefficient
C	Renewable energy directly consumed or stored by the REC
CRD	Crowding Distance
CRF	Capital recovery factor
C_{annual}	Total annualized cost
C_{bat}	Cost per kWh of the batteries
C_{cap}	Initial capital cost
$C_{O\&M}$	Maintenance and operation cost
C_{PV}	Cost of each PV module
C_R	Crossover rate constant
C_{WT}	Cost of each wind turbine
d	Dimension of the multidimensional search space / dimension of the problem
E	Young's modulus
$Edist$	Euclidean distance
E_{Bat}	Sum of the participants' battery-rated capacities
$E_{Bat_{Charge}}$	Charging energy used to charge the batteries
$E_{Bat_{Discharge}}$	Discharging energy used to discharge the batteries
E_{exp}	Exported energy exchanged by the REC with the electrical grid
$E_{Exp_{Com.}}$	Intra-community energy exportation
E_{imp}	Imported energy exchanged by the REC with the electrical grid
$E_{Imp_{Com.}}$	Intra-community energy importation
E_{PV}	PV energy produced
E_{served}	Annual electrical energy served by the system

E_{Total}	Total energy transacted
E_{Wind}	Wind energy produced
f	Objective function
F	Objective function vector
$FEdist$	Function to calculate the Euclidean distance
g	Inequality constraints
$gbest$	Global best position
G	Solar irradiance
G_{beam}	Shearing modulus of the beam material
G_{NOCT}	Irradiance under Nominal Operating Cell Temperature conditions
G_{STC}	Irradiance under STC
h	Equality constraints
h_a	Anemometer height
h_h	Hub height
$\mathrm{h_{weld}}$	Thickness of the weld
h_1	Height of available energy
h_2	Height of bound energy
int	Nominal interest rate
IGD	Inverted Generational Distance index
i,j	Index
J	Polar moment of inertia of weld
k	Iteration
k_{bat}	Conductance of the battery
k_{max}	Maximum number of iterations
lb	Lower boundaries
$\mathrm{l_{beam}}$	Clamped length of the beam attached to the wall
L	Length
L_{beam}	Overhang length of the beam
L_{vessel}	Length of the cylindrical vessel section
$LCOE$	Levelized Cost of Energy
m	Number of inequality constraints
M	Moment of P about center of gravity of weld setup
$MOAF$	Math Optimizer Accelerated Function
$MOAF_{max}$	Maximum value of the Math Optimizer Accelerated Function
$MOAF_{min}$	Minimum value of the Math Optimizer Accelerated Function
$MOPF$	Math Optimizer Probability Function

MS	Maximum Spread index
n	Number of participants in the REC
np	Number of solutions / search particles
nt	Number of true Pareto optimal solutions
N	Project's lifetime
$NOCT$	Nominal Operating Cell Temperature
NPC	Net present cost
N_p	Number of PV modules connected in parallel
N_{PV}	Sum of the PV modules of the participants
N_s	Number of PV modules connected in series
N_{WT}	Sum of the wind turbines of the participants
o	Number of objective functions
p	Participant
P	Load
P_c	Maximum charging power of the battery
P_{cd}	Maximum charge or discharge power of the battery
P_d	Maximum discharging power of the battery
P_C	Bar buckling load
P_{PV}	Power output of the PV system
P_{STC}	Maximum power under STC
q	Number of equality constraints
q_{bat}	Total energy of the battery
q_1	Available energy of the battery in the beginning of each time step
q_2	Bound energy of the battery in the beginning of each time step
q'_1	Available energy of the battery at the end of each time step
q'_2	Available energy of the battery at the end of each time step
rep	Repository size
rep_{max}	Repository maximum size
r	Random generated index
R	Inner radius of the vessel
R_{beam}	Moment of the load about the center of gravity of the weld setup
SCR	Self-Consumption Ratio
SP	Spacing index
SSR	Self-Sufficiency Ratio
t	Hour
$\mathrm{t_{beam}}$	Height of the beam

t_{SP}, $\overline{t_{SP}}$	Index of the Spacing indicator
T_{amb}	Ambient temperature
T_{cell}	Cell temperature
T_h	Thickness of the hemisphere head
T_{NOCT}	Temperature under Nominal Operating Cell Temperature conditions
T_s	Thickness of the shell
T_{STC}	Cell temperature under STC
ub	Upper boundaries
U	Vector resultant of the crossover process
v	Velocity of each particle
V	Vector resultant of the mutation process
V_a	Wind speed at anemometer height
V_h	Wind speed at hub height
x,y	Solution / individual
Z	Number of teeth of the gears
Z_a	Number of teeth in the driven gear
Z_b	Number of teeth of the gear attacked to the driven gear
Z_d	Number of teeth on the driving gear
Z_f	Number of teeth in the final gear
α_{Wind}	Power law exponent / Friction coefficient
α_{VOC}	Temperature coefficient of the open-circuit voltage under STC
α, μ	Control parameter of the AOA
β	Mutation scaling factor
δ	Bar deflection
δ_{max}	Maximum deflection
Δt	Time step
ϵ	Random tiny positive number
Θ	Multidimensional search space
μ_{mppt}	Photovoltaic system efficiency of the maximum power point tracking method
σ	Normal stress
σ_{beam}	Bar bending stress
$\sigma_{beam_{max}}$	Design normal stress for the beam material
τ	Weld stress
τ'	Primary stress acting over the weld throat
τ''	Secondary torsional stress

τ_{max}	Design stress of the weld
Ψ	Objective search space
ω	Inertia factor
Ω	Feasible space
$\overline{\Omega}$	Infeasible space

CHAPTER 1

Introduction

In this chapter, the framework and the importance of the study of this dissertation is exposed, followed by the corresponding motivations and objectives. Lastly, the structure of this dissertation is presented, revealing the contents covered in each chapter.

1.1 Framework

The rapid global increase in population, high living standards, infrastructural development, and industrialization, have resulted in a massive scale extraction of fossil fuels like coal, gas, and oil, at a very alarming pace [1], [2]. The rapid depletion of these energy sources, as well as its high volatility costs in the past recent decades, adding to the aggravation of the climate change and global warming largely caused by the CO2 emissions during its combustion, have prompted very big concerns regarding the future of planet Earth, as well as an imminent approaching energy crisis [3]. These topics incited a strong impulse to the topic of renewable energies, which has been addressed, to a greater or lesser extent, by governments around the world by the adoption of new regulations and policies, encouraging the employment of renewable energy technologies [4].

The Paris Agreement [5], is the first-ever universal, legally binding global climate change agreement, adopted at the Paris climate Conference of Parties 21 (COP21), in December 2015, setting a bond between today´s policies and climate-neutrality before the end of the century [6]. It established a global framework to avoid a dangerous climate change by restraining the average global temperature increase to well below 2 °C and to pursue efforts to limit the average global temperature increase to 1.5 °C, above pre-industrial average temperature levels, until the year 2100 [6], [7]. This agreement marks a new era in global mobilization to address climate change, and stipulates that to achieve these objectives, the world will need to accomplish carbon neutrality in the second half of the century [7].

To carry though the Paris agreement commitments for reducing greenhouse gas (GHG) emissions, the European Union (EU) overhauled its energy policy framework to

further move away from fossil fuels towards cleaner energy [8]. To show global leadership on renewables, the EU set an ambitious collective of objectives for the period of 2021-2030, through the 2030 Climate and Energy framework [9], stating objectives like reaching at least a 40% reduction in GHG emissions (compared to 1990); attain at least 32% of energy derived from renewable sources [10]; and an improvement of at least 32.5% in energy efficiency [7], [11].

Through the Directive (EU) 2018/2001 of 11 December 2018 [10], the EU defined environmental targets and sustainability criteria that promote energy from renewable energy sources (RES), establishing the concepts of individual and collective self-consumption of renewable energy, and with the latter, the promising concept of Renewable Energy Communities (RECs): RECs emerge as a new mean of renewable production and development of the renewable energy consumption, having the faculty of producing, consuming, storing, sharing, and selling renewable energy, and being able to access all the appropriate energy markets. This directive also provides a legal framework that allows self-consumers of renewable energy to produce, consume, store, share and sell electricity without facing disproportionate requirements [12]. On the other hand, and in accordance with Directive (EU) 2018/1999 [13], it was determined that all State Members should draw up and submit to the European Commission, an integrated national energy and climate plan for 2021 to 2030 [14].

It is worth mentioning that in 2016, the Portuguese government pledged to ensure neutrality of its emissions by the end of 2050 as a contribution to the Paris Agreement and in line with the most ambitious efforts under way at an international level, outlining a clear view on intense decarbonization of the national economy [7]. To achieve this goal, the 2050 Carbon Neutrality Roadmap (RNC2050) [7] was approved by the Resolution of the Council of Ministers no. 107/2019 [15], identifying the main decarbonization vectors in all sectors of the economy, the policy and measures options and the emission reduction path to achieve in different scenarios of socioeconomic development [7].

Moreover, Portugal, being part of the EU, and having comply with the objectives stipulated by the latter, in particular the Directive (EU) 2018/1999, developed, in conjunction with the objectives of the RNC2050, a national strategy policy instrument named the National Energy and Climate Plan 2030 (PNEC 2030) [16], which is the main national energy and climate policy instrument for the current decade, setting new national targets for the reduction of GHG emissions, renewable energy and energy efficiency in line with the objective of carbon neutrality [7]. Its main objective is to meet

the targets established such as achieving a 47% share of energy from RES in gross final consumption by 2030, which means that the contribution of renewables in the electricity sector will have to be at least 80% of total production, and therefore the installed capacity, particularly in solar, will have to reach at least 1 GW by 2030 [12]. To achieve these goals, several national directives and regulations were issued to promote the use of renewable energy in industry, services and by ordinary citizens.

One of those national regulation was the national Decree-Law no. 162/2019 [12], which was based and partially transposed to the Portuguese law from the Directive (EU) 2018/2001, and marked a revolution in the way self-consumption entities can organize themselves, multiplying business possibilities, and ensuring a change in the paradigm of the (National Electrical System) (SEN), affirming that it must necessarily evolve from a system based on centralized production to a decentralized model that includes local production, self-consumption solutions, active management of smart grids and ensuring the active participation of consumers in the markets, or through a combination of centralized instruments for promoting clean energy (e.g. capacity auctions) [12]. Additionally, various concepts like renewable self-consumption, storage energy, and the right to share energy are defined, with the concept of RECs, previously debuting in Directive (EU) 2018/2001, also emerging for the first time in Portuguese regulations.

Despite all of this, the current regulation in law in Portugal, as of the making of this dissertation, is done under the Decree-Law 15/2022 [14], that revoked the previous regulation in law in Portugal, Decree-Law (no. 162/2019). The main objective of this new Decree-Law was concentrating all the information on self-consumption, energy communities (ECs), the SEN as well as all the regimes and laws associated with them, into a single document, transposing the two current European directives: Directive (EU) 2018/2001 (and therefore national Decree-Law no. 162/2019); and Directive (EU) 2019/944 [17], where new rules were established for the internal electricity market and where likewise the EU introduced the concept of ECs in its legislation, notably as Citizen Energy Communities (CECs) and RECs [18].

Decree-Law 15/2022 clarified important aspects for the foundation of ECs as two different legally recognized entities: RECs and CECs, besides the duties for their constitution, the obligations on the part of consumers and producers, as well as the perception of the necessary updating of the SEN. Additionally, it guarantees in a complementary way to the activities of local production, storage, self-consumption, transportation, distribution and commercialization of electricity, and the exercise of the activities covered by it obeys and the principles of rationality and efficiency of resources,

ensuring the economic and financial sustainability of the SEN with universal access, whilst promoting the incorporation of RES, an increase in energy efficiency, greater energy security and an increase in the internal market and research, innovation, and competitiveness [19], [14].

In conclusion, the current European regulatory frameworks, Directive (EU) 2019/944 and Directive (EU) 2018/2001), as well as the current regulation in law in Portugal (Decree-Law 15/2022), state two approaches associated with ECs, specified as two different legally recognized entities: REC and CEC [20].

REC are defined, as of Decree-Law 15/2022, Article 189.º, as a collective person established under the terms of this decree-law, through open and voluntary adhesion of its members, partners or shareholders, who may be singular or collective persons, of a public or private nature, including, in particular, small and medium-sized enterprises or local councils, controlled by them and who, cumulatively: i) the members or participants are located in the vicinity of the renewable energy projects or carry out activities related to the renewable energy projects of the respective energy community, necessarily including self-consumption production unit (UPAC); ii) these projects are owned and developed by the REC or by third parties, provided that they are for its benefit and at its service; iii) the main objective of the REC is to provide environmental, economic and social benefits to the members or the localities in which the community operates, rather than financial profits.

Additionally, it states that RECs have the power to: i) Producing, consuming, storing, buying and selling renewable energy with its members or third parties; ii) share and commercialize among its members the renewable energy produced by UPACs at its service, in compliance with the other requirements set out in this decree-law, without prejudice to the REC members maintaining their rights and obligations as consumers; iii) access all energy markets, including system services, both directly or via aggregation.

As of Decree-Law 15/2022, Article 191.º, CECs are defined as a collective person established under the terms of this decree-law, through open and voluntary adhesion of its members, partners or shareholders, who may be singular or collective persons, of a public or private nature, including, in particular, small and medium-sized enterprises or local councils, and which: i) aims to provide environmental, economic or social benefits to its members or stakeholders or to the local areas in which they operate, and its main objective cannot consist of obtaining financial profits; ii) may engage in the production, including of energy from RES, distribution, marketing, consumption, aggregation,

storage of energy, provision of energy efficiency services, or charging services for electric vehicles or provide other energy services to its members or stakeholders.

Furthermore, it outlines additional differences between CECs and RECs, stating that CECs are governed by the provisions of the articles of RECs with the following specificities: i) they may own, establish, purchase or rent closed distribution networks (RDF) and manage them, under the terms defined in this decree-law; ii) they may produce, distribute, market, consume, aggregate and store energy regardless of whether the primary source is renewable or non-renewable.

Table 1.1 summarizes the main differences and common aspects between these two different legally recognized entities.

Table 1.1 - REC versus CEC: Summary of differentiating and common aspects. Based on [20] and [21].

	Renewable Energy Communities (REC)	**Citizen Energy Communities (CEC)**
Participants	Specific governance & Limited membership	Specific governance & Unlimited membership
Geographical scope	Members or participants located in the vicinity of the renewable energy projects	No geographical limitation
Energy	100% renewable energy production through RES	Operate in the electricity sector and are technology-neutral
Purpose	Primary purpose is to generate social & environmental benefits rather than focus on financial profits.	
Ownership and Control	Emphasize participation and effective control by citizens, local authorities, and smaller businesses whose primary economic activity is not the energy sector	
Governance	Participation must be open and voluntary, and households should find it easy to both enter & leave the energy community	
Activities	Can exercise similar activities: generation, aggregation, energy storage, distribution, consumption, provision of energy related services, supply, and sharing.	
Directives	Defined through Directive (EU) 2018/2001 [10]	Defined through Directive (EU) 2019/944 [17]

Other differentiating factors are the autonomy, and effective control: RECs are capable of remaining autonomous from individual members and other traditional market actors that participate in the community, as members or shareholders, while CECs limit the decision-making powers to those members or shareholders who are not engaged in large-scale commercial activity in the energy sector [10], [17], [21]; relatively to the effective

control, RECs can be controlled Micro, Small and Medium-sized Enterprises (MSMEs) that are obligatorily located in the proximity of the renewable energy project; CECs exclude medium-sized and large enterprises from being able to exercise effective control [21].

Additionally, in Decree-Law 15/2022, Article 3.º, various definitions were updated and/or transposed from the previous regulations, some of which very relevant to REC in general, that are worth stating, for instance: d) «Energy storage» means transference of the end use of electricity to a time after its production by converting it into other forms of energy, namely chemical, potential or kinetic; e) «Self-consumption» means the consumption of electricity produced by one or more UPACs and carried out by one or more self-consumers of renewable energy; hh) «Renewable energy sources» (RES) means renewable non-fossil energy sources, namely wind, solar, aerothermal, geothermal, hydrothermal, oceanic, hydroelectric, biomass and renewable gases; oo) «Hybrid» means a producer or UPAC which, in the prior control procedure, simultaneously presents more than one production unit using several primary renewable energy sources; qqq) «National Electrical System» (SEN) means the set of principles, organizations, agents and electrical installations related to the activities covered by this decree-law, in national territory;

As observed, RECs bond a very wide variety of energy actions, such as generation, distribution, supply, aggregation, consumption, sharing, storage of energy, electromobility and provision of energy-related services, involving local members, partners, or shareholders of public or private nature, who may be singular or collective persons [22]. Therefore, despite their wide recognized potential as aforementioned, the implementation of RECs pose several challenges that need to be carefully addressed and thoroughly analyzed, barriers like priority dispatching, curtailment, ownership, and management of distribution [22]. These barriers can be divided in a couple main aspects as key parts for their success: financial aspects, social/cultural/political or organizational aspects, legal/administrative or bureaucratic aspects, and technical aspects [22], [23], [24], [25]. Financial barriers refer to the access to finance, unfair payments for energy produced, weak incentive to use renewable energy in heating and tax and guarantees injustice; social/cultural/political or organizational aspects refer to the lack of experience setting up communities and low trust in the community model; legal/administrative or bureaucratic aspects refer to the complicated legal framework, bureaucratic barriers to grid connections and microgrids operations inherent and intrinsically linked to the regulation and legal framework defined by each country, perhaps by the lack of authority support and lack of RES support schemes; and finally,

technical aspects refer to the lack of expert knowledge about ECs, addressed with the examination of technologies that are implemented or have the potential to be implemented in an EC environment [22], [24].

One of the technical aspects that have gained large amounts of attention and have been the subject of many scientific articles in recent years, is the design of RES, which is a fundamental aspect of RECs and Hybrid Energy Systems (HES) in general [24], [26]. The selection of the right energy generation technologies and respective sizing is a fundamental part of the successful implementation of RECs and have been identified as a major activity in the implementation of RECs [22], [26]. Furthermore, being aware of the available technologies and their potential impact can unlock great possibilities for new and existing RECs [24].

The task of optimally designing RECs is, however, a very difficult undertaking since these communities face significant variability and unpredictability due to renewable energy production [27], [28]. Nonetheless, this variability and unpredictability can be mitigated by the complementarity of resources (such as wind and solar) to balance the variability in energy production, or by the introduction of energy storage systems (ESSs) [29]. ESSs can store surplus energy produced during times of high production and discharge it during times of low production, enabling RECs to become more self-sufficient and reducing their reliance on the electrical grid. Additionally, the introduction of ESSs in RECs also enables new energy-sharing concepts (such as storage sharing) that enable the sharing of the same energy storage system by different community participants [30]. However, minimizing the reliance on the electrical grid and enabling this type of operation (energy and storage sharing) requires an energy management system to optimize the energy flow and manage the different energy sources within the RECs [31].

One other fundamental aspect that contributes to the efficient operation of an REC and the mitigation of the variability and unpredictability of renewable energy production is the optimal sizing of each participant's production and energy storage units. This is especially important to complement the variability of natural resources used for energy production; ensure a robust, reliable, and efficient energy system; manage the initial investment effectively; and account for the diverse profiles of each participant, whether residential or industrial. Thus, the optimal sizing of energy communities has been the subject of great interest by the scientific community due to the growing maturity of renewable technologies (mainly with the reduction of their cost) and the increase and enormous volatility in electricity prices [32], [33], [34].

In order to determine the most appropriate design and/or sizing of the community's renewable energy infrastructure, several optimization techniques can be applied. In this approach, a wide variety of optimization techniques can be found in the literature, which can be roughly grouped into deterministic and metaheuristic optimization methods [35].

Deterministic methods are a well-known and well-studied technique in optimizing scientific problems, which are very efficient in convex optimization problems (local search) and generally have a low computational cost, such as the Newton Raphson method (NRM) [36], the Levenberg-Marquardt method (LM) [37] and the trust region-reflective method (TRR) [35], [38]. However, these methods can converge prematurely to local minima, they need continuity, convexity, and differentiability conditions to be applicable and, furthermore, their efficiency is extremely dependent on the initial positioning [35], [39].

On the other hand, metaheuristic methods use an iterative process that combines random techniques and historical knowledge acquired (memory), to explore a search space with multiple variables and constraints, to find high quality solution(s), while avoiding any convergences to local optima and being capable to deal with non-convex and multimodal optimization problems [35]. This optimization techniques surpass conventional algorithms due to their black-box optimization nature, gradient free mechanisms, and high local optimal avoidance capability [40], [41], [42]. The reason behind the robustness and effectiveness of the metaheuristic optimization techniques is the harmonization between two search mechanisms: exploration (diversification) and exploitation (intensification) [43], [44]. The former is responsible for the diversification and abroad search of solutions in the multidimensional search space. The latter is responsible for the intensification of search in local optimal solutions. The performance and the efficiency of a metaheuristic heavily depend on a correct balance between the inherent techniques of these two mechanisms: if this balance is not well defined, the metaheuristic algorithm may converge prematurely to optimal local solutions, or the opposite situation, never converging to the global optimal solutions [45].

In the literature, a common way of separating metaheuristics is dividing them into the two following categories: trajectory-based metaheuristics and population-based metaheuristics [43]. Trajectory-based metaheuristic algorithms begin with a single solution that is replaced by the best one, in each iteration, forming a search trajectory in the multidimensional search space. Many trajectory-based metaheuristic algorithms can

be found in the literature, including Simulated Annealing (SA), Tabu Search (TS), Iterated Local Search (ILS), and Guided Local Search (GLS) [46].

Population-based algorithms, however, fundamentally begin by generating a random set of candidate solutions that, in each iteration, is improved based on the set of rules defined in the algorithm and evaluated according to the objective function. The algorithm seeks to find the best global solutions stochastically, by constantly improving the set of best solutions found so far. Countless population-based metaheuristics can be found in the literature, and some of the most popular are Particle Swarm Optimization (PSO) [47], Genetic Algorithms [48], Cuckoo Search Algorithm [49], Whale Optimization Algorithm (WOA) [50], Tabu Search Algorithm [51], Grey Wolf Optimizer [52], Black Widow Optimization (BWO) [53], Self-Adaptive Elephant Herd Optimization (SA-EHO) [54], Mixed Integer Distributed Ant Colony Optimization (MIDACO) [55] and Grasshopper Optimization Algorithm (GHA) [56].

These metaheuristic strategies can, therefore, rely on optimization algorithms to achieve efficient power flow optimization and guaranteeing appropriate sizing of the community's renewable energy infrastructure while ensuring compliance with specific REC constraints.

Next, a literature review is carried out, in Table 1.2, focusing on recent research and review papers on optimal design and/or sizing of ECs.

Table 1.2- Literature review of recent research and review papers on optimal design and/or sizing of ECs.

Ref.	Year	Work Type		System Technologies			Optimal sizing	Optimization Approach		Objective/s	Short description of contents
		Review	Research	PV+ESS	Wind	Thermal		SOO	MOO		
[57]	2021	-	X	X	-	-	-	X	-	Minimize the total cost of the EC	The authors proposed an optimization model to schedule peer-to-peer transactions via local electricity market, grid transactions in retail market, and battery management considering the photovoltaic production of households.
[58]	2022	X	-	-	-	-	-	-	-	-	Reviews the most recent research on the mathematical formulation of optimization models for optimal scheduling of resources in ECs.
[59]	2021	-	X	X	-	-	X	X	-	Minimize the Net Energy Exchanged with the Grid (NEEG)	The authors studied the optimal design and control of a PV plant and ESS of a metro station.
[60]	2021	-	X	X	-	-	-	X	-	Maximize the overall revenues of the REC	The authors proposed different strategies for scheduling a battery energy storage system (BESS) in a REC.
[61]	2022	-	X	X	-	-	X		-	Maximize the energy cost reduction	The authors performed an in-depth optimization analysis related to the sizing of RES systems and storage capacity of a REC, in a port.
[62]	2021	-	X	X	-	-	X	X	-	Minimize the total annual energy costs	The authors realized a case study in a real REC with nine EC members of a municipality in Austria, with distributed PV systems, ESS, different electricity tariff scenarios and market signals including feed-in tariffs.
[63]	2023	-	X	X	-	-	X	X	-	Maximize the net present value (NPV)	Presents an optimization model to orient energy experts and urban planners in the capacity sizing and flow management of RECs under the Italian regulatory framework
[64]	2018	-	X	X	-	X	X	-	X	Minimize the total annual cost while minimizing the total annual CO_2 emissions	The authors proposed a multi-objective optimization model to obtain the optimized configuration of interconnected distributed energy resource systems in an EC, while considering economic and environmental aspects.
[65]	2021	-	X	X	-	-	X	-	X	Maximizes the self-sufficiency while minimizing the BESS capacity of the REC members	This paper presents and analyses the impact of a bi-objective strategy to optimize the capacity of the BESSs of REC prosumers equipped with PV generators.
[66]	2018	-	X	X	-	-	X	X	-	Maximize the NPV	Presents a novel approach that aims to assist a distribution system operator to intelligently design the community BESSs considering high

											penetration of prosumers equipped with rooftop PV systems and electric vehicles
[67]	2021	-	X	X	-	-	X	X	-	Maximize the NPV	Proposes a business model for aggregators of ECs, and its optimization problem, accounting for crucial aspects.
[68]	2020	-	X	X	-	-	X	X	-	Maximize the BESS NPV	Proposes two different BESS ownership structures, which are compared to the traditional user owned BESS under the peer-to-grid framework
[69]	2019	-	X	X	X	-	X	X	-	Minimize the total cost over the planning horizon	Evaluates the profitability and self-sufficiency of optimally designed microgrids for new proposed business models
[70]	2023	X	-	X	X	-	-	X	-	-	This paper identifies the main drivers behind the optimal investment decision of a REC, which result from the relationship between the marginal realized price and the levelized cost of the electricity generated by each renewable technology.
[71]	2018	-	X	X	-	-	X	X	-	Minimize electricity purchases from the grid	Proposes a new energy management framework and storage sizing for an EC composed of multiple houses and distributed solar generation
[72]	2021	-	X	X	-	-	X	X	-	Minimize NEEG trading costs	Analyses the sizing and placement of a community storage at a district level using Multi-Period Power Flow, considering PV sizing and power flow conditions.
[73]	2022	-	X	X	-	X	X	X	-	Minimize the economic and environmental impact	Proposes a mixed-integer linear algorithm implementing a partitioned clustering program for subsequent classification of typical demand.
[74]	2021	-	X	X	-	-	X	X	-	Maximize the social welfare	This study maximizes the net profit by deducting the gain to customers from the use of PV and BESS from their costs.

1.2 Motivations and Objectives

The motivations of the current dissertation are grounded on the lack of investigation and application of RECs in a multi-objective optimization approach, with multiple objectives. Multi-objective optimization problems (MOPs) are, in general, and particularly in REC design and sizing, a difficult and challenging investigation process, demanding the analysis of perhaps multiple conflicting interrelated objectives, of economic, technical and/or environmental nature, simultaneously, while considering multiple design constraints and limitations. Nevertheless, the solutions of multi-objective optimization problems, in contrast to single-objective optimization problems (SOPs), provide more robust, viable, and optimized solutions/results.

To increase efficiency and spread the adoption of RECs, this paper aims to determine the optimal sizing of multiple renewable energy production units with a storage system, within an REC, regardless of the number of participants, in a multi-objective optimization approach. Through the optimal sizing of the various energy production and storage units, participants can produce, consume, share, store, and sell the energy produced by RECs, actively contributing to a more accurate, capable, and rational long term energy transition.

Likewise, this paper targets to comprehensively analyze and compare the effectiveness of different real-world based energy management strategies (EMSs), in RECs, replicating the practical challenges encountered in actual RECs operations. These strategies can encompass different levels of cooperation, participation, and collaboration among the various production and storage units of electric energy.

1.3 Thesis Structure

This dissertation is organized in six chapters. Below is a brief description of the contents addressed in each chapter.

The current chapter, CHAPTER 1, realizes the introduction of this dissertation. As aforementioned, it presents the frameworks, the motivations and objectives, and currently describes the structure of this dissertation.

CHAPTER 2 presents the mathematical models of the system components, the EMSs chosen, and devises the problem formulation.

CHAPTER 3 regards all the concepts and definitions of Multi-Objective Optimization (MOO). It presents the conceptualization of the Multi-Objective Particle Swarm Optimization (MOPSO) algorithm, and likewise the distinctive aspect of this study, the novel proposed Multi-Objective Optimization Algorithm (MOA) named MOADEO – Multi-Objective Arithmetic & Differential Evolution Optimization, both with the corresponding preliminaries and formulations.

In CHAPTER 4, the effectiveness and performance of the proposed MOADEO algorithm is evaluated and compared to other MOAs commonly utilized in the literature to solve Multi-objective Optimization Problems (MOPs).

CHAPTER 5 presents the optimization strategy implemented, and afterwards discusses the results of the optimal sizing for each EMS implemented.

Lastly, CHAPTER 6 presents the conclusions of the study, and notes possible future works.

CHAPTER 2

System Modeling and Problem Formulation

In this chapter, the mathematical models of the components of the REC are presented and formulated in great detail. Furthermore, the energy management strategies used to simulate the community are established and properly schematized, and the corresponding problem formulation is defined under two different system evaluation criteria.

2.1 System Modeling

Before sizing the system's individual technologies, the models must be defined to simulate the system realistically and accurately. However, simulating any REC as close to reality as possible can be very complex, given the numerous variables and constraints that need to be considered [75].

In this section, the mathematical models of the system components are presented in detail. The simulated community consists of different energy sources (namely solar and wind power) that directly supply the existing electrical load. Additionally, the community includes an energy storage system (specifically batteries) that play a crucial role in storing excess renewable energy for later use. These models are essential for a comprehensive understanding of the renewable energy community's dynamics and for devising effective energy management strategies.

2.1.1 Batteries

In the existing literature, many different models can be found to simulate and describe, in a feasible and detailed way, the behavior of different types of batteries under different operating conditions [76]. They can be divided into four different groups: Electrochemical, Stochastic, Electrical, and Analytical models [77].

The Kinetic Battery Model (KiBaM) is a popular analytical model developed by Manwell and McGowan in [78], that is widely used in energy storage system simulations. As illustrated in Figure 2.1, this mathematical model represents a battery with two

reservoirs (available charge and bound charge) separated by a conductance. The available charge reservoir contains the available energy of the battery (q_1) that can be immediately supplied to the load, and the bound charge reservoir contains the battery's remaining energy (q_2) that cannot be immediately converted into electrical energy since it is only responsible for supplying energy to the available charge reservoir. The battery's capacity ratio of available energy to total energy is defined by c [79]. The energy flow exchange between reservoirs depends on the conductance (k_{bat}) that represents how quickly the energy from the bound charge reservoir is converted to the available charge reservoir or vice-versa, depending on the operating condition, and on their height difference ($h_1 - h_2$), where $h_1 = q_1 / c$ and $h_2 = q_2 / (1 - c)$. The battery's capacity is the sum of both reservoirs' capacity, $q_{bat} = q_1 + q_2$.

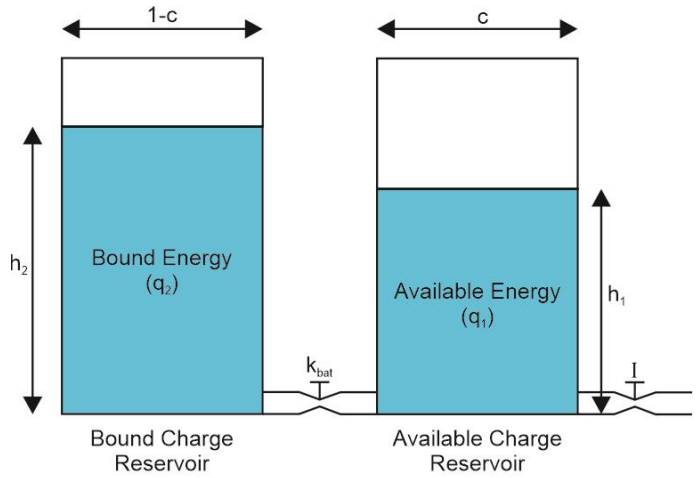

Figure 2.1 - Kinetic Battery Model (KiBaM).

When the battery is discharging, the available charge reservoir supplies its energy to the connected load, while the bound charge reservoir supplies its energy to the available charge reservoir at a slower rate, causing the height difference of both reservoirs to increase. When the battery is charging, the available charge reservoir charges at a faster rate than the bound charge reservoir. When the battery is not being used, a flow of energy occurs between both reservoirs, causing the reservoirs to balance each other until both reservoirs' heights are equal ($h_1 = h_2$). The amount of energy contained in each reservoir, in each time step, is represented by the following Equations (2.1) and (2.2) [79]:

$$q'_1 = q_1 e^{-k_{bat}\Delta t} + \frac{(q_{bat}k_{bat}c - P_{cd})\left(1 - e^{-k_{bat}\Delta t}\right)}{k_{bat}} - \frac{P_{cd}c\left(k_{bat}\Delta t - 1 + e^{-k_{bat}\Delta t}\right)}{k_{bat}} \quad (2.1)$$

$$q'_2 = q_2 e^{-k_{bat}\Delta t} + q_{bat}(1-c)\left(1 - e^{-k_{bat}\Delta t}\right) - \frac{P_{cd}(1-c)\left(k_{bat}\Delta t - 1 + e^{-k_{bat}\Delta t}\right)}{k_{bat}} \quad (2.2)$$

where q'_1, q'_2 and q_1, q_2 are the available charge and bound energy at the end and beginning of each time step, respectively, in $[kWh]$ [79]; Δt is the time step; and P_{cd} is the charge or discharge power of each time step $[kW]$, depending on the operating conditions. A positive value of P_{cd} means the discharging power of the battery being used to cover the demand, while a negative value means the charging power of the battery being used to store surplus energy.

The maximum discharging and charging power of the battery in kW, in each time step, is given by the following Equations (2.3) and (2.4), respectively:

$$P_d = \frac{k_{bat}q_1 e^{-k_{bat}\Delta t} + q_{bat}k_{bat}c\left(1 - e^{-k_{bat}\Delta t}\right)}{1 - e^{-k_{bat}\Delta t} + c(k_{bat}\Delta t - 1 + e^{-k_{bat}\Delta t})} \quad (2.3)$$

$$P_c = \frac{-k_{bat}cq_{bat} + k_{bat}q_1 e^{-k_{bat}\Delta t} + q_{bat}k_{bat}c\left(1 - e^{-k_{bat}\Delta t}\right)}{1 - e^{-k_{bat}\Delta t} + c(k_{bat}\Delta t - 1 + e^{-k_{bat}\Delta t})} \quad (2.4)$$

This mathematical model is computationally efficient and allows for the description of electrochemical processes occurring within the battery using a reduced set of parameters: the total charge ratio stored in the available charge reservoir (c), the conductance (charge flow rate) between both reservoirs (k_{bat}), and the maximum capacity of the battery (q_{bat}). These parameters can be estimated through a series of experimental measurements with constant discharge currents or by using the battery datasheet (at least three discharge curves). Furthermore, it can capture nonlinear effects during charging and discharging, such as recovery effects and capacity rate. However, it does not account for the effects of temperature and battery aging [80].

2.1.2 Photovoltaic System

The Photovoltaic (PV) system is a crucial and impactful component of an REC, although it provides intermittent production with large variability and unpredictability.

Therefore, carefully selecting a model that best suits each specific application is essential. Various models in the literature are used to simulate the behavior of PV modules under different operating conditions, including factors such as dust, cell temperature, partial shading, irradiance, and others [76]. Various models with one, two, or even three or more diodes are commonly used in literature. However, these models imply a considerable amount of computational time and effort, unnecessary for this type of simulation. In this paper, to reduce the computation effort, a synthesized model is used to determine the output power of the PV modules, defined as a function of the PV cell temperature and solar irradiance (G). The power output of the PV system in each time step, with N_s modules connected in series and N_p modules connected in parallel, is given by Equation (2.5) [81], [82].

$$P_{PV} = \mu_{mppt}\left(P_{STC}\frac{G}{G_{STC}}\left(1+\alpha_{VOC}(T_{cell}-T_{STC})\right)\right)N_sN_p \tag{2.5}$$

where μ_{mppt} is the photovoltaic system efficiency of the maximum power point tracking method (MPPT) [%]; P_{STC} is the maximum power under Standard Test Conditions (STC) [W], i.e., a solar irradiance of 1000 $W/m^2$and a temperature of 25 °C; G is the given solar irradiance in each time step [Wm^{-2}]; G_{STC} is the irradiance under STC [Wm^{-2}]; α_{VOC} is the temperature coefficient of the open-circuit voltage under STC [V °C^{-1}]; T_{STC} is the cell temperature under STC conditions [°C]; and T_{cell} is the cell temperature in each time step [°C] given by Equation (2.6) [83], [84]:

$$T_{cell} = T_{amb} + \frac{G}{G_{NOCT}}(NOCT - T_{NOCT}) \tag{2.6}$$

where T_{amb} is the ambient temperature in each time step [°C]; $NOCT$ is the Nominal Operating Cell Temperature [°C], measured with 800 W/m² irradiance, 20 °C ambient temperature and wind speed of 1 m/s; G_{NOCT} is the irradiance under $NOCT$ [Wm^{-2}]; and T_{NOCT} is the temperature under $NOCT$ conditions [°C].

2.1.3 Wind Turbine Generator

The power output of a wind turbine generator is influenced by both the site characteristics and the technical features of the wind turbine. The most significant factors are the wind speed at the turbine hub height and the power output curve.

The wind speed measured by an anemometer is not directly at the turbine hub height. Therefore, it must be converted to that height to accurately estimate the true wind speed. This conversion is essential to ensure precise calculations and effective evaluation of the wind turbine's power generation [85], [86]. A widely used conversion approach employs the power law expressed by Equation (2.7):

$$V_h = V_a \left(\frac{h_h}{h_a}\right)^{\alpha_{Wind}} \tag{2.7}$$

where V_h $[ms^{-1}]$ is the wind speed at hub height h_h $[m]$; V_a $[ms^{-1}]$ is the wind speed at the anemometer height h_a $[m]$; and α_{Wind} is the power law exponent or friction coefficient.

Many different models are used in the literature to simulate and obtain the power curve of a wind turbine regarding the wind speed and hub height, such as physical, linear, and nonlinear models. Although these methods are straightforward to implement in any REC simulation, they are not always accurate when simulating stall-controlled wind turbines. In this type of wind turbine, the pitch angle is fixed, so when the wind speed is above the rated wind speed the turbine power output cannot be held constant and decreases because of aerodynamic losses between the blades and the wind. Thus, in this paper, the power output curve provided by the manufacturer is used to accurately simulate the wind power system.

2.2 Energy Management Strategies and Problem Formulation

In this section, the employed energy management strategies, optimization strategy, and problem formulation for determining the optimal sizes of the system components within the REC is mounted. The management strategies were designed with a focus on real-world operations, aiming to replicate the practical challenges encountered in actual RECs, thus enhancing the approach's realism and applicability. The problem formulation defines the objective function and constraints that describe the purpose/goals of the optimization problem.

2.2.1 Energy Management Strategies

To test the performance of the REC in different operating conditions, four energy management scenarios proposed in [87] were implemented. A summarized description of these scenarios can be found in Table 2.1.

Table 2.1 - Renewable Energy Community Scenarios.

Scenarios	Description
Scenario 1	Independent microgrid participants.
Scenario 2	Sharing renewable energy after charging individual batteries.
Scenario 3	Sharing renewable energy before charging individual batteries.
Scenario 4	Sharing distributed renewable energy and battery storage systems among participants before charging individual batteries.

In Scenario 1, an individualist position is assumed by all the community participants, mimicking a conventional microgrid with no energy transactions between them. In Scenario 2, the surplus energy from distributed renewable systems is shared within the community after fully charging the individual batteries. In contrast, in Scenario 3, the surplus renewable energy is shared directly to cover other community participants' load demand before being dispatched to the individual batteries. In Scenario 4, all the batteries and renewable energy sources are shared to enhance renewable penetration and minimize grid dependence.

Figure 2.2 depicts the flowchart of the energy community strategy in Scenario 1. In this scenario, the participants don't consider any type of energy transactions or storage sharing. If a participant has energy shortage ('Deficit' > 0), it will rely on the

individual batteries to cover the energy shortage. If the individual batteries reach the lower limit of state of charge (SOC_{min}), this participant will import the remaining energy from the electrical grid. In contrast, if a participant has energy surplus ('Deficit' < 0), it will exclusively resort on the individual batteries to store the energy surplus. If the battery reaches its upper limit (SOC_{max}), any remaining excess energy is exported to the electrical grid.

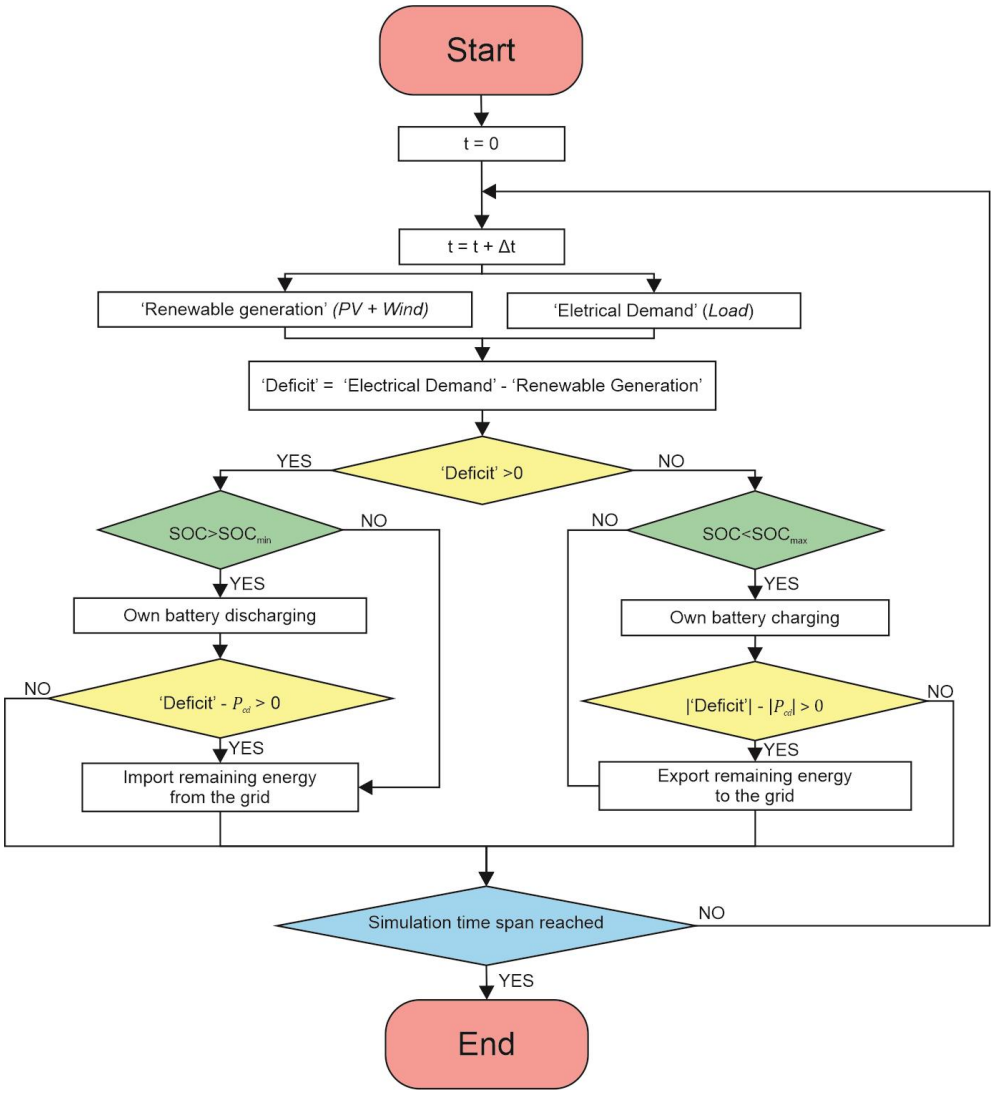

Figure 2.2 - Scenario 1 energy management strategy flowchart. Adapted from [87].

Figure 2.3 shows the Scenario 2 energy strategy. In this scenario, the community participants prioritize charging or discharging their own individual batteries when they have an energy surplus or shortage. If the battery reaches the upper limit of its state of charge (SOC_{max}) when in an energy surplus ('Deficit' < 0), any remaining excess energy is shared within the community before being exported to the electrical grid. Inversely,

when a participant has energy shortage ('Deficit' > 0) if the individual battery cannot cover the required demand energy ('Deficit' $- P_{cd} < 0$), any remaining required energy is supplied by available energy from other prosumers, before importing from the grid.

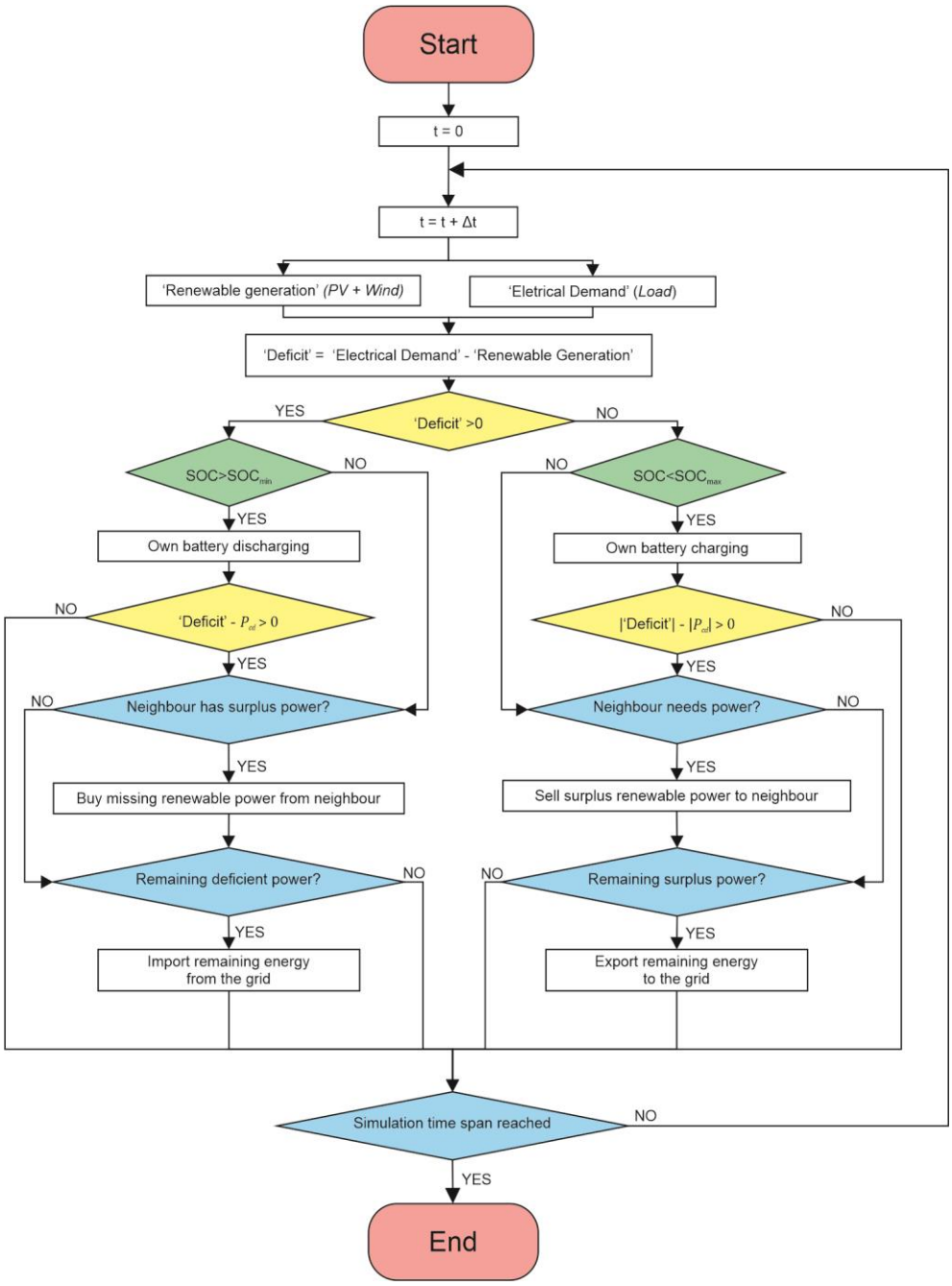

Figure 2.3 - Scenario 2 energy management strategy flowchart. Adapted from [87].

Scenario 3 EMS is shown in a flowchart in Figure 2.4. In this scenario, the community participants prioritize sharing renewable energy before charging or discharging their own individual batteries, when they have an energy surplus or shortage, respectively. When a participant has energy shortage ('Deficit' > 0), if any of the other

community participants has surplus energy, they will trade the remaining energy and try to meet the load demand of the other, otherwise this participant will rely on the individual batteries before resorting to grid exchanges. In the case of a participant having energy surplus ('Deficit' < 0), this participant will try and trade the excess energy with a participant with energy shortage, before resorting to the individual batteries to store the energy surplus. If this participant cannot trade and/or store on the individual batteries the energy surplus completely, the remaining surplus energy will be exported to the grid. This scenario considers the efficiency losses associated with battery operations and ensures that the excess renewable energy is efficiently utilized to meet the REC's energy needs.

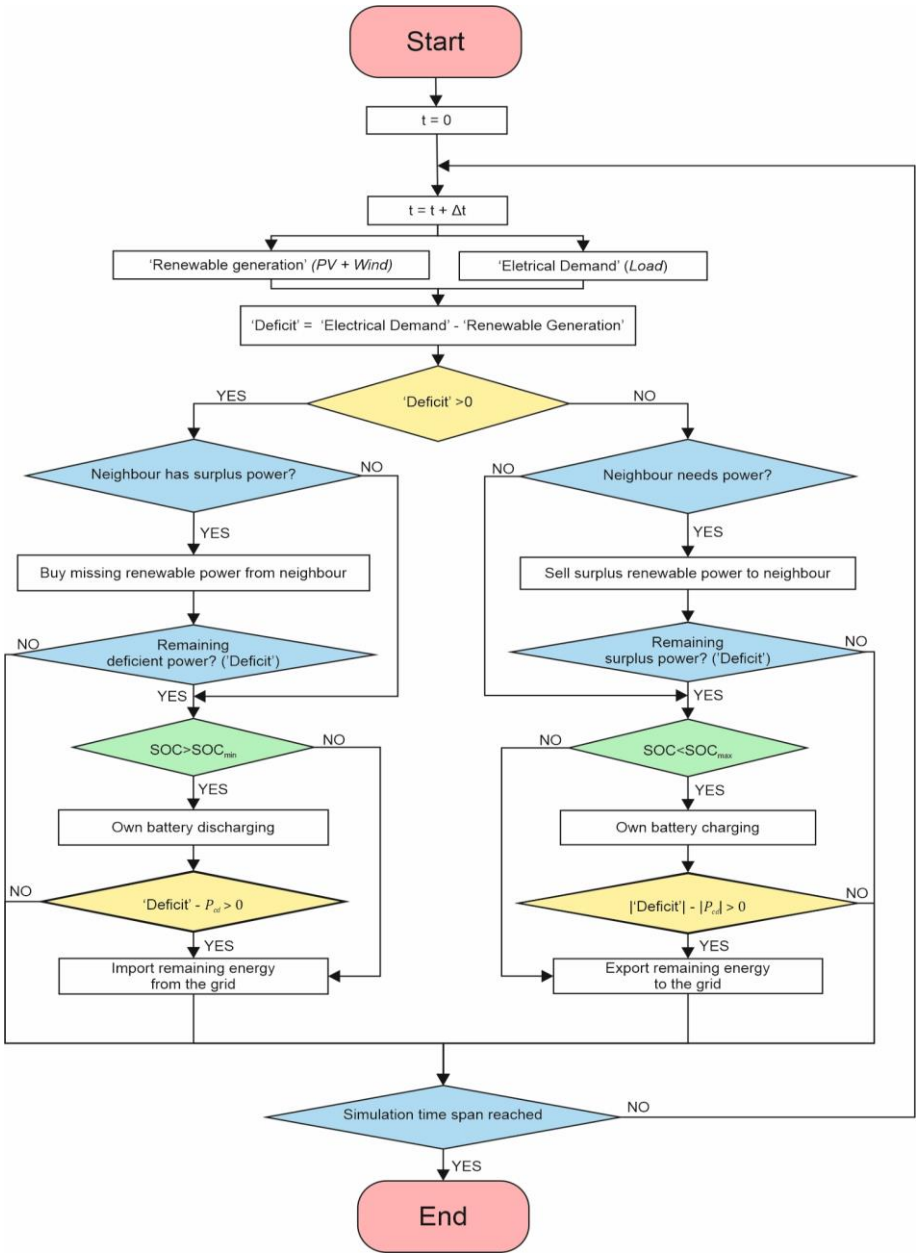

Figure 2.4 - Scenario 3 energy management strategy flowchart. Adapted from [87].

Figure 2.5 depicts the flowchart of the energy community strategy in Scenario 4.

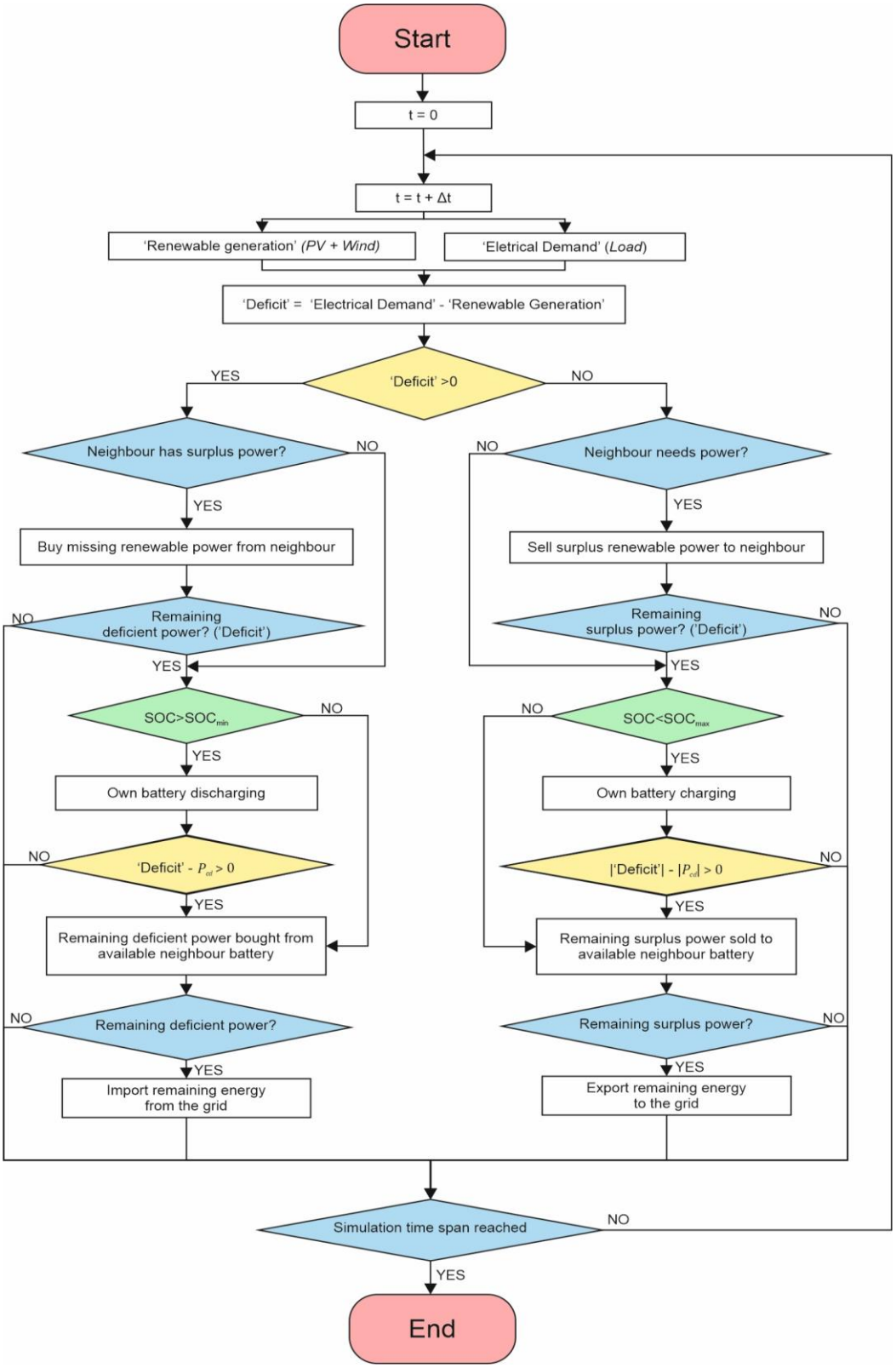

Figure 2.5 - Scenario 4 energy management strategy flowchart. Adapted from [87].

The operation in this scenario follows a specific rule: when one participant has surplus power ('Deficit' < 0), it can be utilized to meet the load demand of other peers. The participants first charge their own batteries to $\mathrm{SOC}_{\max}$ and then proceed to charge other peers' batteries sequentially. Conversely, when a participant faces an energy deficiency ('Deficit' > 0), they can purchase redundant generation from other peers, then discharge their own battery to $\mathrm{SOC}_{\min}$, and finally discharge other peers' batteries, if needed. This collaborative approach allows for improved renewable integration and effective utilization of distributed energy resources within the community.

2.2.2 Problem Formulation

The optimal sizing and design of the studied REC is outlined based on two different system evaluation criteria: economic and flexibility criteria. The economic criteria involve analyzing cost-related factors, while flexibility criteria assess the system's ability to adapt to varying demand and supply conditions, ensuring an efficient and reliable energy management.

2.2.2.1 Economic Criteria

The Levelized Cost of Energy (LCOE) is widely recognized as a crucial economic factor in the optimal planning and design of Hybrid Energy Systems (HES) [88]. Its prominence attracts investors, policymakers, and consumers, making it a pivotal consideration in the design of the REC [89]. LCOE can be defined as the effective cost of energy generated by the REC, in $\$/kWh$ [90]. It is calculated by the ratio of the sum of the total annualized cost (C_{annual}) and the annual electrical energy served by the system (E_{served}), as expressed in Equation (2.8):

$$LCOE = \frac{C_{annual}}{E_{served}} \tag{2.8}$$

where C_{annual} is the product of the net present cost (NPC) and the capital recovery factor (CRF), as expressed by Equation (2.9):

$$C_{annual} = NPC \cdot CRF(int, N) \tag{2.9}$$

The Net Present Cost (NPC) of a system, representing its life-cycle cost, is determined by Equation (2.10), where int denotes the nominal interest rate and N represents the project's lifetime [84]:

$$NPC = C_{O\&M} + C_{cap} \tag{2.10}$$

$$C_{cap} = E_{bat} \cdot C_{bat} + N_{PV} \cdot C_{PV} + N_{WT} \cdot C_{WT} \tag{2.11}$$

In Equation (2.11), C_{cap} is the initial capital cost, where $C_{O\&M}$ is the maintenance and operation cost; E_{bat} is the sum of the participants' battery-rated capacities; N_{PV} and N_{WT} are the sum of the PV modules and wind turbines of the participants, respectively; and C_{bat}, C_{PV} and C_{WT} define the cost per kWh of the batteries, the cost of each PV module, and the cost of each wind turbine, respectively. The capital recovery factor (CRF) is calculated with Equation (2.12):

$$CRF(int, N) = \frac{int(1 + int)^N}{(1 + int)^N - 1} \tag{2.12}$$

2.2.2.2 Flexibility Criteria

The flexibility criteria are crucial parameters for optimizing both energy consumption and production [91]. The Self-Consumption Ratio (SCR) and Self-Sufficiency Ratio (SSR) are two well-known parameters that enhance the flexibility of energy systems. These criteria play a significant role in achieving an efficient and resilient renewable energy community.

SCR can be defined as the quantity of energy produced internally by the system's renewable energy sources, which is also used internally for consumption [91]. This includes both the energy directly used by the load, as well as the batteries' charging energy (acting like an additional load) [92]. Figure 2.6 shows a typical power profile of an REC with this type of renewable energy production system. In this Figure, Area B represents the surplus energy produced during that day, Area C represents the renewable energy directly consumed or stored by the REC, while Area A shows the energy deficit that must be imported to satisfy the load demand.

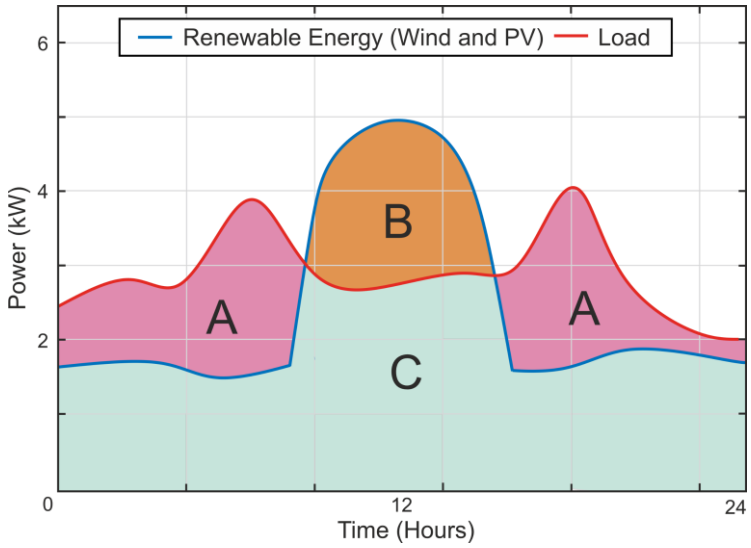

Figure 2.6 - Typical load and production profile.

Using the nomenclature in Figure 2.6, SCR can be defined by Equation (2.13):

$$SCR = \frac{C}{B + C} \tag{2.13}$$

Although SCR is a valuable and viable parameter for designing an REC, if the optimization problem were solely formulated to maximize SCR, the resulting configuration would always be the smallest possible in terms of produced energy. This limitation underscores the need to use SCR in combination with other criteria when formulating an REC optimization problem. By incorporating multiple criteria, the solution can achieve a more comprehensive and balanced configuration that optimizes both energy production and consumption, ensuring the REC's effectiveness and practicality [58]. SSR is also considered to minimize energy community transactions with the electrical grid. SSR represents the proportion of energy consumption supplied by internally produced energy. Using the nomenclature depicted in Figure 2.6, SSR can be defined by Equation (2.14):

$$SSR = \frac{C}{A + C} \tag{2.14}$$

2.2.2.3 Variables and Constraints

For each participant p, the design variables considered for the optimal sizing and design of the REC are the battery-rated capacity (C_{bat_p}) [kWh]; the number of PV

modules (N_{PV_p}); and the number of wind turbines (N_{WT_p}), each subject to upper and lower bounds, as enumerated in Equation (2.15). These bounds were designed based on a typical renewable energy installation in residential areas.

$$\begin{cases} 0 \leq C_{bat_p} \leq 25 \\ 0 \leq N_{PV_p} \leq 50 \\ 0 \leq N_{WT_p} \leq 10 \end{cases} \tag{2.15}$$

The primary goal of any REC is to minimize its exchanges with the electrical grid by enabling the exchange of surplus energy consumed or produced among participants. To achieve this objective in the simulated REC discussed in this paper, two additional design restrictions were implemented in the simulation parameters to further optimize the results. To significantly increase independence from the grid, the energy interactions with the electrical grid were limited to 25% of the total energy transacted in the REC, as specified by Equation (2.16). This limitation was implemented to foster a greater reliance on intra-community energy exchanges and storage, leading to reduced reliance on the grid and enhancing the overall self-sufficiency of the renewable energy community.

$$\sum_{t=1}^{8760} E_{Imp}^{p}(t) + E_{Exp}^{p}(t) < 0.25 \cdot E_{Total}^{p}(t) \tag{2.16}$$

where $\mathrm{E}_{\mathrm{Imp}}^{\mathrm{p}}$ and $\mathrm{E}_{Exp}^{\mathrm{p}}$ are the imported and exported energy exchanged by the REC with the electrical grid by each participant p, respectively, in each hour t. Furthermore, E_{Total}^{p} is the total energy transacted by the participant p, as given by Equation (2.17):

$$E_{Total}^{p} = \sum_{p=1}^{n} \left(\sum_{t=1}^{8760} E_{PV}^{p}(t) + E_{Wind}^{p}(t) + E_{Bat_{Charge}}^{p}(t) + E_{Bat_{Discharge}}^{p}(t) + E_{Imp_{Com.}}^{p}(t) + E_{Exp_{Com.}}^{p}(t) + E_{Imp}^{p}(t) + E_{Exp}^{p}(t) \right) \tag{2.17}$$

where E_{PV}^{p} and E_{Wind}^{p} are the PV and wind energy produced by each participant p, respectively; $E_{Bat_{Charge}}^{p}$ and $E_{Bat_{Discharge}}^{p}$ are the charging and discharging energy used to charge and discharge the batteries, respectively; and $E_{Imp_{Com.}}^{p}$ and $E_{Exp_{Com.}}^{p}$ represent the intra-community transactions of each participant: $E_{Imp_{Com.}}^{p}$ defines the intra-community energy importations, while $E_{Exp_{Com.}}^{p}$ defines the intra-community energy exportation by each participant p.

The other optimizing restriction promotes intra-community energy interactions, encouraging participants to exchange surplus or required energy among themselves, as shown in Equation (2.18). This equation sets a lower limit for the intra-community energy value traded between participants, ensuring that it remains above 30% of the total energy imported by the REC. By encouraging such interactions, the renewable energy community fosters a collaborative approach, optimizing energy utilization and minimizing dependency on external sources.

$$\sum_{p=1}^{n}\left(\sum_{t=1}^{8760} E_{Imp_{Com.}}(t) + \sum_{t=1}^{8760} E_{Exp_{Com.}}(t)\right) > 0.3 \cdot \sum_{t=1}^{8760} E_{Imp}(t) \tag{2.18}$$

where $E_{Imp_{Com}}$ and $E_{Exp_{Com}}$ defines the sum of all the REC participant's intra-community energy importations and exportations, respectively.

CHAPTER 3

Multi-Objective Optimization

In this chapter, the concepts and definitions of Multi-Objective Optimization are primarily done. Subsequently, the meta-heuristic algorithms are introduced as a bridge towards the conceptualization of the Multi-Objective Particle Swarm Optimization (MOPSO) algorithm, and afterward, the proposed Multi-Objective Optimization Algorithm named MOADEO – Multi-Objective Arithmetic & Differential Evolution Optimization, both with the corresponding preliminaries and formulations.

3.1 Multi-Objective Optimization Concepts

In this section, the conceptualization of Multi-Objective Optimization is done, firstly by explaining the types of Multi-Objective Optimization Problems, and afterwards addressing the necessary formulations and concepts for its understanding.

3.1.1 Multi-Objective Optimization Problems

According to the number of objective functions, optimization problems can be divided into 2 categories: single-objective optimization problems (SOPs) and multi-objective optimization problems (MOPs). In recent years, with the development of the optimization techniques and strategies, MOPs most commonly refer to optimization problems with up to 3 objective functions, and due to the increasing complexity of further number of objective problems, MOPs with 4 or more objective functions are referred, in the literature, as many-objective optimization problems (MaOPs) [93], [94]. As perceptible, SOPs refer to problems that have a single objective function, i.e. the goal of the optimization problem is to maximize or minimize one and only one objective, for example, the minimization of a mathematical equation. MOPs, however, refer to optimization problems where the goal is the maximization and/or minimization of two or more objectives, simultaneously, while possibly being contradictory to each other.

A natural and perhaps the simplest approach of solving MOPs is usually done by weighting (combining) each individual objective function into a single equation, resulting in a SOP. This is a very advantageous strategy since SOPs have been relatively

well and extensively studied, in which the weights can be fixed or dynamically changed [95]. Another simple approach widely known is done by selecting one objective function of the problem and considering the remaining as problem constraints, resulting in a single-objective function [95]. This approach of solving optimization problems requires, however, an expanded knowledge relative to the objective functions, like their importance in the overall objective, limits, etc. Though, in other MOPs, the previous' options are not a solution because the objective functions are conflicting or antagonistic with each other; therefore, the problem must be addressed as a multi-objective optimization problem (MOP) [96].

A simple example of real-world MOP with antagonistic objective functions can be purchasing a car: the best purchase is the one least expensive which offers the best performance. These objectives functions, being the cost and the performance, are contradictory to each other since there are cheap cars with low performance all the way to very expensive cars with top performance. A car with less cost and performance cannot be considered as a better option than a car with a higher cost and performance, and vice versa. Nevertheless, a car has the same cost as others along with better performance, should be considered a better solution. The same happens when one car has the same performance as another but is cheaper: it should also be considered a better option. Figure 3.1 portrays this real-life MOP example in a figure.

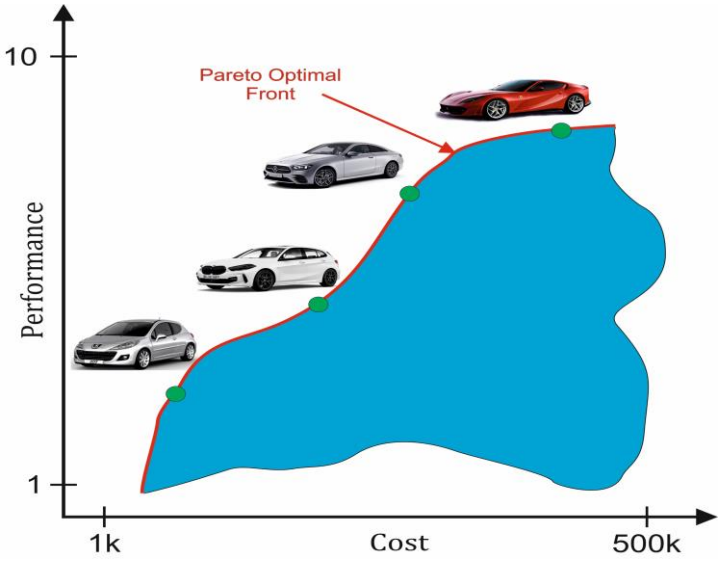

Figure 3.1 - Illustration of an example real-life MOP.

MOPs are in general much more complicated to solve than SOPs. For single-objective optimization problems, *gbest* and *pbest* represent the global and personal best

positions, respectively. In MOPs, however, there is more than one global optimal solution, requiring the determination of a set of acceptable trade-off optimal solutions, commonly referred to as Pareto optimal front [95]. Moreover, one of the biggest difficulties of MOPs is that the objective functions, in most of the cases, are contradictory to each other, meaning one solution can be good to a certain objective function, while simultaneously being bad to another or other objective functions. Additionally, as seen in the example given before, in a MOP a solution cannot be compared to another by relational operators since there is not a single global optimal solution.

3.1.2 Multi-Objective Optimization Formulation

The nature of a MOP can be of maximizing the objective functions (maximization problem) or minimizing the objective functions (minimization problem). Regardless, the expressions that describe both optimization problems can be related by multiplying by negative one [97], [98]. A general MOP, with o number of objective functions, can consequently be formulated as a minimization problem using the following common mathematical formulation [99], [100]:

$$\begin{gathered} Minimize\colon\ F(x) = \{f_1(x), f_2(x), \dots, f_o(x)\} \\ Subject\ to\colon \begin{cases} g_i(x) \geq 0, & i = 1,2, \dots, m \\ h_i(x) = 0, & i = 1,2, \dots, q \\ lb_i \leq x_i \leq ub_i, & i = 1,2, \dots, d \end{cases} \end{gathered} \tag{3.1}$$

where $F(x)$ is the objective function vector; $g(x)$ and $h(x)$ are the inequality and equality constraints, respectively, with m and q number of inequality and equality constraints, respectively; lb and ub are the lower and upper boundaries, respectively, of the multidimensional search space commonly represented as Θ, with dimension d.

For a given candidate solution x, limited by the upper and lower boundaries, if it satisfies both the inequality constraints g_i and equality constraints h_i, for every $i = 1,2, \dots, m$ and $i = 1,2, \dots, q$, respectively, it is defined as a feasible solution, otherwise it is defined as an infeasible solution [101]. The space spanned by the feasible solutions is called the feasible space, commonly represented by Ω, while the space spanned by the infeasible solutions makes up the infeasible space, $\overline{\Omega}$. Apparently, $\Omega + \overline{\Omega} = \Theta$, where $\Omega \subseteq \Theta$ and $\overline{\Omega} \subseteq \Theta$ [101]. Additionally, the space spanned by the objective functions is called the objective search space (Ψ), determined by the feasible space Ω, and the objective function vector $F(x)$, and represents all the possible values of the objective functions [102]. Nevertheless, in a multidimensional search space a candidate solution cannot be

compared with another with relational operators, due to multi-criterion comparison metrics [100], [103]. Other operators are required to measure or find out if a certain solution is better than another solution.

3.1.3 Pareto Optimality Concepts

The concept of comparing two different solutions in a MOP was firstly introduced by Francis Ysidro in 1881 [104], and further developed and investigated by Vilfredo Pareto in 1964 [105]. Without loss of generality, the mathematical definition of Pareto dominance for a minimization problem is as follows [106]:

Definition 1 – Pareto Dominance

A feasible solution $x = \{x_1, x_2, \dots, x_d\}$, dominates, or is non-dominated to another feasible solution $y = \{y_1, y_2, \dots, y_d\}$, denoted as $x \prec y$, if:

$$\forall i \in \{1,2,\dots,o\}: f_i(x) \leq f_i(y) \ \wedge \ \exists i \in \{1,2,\dots,o\} : \ f_i(x) < f_i(y) \tag{3.2}$$

A nondominated solution is one that is better than other solutions in at least one objective function, yet not the worst solution in any of the remaining functions. The solutions that are outperformed are the dominated solutions.

Definition 2 – Pareto Optimality

A feasible solution is called Pareto-optimal if it is not dominated by any other feasible solution in the multidimensional search space. A Pareto-optimal solution cannot be improved in any objective function without there being any worsening for at least some other objective function [98].

Definition 3 – Pareto Optimal Set

The group including all the Pareto optimal solutions of a problem constitute the global Pareto Optimal Set.

Definition 4 – Pareto Optimal Front

The set containing the values of the objective functions of the Pareto Optimal Set is designated as the Pareto Optimal Front, nondominated front, or simply Pareto front.

Figure 3.2 shows a depicts the relationship between the multidimensional search space and the corresponding objective space of a random MOP with two objective functions. The multidimensional search space, presented on the left, contains the feasible space defined by the feasible solutions, which are established by the constraints and the labeled boundaries of the MOP, and also contains the infeasible space, defined by the infeasible solutions. The corresponding values of the solutions in the objective search space are presented on the right: a feasible solution in the multidimensional search space presents a feasible solution in the objective search space, and an infeasible solution defines an infeasible solution in the objective search space. In Figure 3.2, within the objective search space, the nondominated solutions (exhibited in green circles) that form the Pareto front (yellow), are distinguished from the set of dominated solutions (presented in green circumferences).

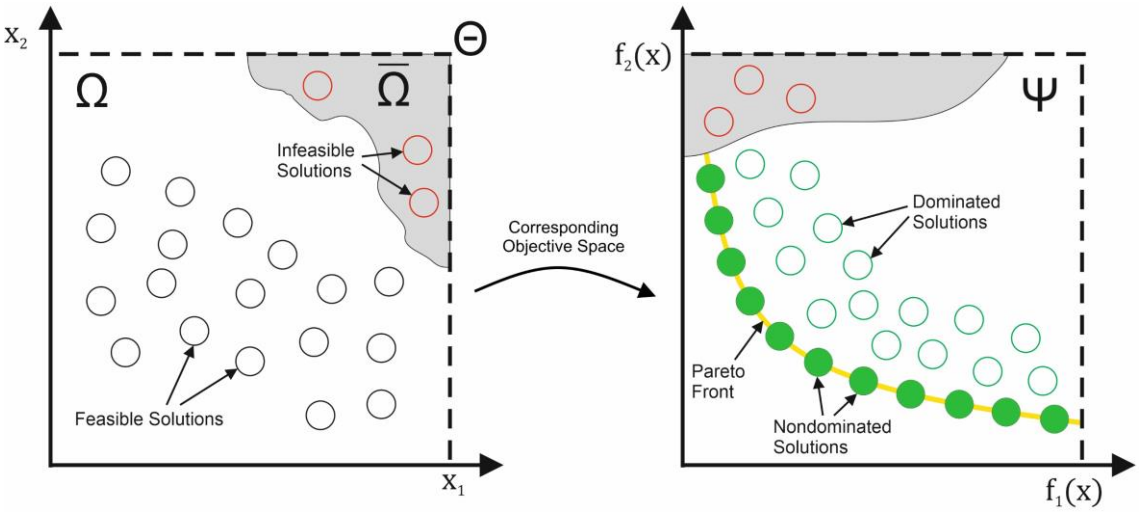

Figure 3.2 - Relationship between the multidimensional search space and the objective search space.

3.2 Meta-heuristics

In recent years, the over-increasing appearance of high complexity and difficulty real-world problems urged for an increasingly need of more reliable, flexible, and fast optimization techniques, especially metaheuristic optimization algorithms [107]. The word “metaheuristic” was introduced in 1986 by Fred Glover [108], as an evolutionary word for “heuristic”. The major difference between heuristic and metaheuristic is that heuristic is problem-dependent: it can be efficient to some problems, while being the opposite to other problems. Metaheuristic however can be used in basically all optimization problems and seem to be a generic algorithm framework [107]. Metaheuristic optimization algorithms use an iterative process that combines random techniques and historical knowledge acquired (memory) to find high quality solution(s) in a multidimensional search space, while avoiding any convergences to local optima. This optimization techniques surpass conventional algorithms due to their black-box optimization nature, gradient free mechanisms, and high local optimal avoidance capability [40], [41], [42].

The reason behind the robustness and effectiveness of the metaheuristic optimization techniques is the harmonization between two search mechanisms: exploration (diversification) and exploitation (intensification) [43], [44]. The former is responsible for the diversification and abroad search of solutions in the multidimensional search space. Exploration mechanisms obtain highly distributed values of the solutions, derived of the high nature of distribution, therefore increasing the exploration area of unexplored areas in the multidimensional search space; this ability is directly related to the avoidance of premature convergence in local optima [44]. The latter is responsible for the intensification of search in local optimal solutions. Exploitation mechanisms obtain high-density results through the search calculations, having low dispersion and intensifying the search for solutions in already explored regions, where high quality solutions have been found [109]. The performance and the efficiency of a metaheuristic heavily depend on a correct balance between the inherent techniques of these two mechanisms: if this balance is not well defined, the metaheuristic algorithm may converge prematurely to optimal local solutions, or the opposite situation, never converging to the global optimal solutions [45].

In the literature, metaheuristics can be classified and divided in many different ways. A common way of separating them is dividing them into the two following categories: trajectory-based metaheuristics and population-based metaheuristics [43]. Trajectory-based metaheuristic algorithms begin with a single solution that is replaced

by the best one, in each iteration, forming a search trajectory in the multidimensional search space. Many trajectory-based metaheuristic algorithms can be found in the literature, including Simulated Annealing (SA), Tabu Search (TS), Iterated Local Search (ILS), and Guided Local Search (GLS) [46]. Population-based algorithms, however, fundamentally begin by generating a random set of candidate solutions that, at each iteration, is improved based on the set of rules defined in the algorithm and evaluated according to the objective function. The algorithm seeks to find the best global solutions stochastically, by constantly improving the set of best solutions found so far. Countless population-based metaheuristics can be found in the literature, namely: Particle Swarm Optimization (PSO) [110], Grey Wolf Optimizer (GWO) [111], Whale Optimization Algorithm (WOA) [112], Differential Evolution (DE) [113], Ant Lion Optimizer (ALO) [114], Genetic Algorithm (GA) [115], Flower Pollination Algorithm (FPA) [116], Arithmetic Optimization Algorithm (AOA) [117], etc.

The general frameworks of population-based algorithms, for solving MOPs, is always very similar [99]: the optimization starts by generating a random set of candidate solution in the multidimensional search space. The candidate solutions, if feasible, are then compared with each other by the Pareto operators, and the set of nondominated solutions is determined and stored in a repository with limited capacity. What makes a multi-objective optimization algorithm (MOA) different from another is the use of different methods to enhance the nondominated solutions [99]. In each iteration, the algorithm generates new candidate solutions and tries to improve the set of nondominated solutions. The iterative process ends when the stopping criterion is reached. The stopping criterion may reflect several aspects inherent to the optimization problem: simulation time; maximum number of iterations; the maximum number of objective function evaluations; and population stagnation, i.e., if there is no significant improvement of the solutions during a certain number of iterations; among others. A final optimal solution can, only afterward, be chosen from the Pareto front, according to the preferences or decision-making factors outlined by the designer.

3.3 Multi-Objective Particle Swarm Optimization (MOPSO)

Multi-Objective Particle Swarm Optimization (MOPSO) is a population-based, stochastic metaheuristic algorithm that is very effective in solving multi-objective optimization problems, i.e., optimization problems involving two or more objective, typically antagonistic, functions [118]. It is a metaheuristic algorithm inspired by the foraging behavior of certain animal species involving a population of particles that represent possible solutions. The particles can communicate and cooperate with each other to determine a set of promising solutions, i.e., a set of solutions with a good trade-off between the different objective functions (nondominated solutions). The particles are randomly positioned within the multidimensional search space (d) and evaluated using the objective functions inherent to the optimization problem (with or without constraints). Particles move based on their current velocities and positions, the individual experience of each particle (cognitive factor), and the collective experience of the population's particles (social factor). Thus, during the optimization process, the velocity and position vector are updated according to Equations (3.3) and (3.4), respectively:

$$v_{i,d}^{k+1} = \omega \cdot v_{i,d}^{k} + c_1 \cdot r_1 \cdot \left(pbest_{i,d}^{k} - x_{i,d}^{k}\right) + c_2 \cdot r_2 \cdot \left(gbest_{d}^{k} - x_{i,d}^{k}\right) \tag{3.3}$$

$$x_{i,d}^{k+1} = x_{i,d}^{k} + v_{i,d}^{k+1} \tag{3.4}$$

where $v_{i,d}^{k}$ represents the velocity of each particle i in iteration k; $x_{i,d}^{k}$ is the position of particle i in iteration k; ω is the inertia factor; c_1 and c_2 are the acceleration coefficients used to adjust the cognitive and social contributions when updating the velocities, respectively; and r_1 e r_2 define the stochastic characteristic given by two random numbers evenly distributed in the interval [0, 1]. In each iteration, this set of nondominated solutions is determined, registered in a given hypercube, and stored in a repository with limited capacity.

For the collective experiment ($gbest$), in the MOPSO algorithm, each particle selects a solution from the repository associated with a given hypercube through the roulette wheel selection method that selects a nondominated solution from the repository based on a probability. This probability is calculated using the ratio between the individual fitness of the solutions (objective function value) and the quality of the solutions that compose the repository, i.e., the sum of all the individual fitness of the solutions. Furthermore, for its individual experience ($pbest$), each particle considers the

current/recent nondominated solution produced by the particle itself in the iterative process. These selection procedures of $gbest$ and $pbest$ promote a good diversification in the construction of new solutions (population) and, simultaneously, maximize convergence to the real Pareto optimal front, ensuring a good diversity in the solutions that constitute it.

As aforementioned, the movement of each particle belonging to the population, i.e., its new velocity and position, is calculated through Equations (3.3) and (3.4), respectively. However, it is essential to prevent particles from "traveling" outside the multidimensional search space during the iterative process. This constraint is expressed mathematically by Equation (3.5):

$$\begin{cases} if\ x_{i,d}^{k+1} > ub_d\ then\ x_{i,d}^{k+1} = ub_d \\ if\ x_{i,d}^{k+1} < lb_d\ then\ x_{i,d}^{k+1} = lb_d \end{cases} \tag{3.5}$$

Through this procedure, if any of the lower (lb) or upper (ub) limits are exceeded, the movement of the particle is modified to ensure that the new position is within the search space.

3.4 The proposed Multi-Objective Optimization Algorithm: Multi-Objective Arithmetic & Differential Evolution Optimization (MOADEO)

This section outlines the proposed Multi-Objective Optimization Algorithm named MOADEO – Multi-Objective Arithmetic & Differential Evolution Optimization. It begins by introducing and explaining the associated preliminaries, and after that, describes the algorithm itself, describing the key intrinsic functions and the relevant formulations.

3.4.1 Preliminaries

The proposed MOADEO algorithm was established based on 2 well known population-based optimization algorithms present in the literature: the Arithmetic Optimization Algorithm (AOA) and the Differential Evolution (DE) Algorithm. Prior to the exhibition of the MOADEO algorithm, these 2 algorithms are presented, and the corresponding mathematical formulations are explained in great detail.

3.4.1.1 Arithmetic Optimization Algorithm (AOA)

The arithmetic optimization algorithm (AOA) is one of the latest population-based metaheuristic algorithms, proposed in 2021 by [117]. This optimization algorithm inspires on the four major mathematical operators, i.e., Multiplication, Division, Subtraction, and Addition, to seek and achieve high quality solutions, using the two search mechanisms of metaheuristics: exploration and exploitation [119]. The search mechanism chosen, in each iteration k, is selected according to the value of the Math Optimizer Accelerated Function ($MOAF$), defined by Equation (3.6) [120]:

$$MOAF^k = MOAF_{min} + k\left(\frac{MOAF_{max} - MOAF_{min}}{k_{max}}\right) \tag{3.6}$$

where $MOAF_{min}$ and $MOAF_{max}$ denote the minimum and maximum values of the MOAF, respectively, predefined by the user; k_{max} is the maximum number of iterations.

In the exploration mechanism, the AOA makes use of two of the mathematical operators: the Division operator and the Multiplication operator. This search mechanism

is conditioned by the value of the MOAF for the condition $r_1 < MOAF$, r_1 being a random generated number between [0,1], and it is formulated by Equation (3.7) [117]:

$$x_{i,d}^{k+1} = \begin{cases} best_d^k \div \left(MOPF^k + \epsilon\right) \times \left((ub_d - lb_d) \times \mu + lb_d\right), & r_2 < 0.5 \\ best_d^k \times MOPF^k \times \left((ub_d - lb_d) \times \mu + lb_d\right), & otherwise \end{cases} \quad (3.7)$$

where $x_{i,d}^{k+1}$ denotes the position of the i-th solution in the next iteration, $(k+1)$; $best_d^k$ represents the position of the best solution obtained so far; ϵ is a random tiny positive number to avoid the division by zero [121]; ub_d and lb_d define the upper and lower bound values of the multidimensional search space with dimension d, respectively; μ is a control parameter that controls the search process; r_2 is a random generated number between [0,1]. The Math Optimizer Probability Function (MOPF), is a function defined by Equation (3.8):

$$MOPF^k = 1 - \frac{k^{1/\alpha}}{k_{max}^{1/\alpha}} \quad (3.8)$$

where α represents a critical parameter that controls the exploitation search mechanism efficiency throughout iterations [122].

The exploitation search mechanism is defined by the remaining two mathematical operators: the Subtraction operator and the Addition operator, and it is modeled using Equation (3.9) [117]:

$$x_{i,d}^{k+1} = \begin{cases} best_d^k - MOPF^k \times \left((ub_d - lb_d) \times \mu + lb_d\right), & r_3 < 0.5 \\ best_d^k + MOPF^k \times \left((ub_d - lb_d) \times \mu + lb_d\right), & otherwise \end{cases} \quad (3.9)$$

where r_3 is a random generated number between [0,1]. The pseudo-Code of AOA is displayed in Table 3.1.

Table 3.1 - Pseudo-Code of the AOA.

Pseudo-Code	
1	Initialize the parameters of the AOA: μ and α.
2	Assess the limit values of the MOAF: $MOAF_{min}$, and $MOAF_{max}$
3	Initialize the position of the initial solutions.
4	Assess the fitness values of the given solutions.
5	while $k < k_{max} + 1$
6	Assess the value of the MOAF using Equation (3.6).
7	Assess the value of the MOPF using Equation (3.8).
8	for ($i = 1$ *to Solutions*)
9	for ($j = 1$ *to Positions*)
10	Generate the random number values r_1, r_2 and r_3.
11	if r_1<MOAF

Exploration Mechanism
if r_2>0.5
Update the position of the i-th solution using the Division Operator as of the 1st rule of Equation (3.7).
else
Update the position of the i-th solution using the Multiplication Operator as of the 2nd rule of Equation (3.7).
end
else
Exploitation Mechanism
if r_3>0.5
Update the position of the i-th solution using the Subtraction Operator as of the 1st rule of Equation (3.9).
else
Update the position of the i-th solution using the Addition Operator as of the 2nd rule of Equation (3.9).
end if
end if
end for
end for
Assess the fitness values of the given solutions.
Save the best solutions so far.
$k = k + 1$
end while
Return the best global solution.

3.4.1.2 Differential Evolution (DE) Algorithm

The differential evolution (DE) algorithm, firstly proposed by [123], is a metaheuristic algorithm based on the theory of evolution and natural selection. The algorithm uses a set of candidate solutions to explore the multidimensional search space, where the ones with the best fitness's are maintained and have a great probability of generating descendants with the same characteristics, to the next generation. This algorithm resorts on selection operators and modifications that result of the mutation operators and crossover operators, to generate new solutions. If the fitness of the descendants is better than the fitness of the respective parents, the descendants replace their parents, otherwise the parents´ solutions are kept for the next generation [124].

The mutation process uses the vectorial difference between two random candidate solutions. In the variant "DE/rand/1", a random selected candidate solution $x_{i,d}^k$ undergoes a mutation process, result of the vectorial difference between two other random solutions, weighted by a mutation scaling factor. The position of the new solution result of the mutation process, $V_{i,d}^{t+1}$, for this mutation, is given by Equation (3.10) [125]:

$$V_{i,d}^{k+1} = x_{r_{1,d}}^k + \beta\left(x_{r_{2,d}}^k - x_{r_{3,d}}^k\right), \qquad i \neq r_1 \neq r_2 \neq r_3 \tag{3.10}$$

where β represents the mutation scaling factor, a constant between [0,2] that decides the step onward (weight) in the direction of the defined vectorial difference $\left(x_{r_{2,d}}^{k} - x_{r_{3,d}}^{k}\right)$; r_1, r_2 and r_3 are 3 random integer indexes between [1,np].

The crossover operator is used as an increase mechanism of diversification of the generated solutions, which is normally binomial (bin) or exponential (exp). The binomial crossover awards the descendants with at least one component of the mutation process, and it is defined by Equation (3.11) [125]:

$$U_{i,d}^{k+1} = \begin{cases} V_{i,d}^{k+1}, & if\ r_1 \leq C_R\ or\ j = r_2 \\ x_{i,d}^{k}, & otherwise \end{cases} \tag{3.11}$$

where $U_{i,d}^{k+1}$ is the position of the solution resultant of the crossover process; C_R is the crossover rate constant, a user-defined scalar parameter between [0,1].

The last operator, the selection operator, is an elitist process responsible for selecting the best solutions of the current generation for the next generation, by comparing their fitness´ in the objective functions. The selection operator is given by Equation (3.12):

$$x_{i,d}^{k+1} = \begin{cases} U_{i,d}^{k+1}, & if\ f\left(U_{i,d}^{k+1}\right) \leq f\left(x_{i,d}^{k}\right) \\ x_{i,d}^{k}, & otherwise \end{cases} \tag{3.12}$$

The pseudo-Code of the DE algorithm is shown in Table 3.2.

Table 3.2 - Pseudo-Code of the DE algorithm.

Pseudo-Code	
1	Initialize the parameters of the DE algorithm: C_R and β.
2	Initialize the positions of the initial solutions.
3	Assess the fitness values of the given solutions.
4	while $k < k_{max} + 1$
5	for ($i = 1$ *to Solutions*)
6	for ($j = 1$ *to Positions*)
7	Generate the random number values r_1, r_2 and r_3.
8	**Mutation Stage**
9	New solution is generated result of the mutation process ($V_{i,d}^{k+1}$), as of Equation (3.10).
10	**Crossover Stage**
11	if $r_1 \leq C_R\ or\ j = r_2$
12	New solution ($U_{i,d}^{k+1}$) is awarded with a component of the mutation process ($V_{i,d}^{k+1}$), as of the 1st rule of Equation (3.11).
13	else
14	New solution ($U_{i,d}^{k+1}$) is not awarded with a component of the mutation process, as of the 2nd rule of Equation (3.11).
15	end if
16	end for

Assess the fitness values of the new solutions ($U_{i,d}^{k+1}$).
Selection Stage
if $f(U_{i,d}^{k+1}) \leq f(x_{i,d}^{k})$
New generated solution result of the crossover operator ($U_{i,d}^{k+1}$), replaces the initial solution $x_{r_{1,d}}^{k}$, for the next generation, as of the 1st rule of Equation (3.12).
else
Initial solution $x_{i,d}^{k}$ remains and thrives for the next generation ($x_{i,d}^{k+1}$), as of the 2nd rule of Equation (3.12).
end if
end for
$k = k + 1$
end while
Return the best global solution.

3.4.2 Features and Formulations

As aforementioned, the proposed Multi-Objective Arithmetic & Differential Evolution Optimization (MOADEO) algorithm combines the specificities, i.e., diversification and intensification mechanisms, of two population-based metaheuristic algorithms: the Arithmetic Optimization Algorithm (AOA), and the Differential Evolution (DE) Algorithm. Additionally, the population of the MOADEO algorithm is divided into multiple swarms, allowing it to achieve greater diversification in the construction of new solutions and, simultaneously, to explore the multidimensional search space with greater independence. Each swarm confines a population of individuals who represent possible solutions, with the ability to communicate, cooperate, share cognitive and social experiences, and evolve to achieve high-quality solutions.

Initially, all the variables inherent to the optimization problem and all the required variables for the correct use of the MOADEO optimization algorithm are initialized, for instance: the control parameters inherent to each of the two optimization algorithm ($MOAF_{max}$, $MOAF_{min}$, α, and μ from the AOA and β and C_R from the DE algorithm), the parameters associated with the optimization itself, for example the number of swarms, the number of individuals associated with each swarm, the maximum capacity of the repository of non-dominant solutions (rep_{max}), the maximum number of iterations allowed (k_{max}), and also the parameters related to the MOP such as the dimension of the optimization problem (d), the lower (lb) and upper (ub) bounds, among others. Once all the initializations have been structured, the individuals associated with each swarm are randomly positioned within the multidimensional search space, through the following Equation (3.13):

$$x_{i,d} = lb_d + (ub_d - lb_d) \times r \tag{3.13}$$

In each iteration, the individuals belonging to each swarm are evaluated using the objective functions inherent to the optimization problem (with or without restrictions). Based on this evaluation (quantification), the non-dominated solutions that form the Pareto Front are determined using the concepts presented in subsection 3.1.3. As aforementioned, a non-dominated solution is one that is better than the other solutions in at least one objective function, while being no worse in the others. Once the Pareto optimal front has been determined, this set of non-dominated solutions is stored in a repository with limited capacity (rep). However, the set of non-dominated solutions can exceed the maximum capacity of the reservoir (rep_{max}). In this situation, the non-dominated solutions are sorted and selected based on their Crowding Distance (CRD).

The Crowding Distance (CRD) is a method that evaluates how proximate the solutions of a Pareto Front are to each other. It is used to encourage the diversification and uniform spread of the solutions throughout the best-known Pareto Front [126]. Its value is infinite for the extremal solutions, and the sum of the edge's length of the cuboid for non-extremal solutions, for each respective objective function [127], [128]. Figure 3.3 depicts the cuboid of a non-extremal random Pareto Front solution i, of a random MOP with 2 objectives functions, which is an estimate of the size of the largest cuboid enclosing i without including any other point [129].

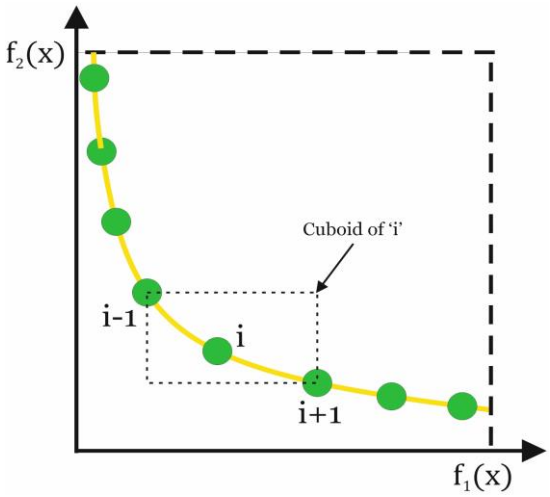

Figure 3.3 – Cuboid of a random non-extremal solution i.

For each extremal solution i, of each objective function j, the CRD value is given by Equation (3.14):

$$CRD_j(x_i) = \infty \tag{3.14}$$

Moreover, for each non-extremal solution i, of each objective function j, the CRD value can be calculated by using Equation (3.15) [128]:

$$CRD_j(x_i) = \frac{f_j(x_{i+1}) - f_j(x_{i-1})}{f_j max - f_j min} \tag{3.15}$$

The total CRD value of a solution x is the sum of the solution´s crowding distances with respect to each objective function [126]. The pseudo-code of the CRD function is given in Table 3.3.

Table 3.3 – Pseudo-code of the Crowding Distance Function.

Pseudo-Code	
1	% input: solutions of the Pareto Front
2	for ($i = 1$ *to number of solutions*)
3	$CRD(x_i) = 0$
4	end for
5	for ($j = 1$ *to number of objective functions*)
6	$Sort(CRD_j)$
7	Attribute an infinite value of CRD to the extremal solutions, as of Equation (3.14).
8	Get the highest and lowest objective function value ($f_j max$ and $f_j min$).
9	for ($i = 2$ *to (number of solutions* – 1))
10	Calculate the CRD of the non-extremal solution, as of Equation (3.15). $CRD(x_i) = CRD(x_i) + CRD_j(x_i)$
11	end for
12	end for
13	Return Crowding Distances.

Once the Pareto front associated with each swarm has been determined, the movement of each individual (new positioning) is carried out using the following Equations (3.16) and (3.17). These equations are based on the AOA optimization algorithm, with several modifications to minimize the problem of premature convergence and converge, at the same time, as much as possible to the true Pareto optimal front. In the MOADEO algorithm, each particle selects to the collective experiment, a position of a random solution ($x_{r_1,d}$).

$$x_{i,d}^{k+1} = \begin{cases} x_{r_1,d}^k \div \left(MOPF^k + \epsilon\right) \times \left((ub_d - lb_d) \times \mu + lb_d\right), & r_2 < 0.5 \\ x_{r_1,d}^k \times MOPF^k \times \left((ub_d - lb_d) \times \mu + lb_d\right), & otherwise \end{cases} \tag{3.16}$$

To the AOA intensification mechanism, some modifications were likewise introduced with the aim of achieving a good diversification of the solutions that make up

the Pareto front. In particular, vectorial differences were used between two individuals selected at random from the repository, as shown in equation (3.17)

$$x_{i,d}^{k+1} = \begin{cases} x_{r_1,d}^{k} - MOPF^{k} \times \left(\left(x_{r_2,d}^{k} - x_{r_3,d}^{k} \right) \times \mu + lb_d \right), & r_4 < 0.5 \\ x_{r_1,d}^{k} + MOPF^{k} \times \left(\left(x_{r_2,d}^{k} - x_{r_3,d}^{k} \right) \times \mu + lb_d \right), & otherwise \end{cases} \tag{3.17}$$

Nonetheless, in the MOADEO algorithm, the movement of each individual undergoes a crossing process, i.e. the new positions calculated using Equations (3.16) and (3.17) undergo a binomial crossing process, through Equation (3.11). Once the movement of the individuals (new position) has been determined, it is crucial to ensure that it is within the multidimensional search space. This procedure is carried out using Equation (3.5). The iterative process ends when the stop criterion is reached. Table 3.4 shows the Pseudo-code of the MOADEO algorithm.

Table 3.4 – Pseudo-Code of the MOADEO algorithm

	Pseudo-Code
1	Initialize the parameters of the AOA: μ, α.
2	Initialize the parameters of the DE algorithm: C_R and β.
3	Place the initial solutions, associated with each swarm, withing the multidimensional search space, using Equation (3.13).
4	Spread the solutions equally, amongst the multiple swarms.
5	while $k < k_{max} + 1$
6	Assess the value of $MOPF$ using Equation (3.8).
	for ($i = 1$ *to Number of swarms*)
7	Assess the fitness values of the given solutions.
8	Find the non-dominated solutions withing the swarm, using the concepts presented in subsection 3.1.3.
9	end for
10	Store the set of non-dominated solutions in a common repository (rep).
11	Assess the CRD values of the given solutions Equations (3.14) and (3.15).
12	if $rep > rep_{max}$
13	Select the best rep_{max} solutions from the repository, based on their CRD.
14	end
15	Assess the new positions of each individual, using Equations (3.16) and (3.17).
16	Update the new positions using the binomial crossing process, as of Equation (3.11).
17	Ensure the new positions are within the multidimensional search space, using Equation (3.5).
18	$k = k + 1$
19	end while
20	Return the best global solution.

CHAPTER 4

Evaluation of the Proposed Multi-Objective Optimization Algorithm

In this chapter, the effectiveness and performance of the proposed MOADEO algorithm is evaluated and compared to other MOAs commonly utilized in the literature.

4.1 Evaluation on Benchmark Functions

In this section, to assess the effectiveness and performance of the proposed MOADEO algorithm, this algorithm is compared to a set of MOAs selected from the literature based on their competitive performance and results, specifically: Multi-objective Arithmetic Optimization Algorithm (MAOA) [42], Multi-objective Flower Pollination Algorithm (MOFPA) [130], Multi-objective Lichtenberg Algorithm (MOLA) [131], Multi-objective Particle Swarm Optimization (MOPSO) [132], Non-dominated Sorting Genetic Algorithm (NSGA-II) [133], and Non-Dominated Sorting Whale Optimization Algorithm (NSWOA) [134].

Each of the selected MOAs, jointly with the proposed MOADEO algorithm, are tested and subsequently evaluated in 20 widely utilized benchmark functions selected from the literature, explicitly the DTLZ [135], [136], [137], [138], [139], [140], [141]. The formulation of each benchmark function is exhibited in Appendixes A, and the respective individual specifications and settings are also depicted, explicitly: the number of objective functions, the dimension, and the boundaries.

It should be mentioned that some of the codes for the simulation purposes were taken from existing frameworks present in the literature, commonly used for comparations and benchmarking purposes and analytical test problems [142]: the DTLZ benchmark functions were taken from [143]; the remaining benchmark functions were taken from [144], [145], [146]; the MOPSO algorithm was taken from [147]; the remaining MOAs were taken from the MATLAB File Exchange Central [148]; lastly, the performance metrics used, described in the following Subsection 4.1.2, were taken from the PlatEMO framework [149].

4.1.1 Parameter Settings

A fair comparison between the performances of different metaheuristics demands some degree of equality [45]. Thus, the MOAs used in the simulation were governed and simulated under the same global simulation parameters: the number of maximum iterations (k_{max}) was set to 500; the repository maximum size (rep_{max}) was limited to 90; and the number of search particles (np) in the multidimensional search space was also set to 90. Additionally, due to the stochastic nature of the optimization, each MOA was run 30 times for each benchmark function [150]. Moreover, to execute a fair and coherent evaluation of the MOAs used in the simulation, for each run, the initial positions of the search particles, that are generated randomly within the boundaries of the problem using Equation (3.13), were considered the same for all the MOAs, giving the algorithms the same starting situation and resulting in coherent convergence and convergence results.

The control parameters used in the simulation, for each individual MOA, are disclosed in Table 4.1 with the respective values, and nomenclatures if existent.

Table 4.1 - Individual parameter settings of the different MOAs.

Algorithm	**Control Parameters**
MOADEO	$MOP_{max} = 1$ $MOP_{min} = 0.2$ A = 5 $M_u = 0.2$ $C_R = 0.9$ Number of swarms = 3
MAOA	Grid Inflation Parameter: A = 0.1 Leader Selection Pressure Parameter: $\beta = 4$ $\gamma = 2$ $\alpha = 5$ $M_u = 0.1$ $MOPF_{max} = 1$ $MOPF_{min} = 0.2$ Number of grids per each dimension = 30
MOFPA	Probability Switch: $p = 0.8$
MOLA	$Ref = 0.4$ $Int_{Con} = 0$ Stick Probability: $S_c = 1$ Creation Radius: $R_c = 150$ $M = 0$ Number of grids per each dimension = 30
MOPSO	Inertia weight: $\omega = 0.7$ Individual confidence factor: $C_1 = 2$ Swarm confidence factor: $C_2 = 2$ Maximum velocity in percentage = 5 Uniform mutation percentage = 0.5 Number of grids per each dimension = 20

NSGA-II	*
NSWOA	*

*No additional parameters required besides the global parameters.

The values used in the control parameters were selected according to the most utilized values in the literature, and the most adequate to the simulation environment. The computational tasks were executed using Matlab® 2021a, in a computer with an Intel(R) Xeon(R) 5-2637 v2 @ 3.50GHz CPU processor, 32 GB RAM and Windows 10 Professional 64-bit operating system.

4.1.2 Performance Criteria

A collective of performance metrics should be applied to correctly evaluate and quantify the performance of multi-objective optimization algorithms in MOPs. For the extension of the non-dominated solutions, two important concepts should be considered: Convergence and Diversity/Coverage. The former refers to the general quality of the solutions found by the MOA, and the process of improvement of the accuracy of the non-dominated solutions [99]. The latter refers to the distribution or the coverage of the solutions and number of solutions found, that cover the entire True Pareto front.

In this paper, three metrics were chosen from the literature to quantify the convergence and coverage of the MOAs: Inverted Generational Distance (IGD) [151], Spacing (SP) [152] and Maximum Spread (MS) [153].

The IGD index can describe the convergence of a set of optimal solutions, represented by the distance between the obtained Pareto optimal solutions of the MOA and the true Pareto optimal front of the MOP, and it's given by Equation (4.1) [100]:

$$IGD = \frac{\sqrt{\sum_{i=1}^{nt} Edist'^{2}_{i}}}{nt} \tag{4.1}$$

where nt is the number of true Pareto optimal solutions; $dist'_i$ is the Euclidean distance between the i-th true Pareto optimal solution and the closest Pareto optimal solution in the obtained repository.

The coverage of the algorithms must also be analyzed, to evaluate if the non-dominated solutions are evenly spread and spaced out in the objective search space. The index SP and MS describe the coverage of the solutions in the multidimensional search space. The SP index formulation is given by Equation (4.2).

$$SP = \sqrt{\frac{1}{nt-1}\sum_{i=1}^{nt}(\overline{t_{SP}} - t_{SP_i})^2} \tag{4.2}$$

where $\overline{t_{SP}}$ is the average of all t_{SP_i}; $t_{SP_i} = \min_j(|f_1^i(x) - f_1^j(x)| + |f_2^i(x) - f_2^j(x)|)$ for all $i, j = 1,2,\dots,nt$. The MS index can be defined by Equation (4.3):

$$MS = \sqrt{\sum_{i=1}^{o}\max\left(FEdist(a_i, b_i)\right)} \tag{4.3}$$

where $FEdist$ is a function to calculate the Euclidean distance; a_i and b_i represent the maximum and minimum value in the i-th objective function, respectively.

It is worth mentioning that for the index´s IGD and SP, lower values represent better values, i.e., the better the algorithm is. The contrast occurs in index MS, where a higher value represents a better coverage of non-dominated solutions in the objective search space. Therefore, the higher value it has, the better the algorithm is.

4.1.3 Results and discussion

Table 4.2, Table 4.3 and Table 4.4 present the results of the simulation, for each performance metric evaluated: IGD, SP and MS, respectively. Each table presents the results obtained by each MOA in the benchmark functions selected, for the 30 runs, resumed on 3 statistical metrics: the mean value, the standard deviation (STD), and lastly the minimum (Min) or maximum (Max) value of the results, depending on the performance metric (minimum value for IGD and SP, and maximum value for MS). The best results were shaded to emphasize the best algorithm and the respective value. Moreover, the mean results obtained for each MOA selected from the literature were compared to the proposed MOADEO algorithm through "+","=", and "-" respective whether that algorithm won, tied or lost to the value of the proposed MOADEO algorithm. The results were considered tied “=” when the mean value of the MOA in question is within 5% of the proposed MOADEO algorithm. In the bottom of each table,

these evaluations are summarized to show in how many benchmark functions that MOA won, tied or lost to the proposed MOADEO algorithm.

As Table 4.2 exhibits, relatively to the IGD performance metric, the proposed MOADEO algorithm obtained the best performance in terms of the mean value in the F6, F7, F10, F12, F14, F15, F16, F18, and F10 benchmark functions, where it additionally obtained the best STD value in the F6, F7 F16, F18, and F20 benchmark functions. The proposed algorithm also obtained the minimum value of the IGD metric in various benchmark functions, explicitly the F6, F7, F10, F13, F14, F16, F17, F18, and F20 benchmark functions. These results show that the proposed MOADEO algorithm has a good convergence of the set of optimal solutions in the 500 iterations, compared to the remaining MOAs. Considering the set of MOAs selected from the literature, the proposed MOADEO algorithm won 16, 10, 12, 8, 11, and 6 times, respectively. However, the proposed MOADEO algorithm did not beat the majority of the IGD results of the MOPSO and the NSWOA algorithm: the proposed algorithm won 8 and 6 times, tied 3 and 5 times, and lost in 7 and 9 times, respectively.

Nevertheless, in general the proposed MOADEO algorithm won against most of the MOAs selected from the literature, having a similar convergence performance to the MOPSO algorithm and to the NSWOA, meaning it has a very competent performance in approximating the optimal set of solutions to the real Pareto Front, regardless of the MOP.

Additionally, a collective of figures were created to better interpret the convergence values of the proposed MOADEO algorithm and the remaining MOAs, in the 20 benchmark function. Figure 4.1 exhibits a qualitative and quantitative evaluation of the results presented in Table 4.2, relative to the IGD metric. For each benchmark function, two figures are displayed: the figures on the left present the true Pareto Front and the Pareto Front of each MOA correspondent to the best IGD value (best convergence result), in the given benchmark function; the figures on the right show the boxplot of the IGD results (presented in Table 4.2), for each MOA, exhibiting the minimum, maximum, mean, the percentiles and median value of the results of the 30 repetitions executed, in the given benchmark function. As evident, the MOAs with a better minimum value present more coherent Pareto Fronts, with better convergence towards the true Pareto Front (presented in blue), whereas MOAs with worse IGD minimum values present more disperse and less approximate solutions to the true Pareto Front.

Relatively to the diversity results of the MOAs in the 20 benchmark functions, shown in Table 4.3 relatively to the SP metric, and in Table 4.4 relatively to the MS metric, the proposed MOADEO algorithm did not show as much potential compared to the convergence of the optimal set of solutions.

Relatively to the SP performance metric, in Table 4.3, the proposed algorithm showed competent results, however, did not present as competent values as the results in the convergence performance metric (IGD). The proposed MOADEO algorithm only proved to have a better mean value in two benchmark functions: F12 and F14, though tying (having similar results) a bunch of times, to other MOAs: it tied 0, 3, 2, 5, 4, and 3 times, respectively, to the set of MOAs selected from the literature. 2 MOAs in particular had a better performance in this metric than the proposed MOADEO algorithm: the MOFPA and the NSGA-II algorithms. These won 10 and 13 times, and only lost 7 and 3 times, respectively, to the proposed MOADEO algorithm. Interestingly, there also is a particularity in the results of this table, where some of the MOAs presented a minimum value of zero, in some benchmark functions. The reason behind this is that the some of the MOAs couldn´t diverge early enough (or converged too early to local optima's) throughout the iterations and ended up with only 2 (or more) solutions in the repository with the same exact coordinates, thus the SP value of 0. Furthermore, the proposed MOADEO algorithm also presented a peculiar value of SP for the benchmark function F19: not a number (NaN). This result is caused from the same reasons described in this paragraph, but in this case this MOP, it only presented a single solution in the repository, and therefore an undefined result of SP.

In general, the proposed MOADEO algorithm presented capable results in this divergence performance metric, indicating to be a skilled MOA compared to those in the literature.

Relatively to the MS performance metric results, shown in Table 4.4, where the higher value represent a better coverage of non-dominated solutions in the objective search space, the proposed MOADEO algorithm, similarly to the Table 4.3, did not salient itself to the MOAs in the literature. The MAOA had outstanding results, winning in most of the benchmark functions. However, the proposed MOADEO algorithm obtained very competitive results compared to the rest of the MOAs, shown by the high value of times the rest of the MOAs lost to the value of it: 15, 10, 14, 10, and 14, respectively. Equally to Table 4.3, the proposed MOADEO algorithm got stuck on benchmark function F19, where it yet again obtained not a number (NaN).

Table 4.2 - Results of the simulation of the 20 benchmark functions, relative to the IGD performance metric.

Benchmark Function/Metric		MOADEO	MAOA		MOFPA		MOLA		MOPSO		NSGA-II		NSWOA	
F1	Mean	3.282245	4.556052	-	2.424277	+	3.666486	-	3.260895	=	2.563799	-	0.323592	+
	STD	3.261663	4.178479		3.015336		1.719423		3.102368		2.664681		0.214495	
	Min	0.152958	0.279453		0.029223		0.514310		0.048351		0.195941		0.045662	
F2	Mean	0.137415	0.358278	-	0.082993	+	0.196294	-	0.104964	+	0.117274	+	0.076880	+
	STD	0.008052	0.065451		0.005808		0.029456		0.004642		0.006531		0.003376	
	Min	0.118141	0.219692		0.071707		0.140690		0.095756		0.104773		0.070216	
F3	Mean	142.7817	147.5460	=	106.2391	+	34.19851	+	144.3323	=	134.0880	+	58.82618	+
	STD	35.68136	31.93369		25.52198		14.82829		25.98817		28.71300		15.26077	
	Min	84.78603	85.77607		41.17253		5.478579		85.77607		76.47190		30.55352	
F4	Mean	0.178785	0.262065	-	0.157116	+	0.229057	-	0.082719	+	0.083985	+	0.075000	+
	STD	0.093937	0.050621		0.287291		0.128416		0.011940		0.008842		0.012759	
	Min	0.097320	0.154730		0.038092		0.084827		0.061820		0.060657		0.057103	
F5	Mean	0.060607	0.243606	-	0.007538	+	0.028551	+	0.027230	+	0.008499	+	0.007761	+
	STD	0.005657	0.077946		0.001325		0.008934		0.002844		0.001668		0.000839	
	Min	0.045696	0.072478		0.005431		0.016118		0.021651		0.005800		0.006002	
F6	Mean	0.004748	0.027470	-	0.005882	-	0.007434	-	0.005291	-	0.005884	-	0.005393	-
	STD	0.000183	0.005955		0.000572		0.005265		0.000269		0.000368		0.000252	
	Min	0.004482	0.017921		0.005110		0.005140		0.004677		0.005190		0.004931	
F7	Mean	0.063893	0.171787	-	0.094257	-	1.122219	-	0.156197	-	0.135117	-	0.087067	-
	STD	0.002170	0.019010		0.008780		0.022516		0.029268		0.048031		0.006771	
	Min	0.059152	0.138831		0.080741		1.069022		0.119078		0.106890		0.076803	
F8	Mean	0.005383	0.064505	-	0.005899	-	0.005796	-	0.005253	=	0.005634	=	0.005586	=
	STD	0.000183	0.028729		0.000518		0.000478		0.000155		0.000253		0.000316	
	Min	0.005019	0.024463		0.005173		0.005298		0.004928		0.005237		0.005030	
F9	Mean	0.081424	0.359711	-	0.164811	-	0.049521	+	0.049914	+	0.443035	-	0.042729	+
	STD	0.016372	0.186151		0.285717		0.004522		0.003297		0.375084		0.002629	
	Min	0.057330	0.133396		0.042510		0.043888		0.042815		0.044805		0.037539	
F10	Mean	0.069262	0.289087	-	1.583258	-	0.082993	-	0.077069	-	2.440675	-	0.078522	-
	STD	0.004140	0.083493		2.934100		0.006672		0.003322		3.386398		0.004660	
	Min	0.063667	0.200582		0.070613		0.069814		0.070724		0.071827		0.070849	
F11	Mean	2.857105	3.421594	-	2.486506	+	2.574438	+	2.500490	+	2.491928	+	2.489858	+
	STD	0.161519	0.480261		0.002163		0.067805		0.004121		0.004278		0.004119	
	Min	2.593997	2.828668		2.483437		2.503048		2.492777		2.484186		2.482370	
F12	Mean	5.888439	5.911771	=	5.888444	=	5.888446	=	5.888447	=	5.888443	=	5.888441	=
	STD	2.437e-05	0.021524		3.194e-05		2.921e-05		2.488e-05		2.217e-05		2.731e-05	
	Min	5.888386	5.889838		5.888328		5.888401		5.888396		5.888417		5.888395	
F13	Mean	0.165143	0.330217	-	0.160362	=	0.172813	=	0.169879	=	0.233339	-	0.162933	=
	STD	0.010780	0.034420		0.011045		0.011569		0.009875		0.023142		0.008078	
	Min	0.143198	0.273923		0.145302		0.152530		0.155039		0.185197		0.149172	
F14	Mean	0.021836	0.025204	-	0.026260	-	0.027014	-	0.024151	-	0.026402	-	0.022015	=
	STD	0.002060	0.003020		0.005627		0.003162		0.002887		0.003086		0.001594	
	Min	0.016844	0.019187		0.020981		0.020982		0.019703		0.021303		0.018776	
F15	Mean	0.078119	0.203325	-	0.083222	-	0.097277	-	0.083141	-	0.180419	-	0.081958	=
	STD	0.009492	0.093787		0.008659		0.024231		0.009773		0.366834		0.008731	
	Min	0.064280	0.095240		0.066627		0.070303		0.071319		0.054304		0.066935	
F16	Mean	0.004848	0.010789	-	0.005304	-	0.068035	-	0.005728	-	0.005493	-	0.005984	-
	STD	0.000181	0.001129		0.000348		0.051960		0.000235		0.000305		0.000327	
	Min	0.004514	0.009097		0.004815		0.005506		0.005226		0.005030		0.005300	
F17	Mean	0.225022	0.013657	+	0.225434	=	0.235855	=	0.006413	+	0.225529	=	0.005170	+
	STD	0.295711	0.001853		0.295395		0.130451		0.002195		0.295323		0.000167	
	Min	0.004789	0.010143		0.004908		0.010399		0.005147		0.005201		0.004826	
F18	Mean	0.004968	0.013158	-	0.005918	-	0.013425	-	0.013227	-	0.014224	-	0.005793	-
	STD	0.000193	0.001474		0.000311		0.007677		0.001754		0.006451		0.000225	
	Min	0.004612	0.010477		0.005221		0.005816		0.010521		0.006966		0.005345	
F19	Mean	0.847953	0.014534	+	0.839292	=	8.671010	-	0.059559	+	0.796601	+	0.006217	+
	STD	0.003444	0.003811		1.349e-09		4.393905		0.022343		0.160952		0.000311	
	Min	0.841025	0.009651		0.839292		2.825396		0.025427		0.006726		0.005769	
F20	Mean	0.003882	0.014880	-	0.004150	-	0.004009	=	0.004286	-	0.004652	-	0.004193	-
	STD	0.000134	0.003193		0.000393		0.000169		0.000411		0.000374		0.000251	
	Min	0.003609	0.011263		0.003817		0.003620		0.003618		0.004088		0.003870	
Win			2		6		4		7		6		9	
Tie			2		4		4		5		3		5	
Lose			16		10		12		8		11		6	

Table 4.3 - Results of the simulation of the 20 benchmark functions, relative to the SP performance metric.

Benchmark Function/Metric		MOADEO	MAOA		MOFPA		MOLA		MOPSO		NSGA-II		NSWOA	
F1	Mean	0.321530	4.749528	-	0.237794	+	2.232347	-	1.321072	-	0.253488	+	1.970695	-
	STD	0.285751	2.016864		0.251713		0.617096		0.025767		0.254069		2.386650	
	Min	0.043457	0.000356		0.022540		1.128291		1.321072		0.022874		0.060745	
F2	Mean	0.065516	0.089796	-	0.062322	=	0.091503	-	0.069883	-	0.059286	+	0.065053	=
	STD	0.007625	0.022786		0.008424		0.020650		0.010766		0.010654		0.010008	
	Min	0.050828	0.052464		0.048977		0.068041		0.050545		0.036661		0.053388	
F3	Mean	12.33447	33.54520	-	8.327906	+	16.01383	-	36.33942	-	10.36808	+	15.25041	-
	STD	4.862384	12.22930		3.157397		3.890015		8.979350		7.437592		13.69453	
	Min	7.544418	14.56306		3.132692		9.040897		20.22447		3.374710		7.401596	
F4	Mean	0.096448	0.179527	-	0.054543	+	0.039479	+	0.076066	+	0.069458	+	0.107706	-
	STD	0.043094	0.149888		0.021258		0.036846		0.015371		0.007202		0.052060	
	Min	0	0.041718		0		2.142e-07		0.037098		0.056880		0.045447	
F5	Mean	0.029902	0.052292	-	0.010845	+	0.029641	=	0.049058	-	0.011433	+	0.010049	+
	STD	0.006754	0.018671		0.001320		0.037648		0.044003		0.001571		0.001279	
	Min	0.019737	0.026566		0.008700		0.007093		0.016722		0.008365		0.008149	
F6	Mean	0.009385	0.025925	-	0.010060	-	0.093610	-	0.009050	=	0.010165	-	0.010038	-
	STD	0.000811	0.005422		0.001202		0.220038		0.000871		0.000832		0.000813	
	Min	0.007988	0.015031		0.007524		0.007039		0.006568		0.008554		0.008068	
F7	Mean	0.067588	0.161578	-	0.076223	-	0.010549	+	0.075558	-	0.055922	+	0.079427	-
	STD	0.006481	0.055544		0.011338		0.005384		0.016464		0.009087		0.011198	
	Min	0.054513	0.100971		0.049295		0.005352		0.053348		0.040669		0.062505	
F8	Mean	0.005292	0.034047	-	0.007085	-	0.005915	-	0.005197	=	0.007839	-	0.006411	-
	STD	0.000498	0.010027		0.000803		0.000803		0.000555		0.000599		0.000711	
	Min	0.004234	0.019140		0.005611		0.004555		0.003972		0.006837		0.005268	
F9	Mean	0.115271	0.226169	-	0.085333	+	0.090767	+	0.120251	=	0.084169	+	0.080957	+
	STD	0.021943	0.108108		0.026608		0.021142		0.013592		0.024746		0.023623	
	Min	0.066646	0.077282		0.037882		0.045661		0.095161		0.036315		0.045833	
F10	Mean	0.178674	0.233504	-	0.102607	+	0.105782	+	0.162875	+	0.102141	+	0.121947	+
	STD	0.112840	0.068568		0.045782		0.042200		0.114656		0.043060		0.083551	
	Min	0.077388	0.127439		0.076256		0.067801		0.068672		0.072763		0.062026	
F11	Mean	0.735655	0.868739	-	0.089095	+	0.337521	+	0.096277	+	0.097671	+	0.084043	+
	STD	0.287578	0.425698		0.007557		0.188191		0.022702		0.011379		0.007109	
	Min	0.335212	0.381740		0.074847		0.145188		0.069912		0.078159		0.071784	
F12	Mean	0.005381	0.012832	-	0.005835	-	0.005528	=	0.005712	-	0.005806	-	0.005457	=
	STD	0.000411	0.002374		0.000541		0.000573		0.000735		0.000587		0.000914	
	Min	0.004631	0.009547		0.005075		0.004650		0.004549		0.004823		0.004151	
F13	Mean	0.135460	0.217719	-	0.139527	=	0.142388	-	0.138768	=	0.106502	+	0.141832	=
	STD	0.015351	0.062838		0.014088		0.015175		0.011524		0.012173		0.015172	
	Min	0.113865	0.110620		0.110250		0.110488		0.119206		0.080748		0.114854	
F14	Mean	0.014855	0.042114	-	0.019679	-	0.021622	-	0.018514	-	0.016613	-	0.018505	-
	STD	0.001754	0.027267		0.003730		0.008308		0.005786		0.002757		0.002354	
	Min	0.011944	0.019504		0.013373		0.013374		0.011847		0.012870		0.014081	
F15	Mean	0.147948	0.167478	-	0.162329	-	0.167391	-	0.166930	-	0.151351	=	0.170303	-
	STD	0.011287	0.034854		0.010811		0.027306		0.012973		0.045258		0.012888	
	Min	0.121980	0.085570		0.142462		0.133021		0.135448		0.016444		0.150575	
F16	Mean	0.008715	0.037970	-	0.008071	+	0.006256	+	0.004527	+	0.008299	=	0.007340	+
	STD	0.000500	0.021462		0.000761		0.002562		0.000546		0.001050		0.000554	
	Min	0.007935	0.013324		0.006648		0.003648		0.003550		0.006469		0.006152	
F17	Mean	0.005525	0.030122	-	0.005144	+	0.007184	-	0.005356	=	0.005356	=	0.007902	-
	STD	0.004268	0.022738		0.003995		0.007492		0.001961		0.004173		0.000507	
	Min	0	0.007129		0		0.000673		0.003707		0		0.006696	
F18	Mean	0.008501	0.059765	-	0.008977	-	0.012565	-	0.012640	-	0.008822	=	0.007956	+
	STD	0.000492	0.033878		0.000916		0.010136		0.001974		0.001318		0.000817	
	Min	0.007758	0.012060		0.006871		0.005575		0.008131		0.006732		0.006500	
F19	Mean	NaN	0.093915	+	0	=	0.161092	+	0.028548	+	0.000373	+	0.006133	+
	STD	NaN	0.456069		0		0.134451		0.012234		0.001471		0.000561	
	Min	0.017144	0.009415		0		0		0.013357		0		0.005024	
F20	Mean	0.010383	0.023222	-	0.007864	+	0.171539	-	0.104393	-	0.007243	+	0.126669	-
	STD	0.014798	0.037368		0.009079		0.148358		0.130574		0.003431		0.262090	
	Min	0.006657	0.009125		0.005282		0.004958		0.003038		0.005318		0.005328	
Win				1		10		7		5		13		7
Tie				0		3		2		5		4		3
Lose				19		7		11		10		3		10

Table 4.4 - Results of the simulation of the 20 benchmark functions, relative to the MS performance metric.

Benchmark Function/Metric		MOADEO	MAOA		MOFPA		MOLA		MOPSO		NSGA-II		NSWOA	
F1	Mean	0.915883	1.314233	+	0.548752	-	1.162993	+	0.780215	-	0.687218	-	1.194584	+
	STD	0.188971	0.505874		0.043441		0.183364		0.251186		0.059125		0.297624	
	Max	1.261996	2.884921		0.634499		1.507360		1.491297		0.836414		1.681012	
F2	Mean	0.568672	0.693960	+	0.451780	-	0.542044	=	0.384230	-	0.636740	+	0.395081	-
	STD	0.057220	0.076749		0.053506		0.050470		0.040462		0.052927		0.034964	
	Max	0.731746	0.897164		0.568091		0.657809		0.453723		0.759105		0.464959	
F3	Mean	0.857538	0.982543	+	0.735227	-	1.164236	+	0.919545	+	0.832883	=	0.730293	-
	STD	0.188999	0.095846		0.197158		0.130948		0.122966		0.065344		0.120628	
	Max	1.255774	1.180579		1.343636		1.495826		1.218689		1.022882		1.037915	
F4	Mean	0.970601	1.166207	+	0.540985	-	0.763331	-	0.747353	-	0.686211	-	1.162233	+
	STD	0.097978	0.200991		0.181980		0.201188		0.115965		0.047943		0.135569	
	Max	1.196701	1.648566		1.000000		1.280977		1.007034		0.769628		1.505321	
F5	Mean	0.564737	0.665577	+	0.423515	-	0.556686	=	0.560193	=	0.479805	-	0.417469	-
	STD	0.066370	0.066768		0.039639		0.176149		0.144301		0.044332		0.040184	
	Max	0.692092	0.814069		0.506142		1.097258		0.984985		0.547550		0.522476	
F6	Mean	1.020030	1.696094	+	0.446547	-	0.594950	-	0.390520	-	0.473036	-	0.452320	-
	STD	0.082424	0.054043		0.055990		0.444223		0.042435		0.042017		0.053294	
	Max	1.190551	1.823089		0.564319		1.788113		0.504693		0.549741		0.560658	
F7	Mean	0.553829	1.153269	-	0.504436	-	0.874715	+	0.437224	-	0.582085	+	0.495315	-
	STD	0.039458	0.084002		0.059870		0.025678		0.045986		0.053824		0.050592	
	Max	0.627589	1.339061		0.629388		0.922999		0.543019		0.735535		0.589364	
F8	Mean	0.299634	1.307755	+	0.338618	+	0.271281	-	0.230431	-	0.401108	+	0.290935	=
	STD	0.031875	0.075168		0.043433		0.033171		0.029475		0.039710		0.032630	
	Max	0.378274	1.442154		0.421975		0.349530		0.303859		0.522002		0.359618	
F9	Mean	0.566904	1.079915	+	0.410687	-	0.372234	-	0.445732	-	0.565813	=	0.323768	-
	STD	0.080141	0.119633		0.099625		0.032443		0.059908		0.114439		0.038107	
	Max	0.725680	1.350518		0.645564		0.448872		0.631272		0.738147		0.468181	
F10	Mean	0.526459	1.163811	+	0.490121	-	0.374010	-	0.394558	-	0.584118	+	0.393276	-
	STD	0.070425	0.101139		0.187224		0.055736		0.083555		0.207246		0.073390	
	Max	0.658000	1.367711		0.864045		0.501029		0.562848		0.880767		0.581150	
F11	Mean	0.788396	1.300797	+	0.497578	-	0.794339	=	0.482296	-	0.540274	-	0.472176	-
	STD	0.105102	0.082547		0.031748		0.138716		0.043759		0.045670		0.028180	
	Max	1.031061	1.494858		0.547629		1.154222		0.596576		0.643603		0.538203	
F12	Mean	0.975490	1.006256	=	0.972586	=	0.969431	=	0.969554	=	0.973077	=	0.968765	=
	STD	0.002556	0.002565		0.003299		0.003756		0.002940		0.003385		0.002432	
	Max	0.979634	1.013117		0.983999		0.977832		0.974158		0.978910		0.974854	
F13	Mean	0.656915	1.142983	+	0.439016	-	0.429992	-	0.405567	-	0.544852	-	0.419587	-
	STD	0.044174	0.071549		0.039323		0.037855		0.030299		0.060426		0.034347	
	Max	0.754548	1.274065		0.528418		0.496049		0.487759		0.653019		0.496075	
F14	Mean	0.457588	0.923173	+	0.459473	=	0.422754	-	0.394768	-	0.481777	+	0.421932	-
	STD	0.037987	0.088573		0.064892		0.066398		0.045299		0.047032		0.038331	
	Max	0.561167	1.138986		0.643172		0.604501		0.506806		0.619359		0.503632	
F15	Mean	0.941107	1.081687	+	0.902749	=	0.930529	=	0.908970	=	0.918224	=	0.953459	=
	STD	0.043528	0.089768		0.048438		0.049523		0.057238		0.072906		0.042100	
	Max	1.054002	1.292101		0.993967		1.060073		1.045576		1.043367		1.030554	
F16	Mean	0.989797	1.145202	+	0.415685	-	0.506029	-	0.182105	-	0.427721	-	0.342801	-
	STD	0.084346	0.098685		0.053316		0.125186		0.021452		0.041736		0.036380	
	Max	1.171762	1.324253		0.510055		0.732797		0.229038		0.489692		0.406862	
F17	Mean	1.021679	1.144491	+	0.616891	-	0.834297	-	0.227009	-	0.645616	-	0.395765	-
	STD	0.050296	0.139300		0.295588		0.149560		0.095232		0.274192		0.036453	
	Max	1.127577	1.380912		1.000000		1.165913		0.613448		1.000000		0.467236	
F18	Mean	0.797354	1.153333	+	0.415925	-	0.457369	-	0.684490	-	0.441817	-	0.361810	-
	STD	0.082862	0.142471		0.042262		0.088036		0.085949		0.056067		0.045736	
	Max	0.953747	1.445599		0.511559		0.646714		0.866737		0.563110		0.501696	
F19	Mean	NaN	1.076436	+	1.000000	+	0.994322	+	0.678776	+	0.977821	+	0.272862	+
	STD	NaN	0.178939		0		0.046199		0.122714		0.095367		0.029327	
	Max	1.018464	1.971755		1.000000		1.059346		1.020458		1.000000		0.336789	
F20	Mean	0.726142	1.276185	+	0.393071	-	1.161179	+	0.814158	+	0.423407	-	0.657433	-
	STD	0.131233	0.110838		0.091089		0.450512		0.539566		0.064102		0.541844	
	Max	1.236383	1.641778		0.806657		1.719191		1.658508		0.584723		1.807766	
Win			18		2		5		3		6		3	
Tie			1		3		5		3		4		3	
Lose			1		15		10		14		10		14	

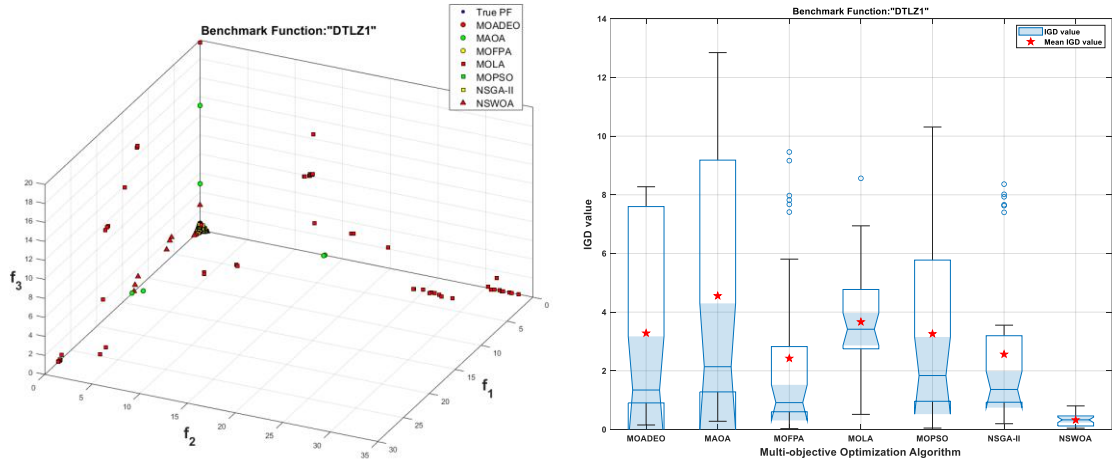

a) Results obtained on the DTLZ1 benchmark function.

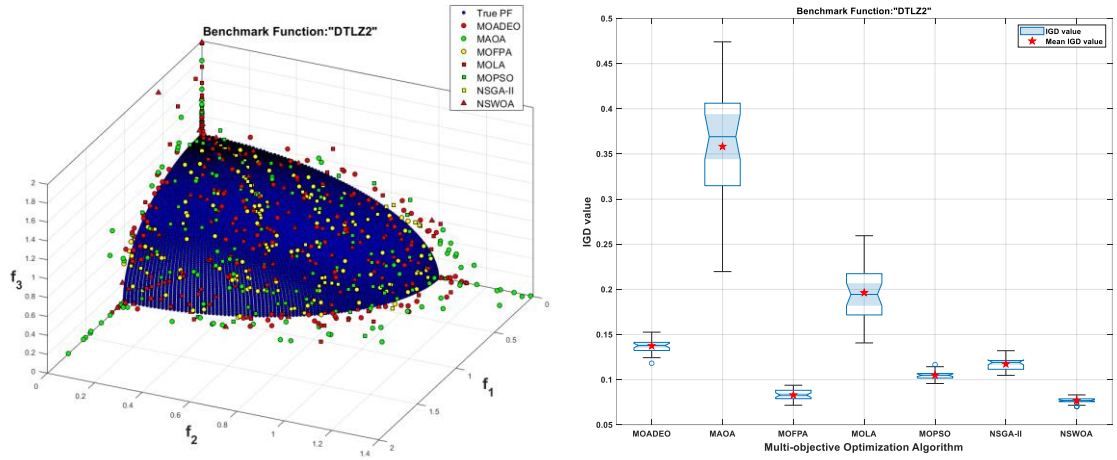

b) Results obtained on the DTLZ2 benchmark function.

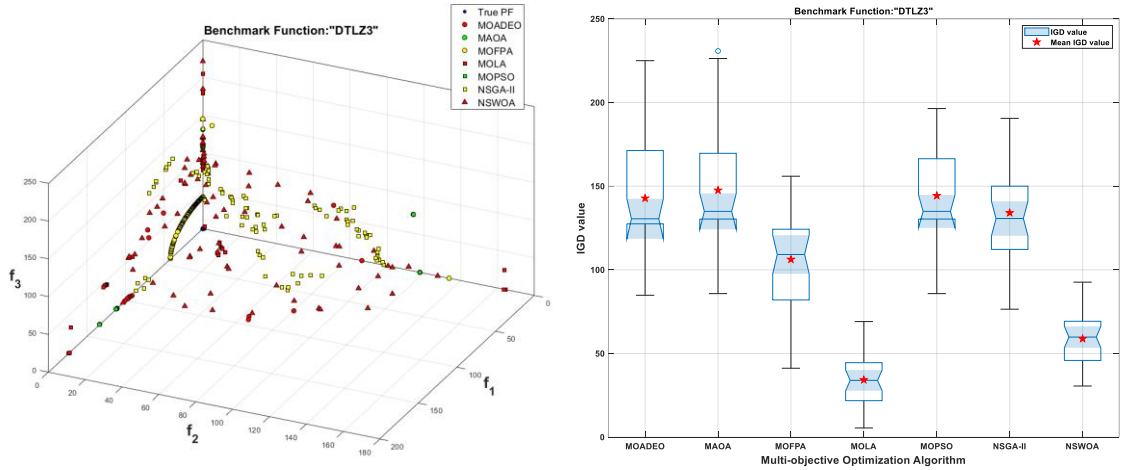

c) Results obtained on the DTLZ3 benchmark function.

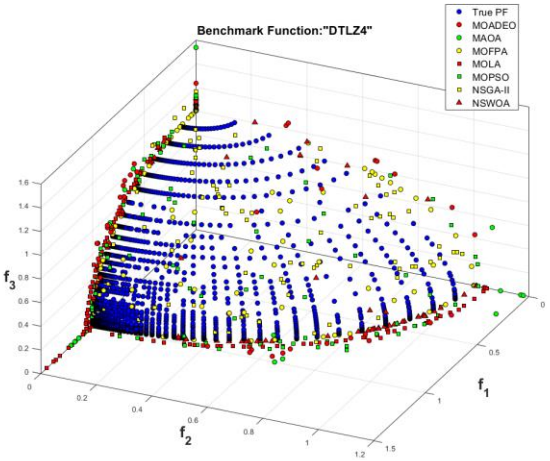

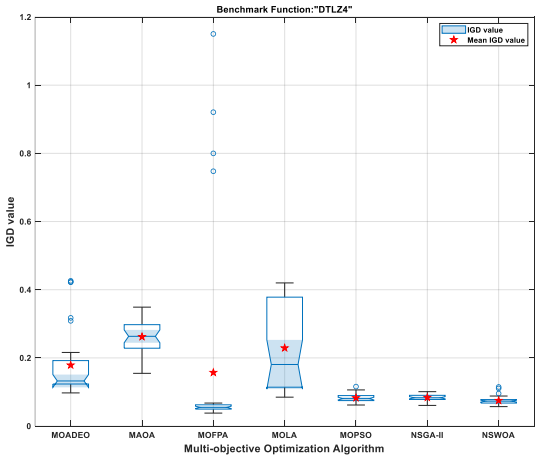

d) Results obtained on the DTLZ4 benchmark function.

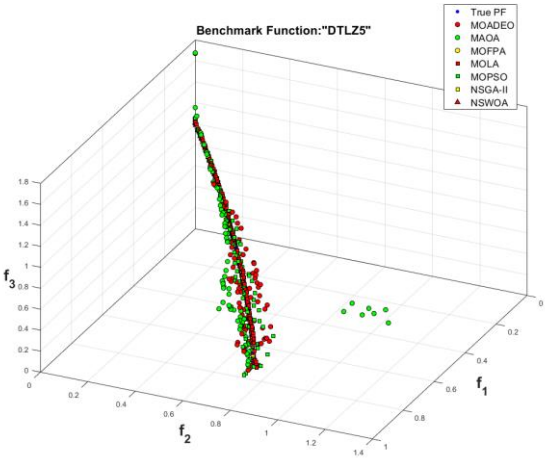

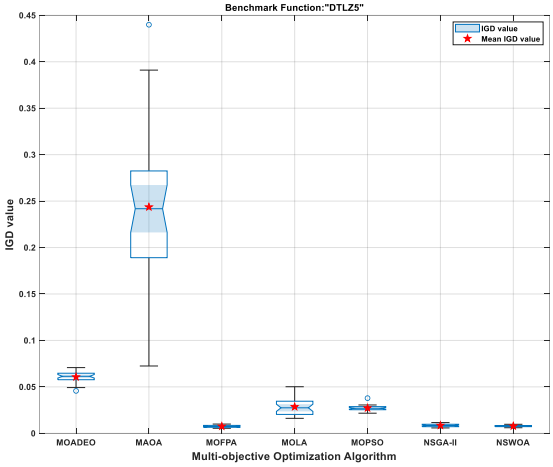

e) Results obtained on the DTLZ5 benchmark function.

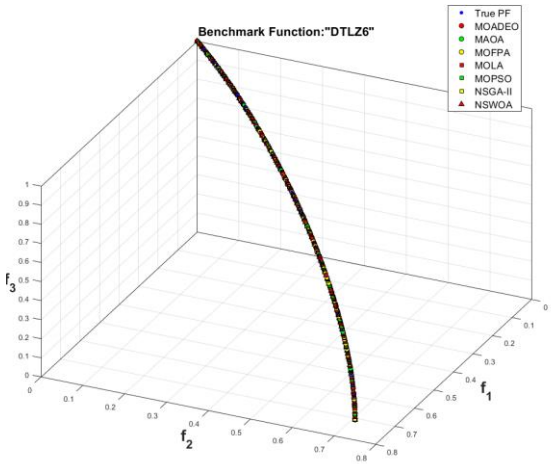

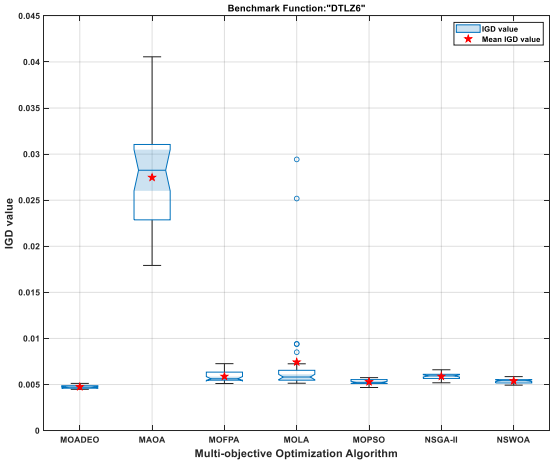

f) Results obtained on the DTLZ6 benchmark function.

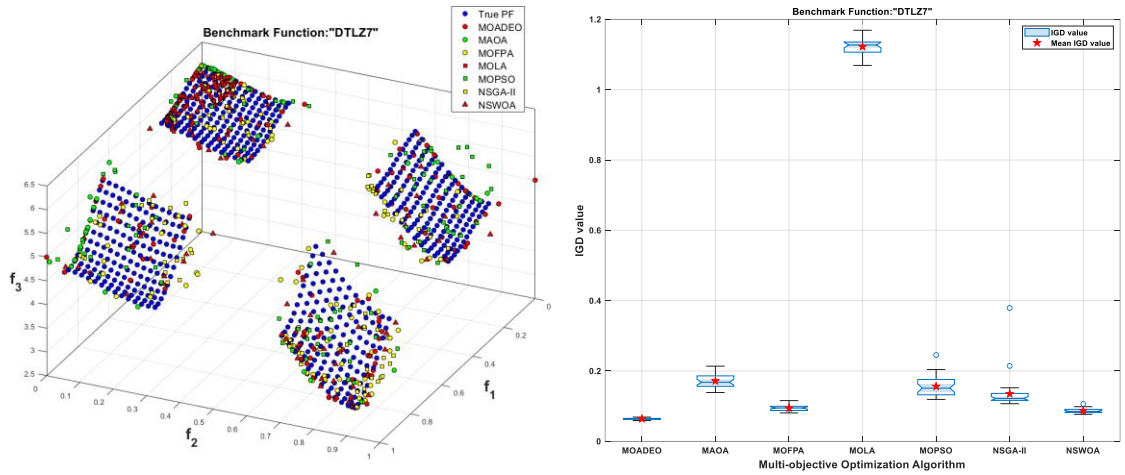

g) Results obtained on the DTLZ7 benchmark function.

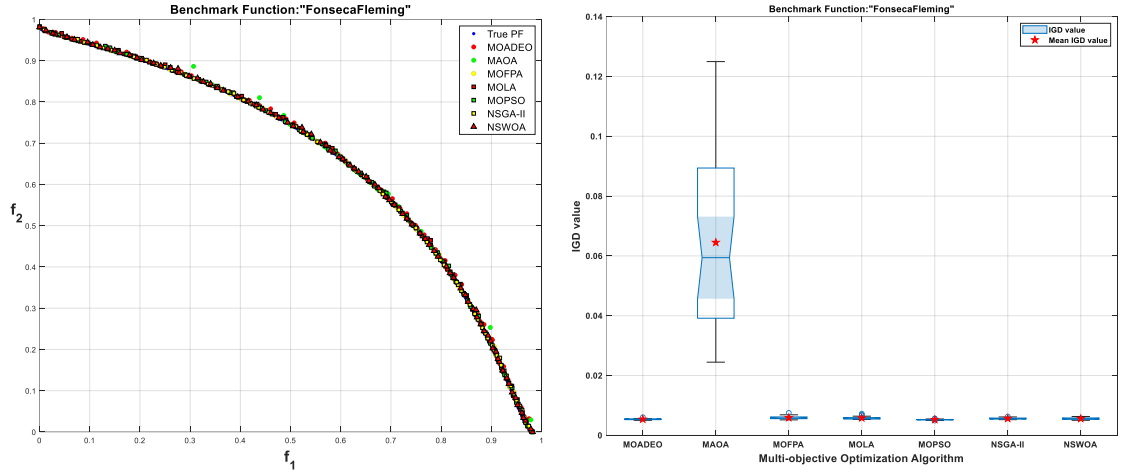

h) Results obtained on the Fonseca-Fleming benchmark function.

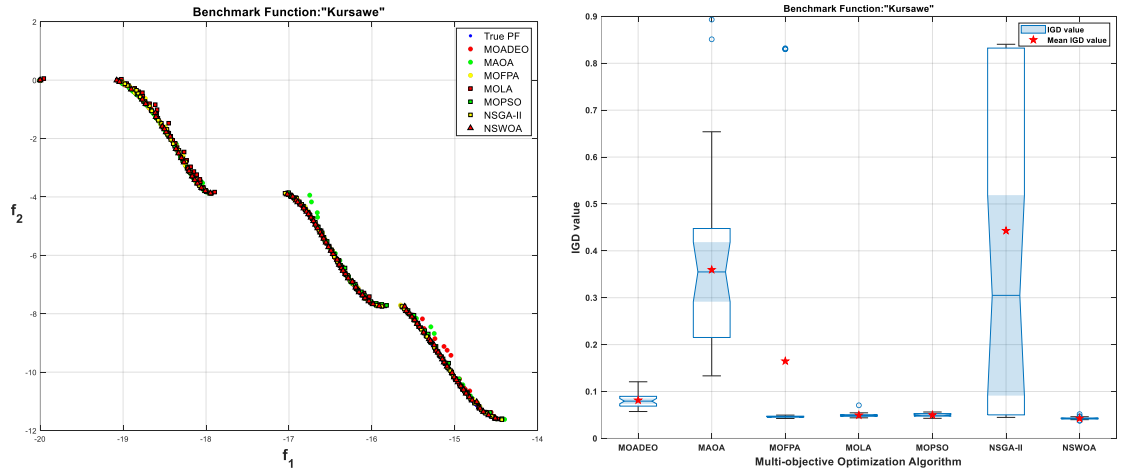

i) Results obtained on the Kursawe benchmark function.

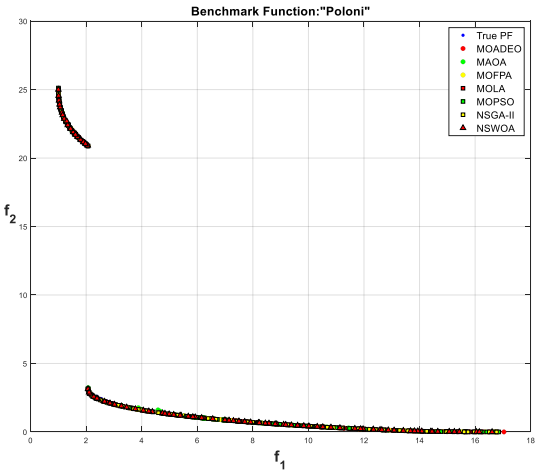

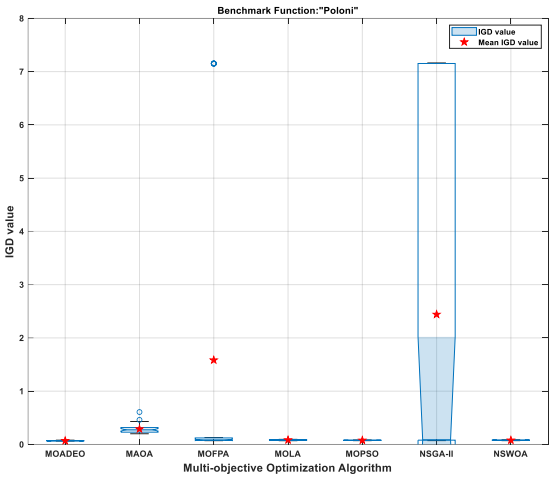

j) Results obtained on the Poloni benchmark function.

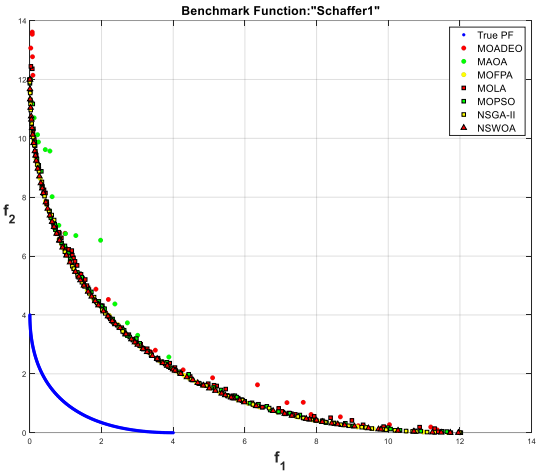

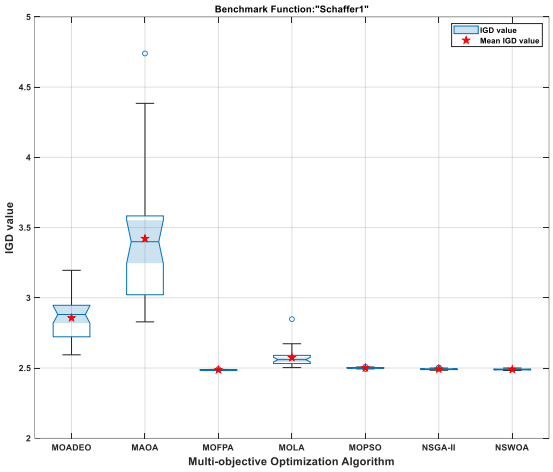

k) Results obtained on the Schaffer1 benchmark function.

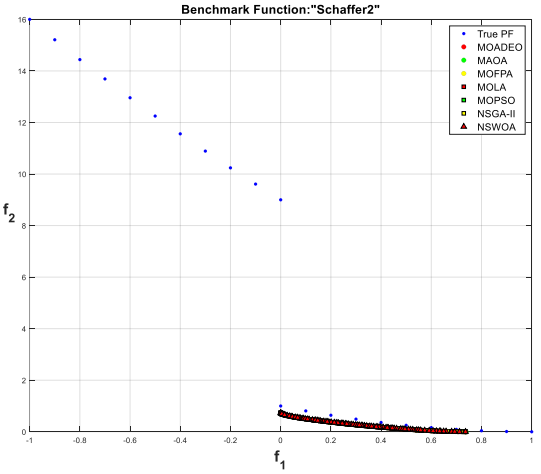

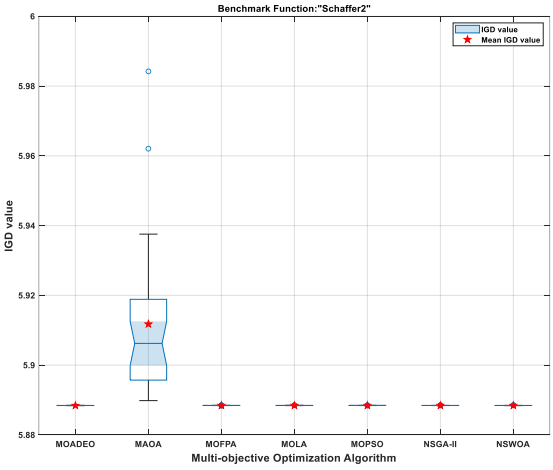

l) Results obtained on the Schaffer2 benchmark function.

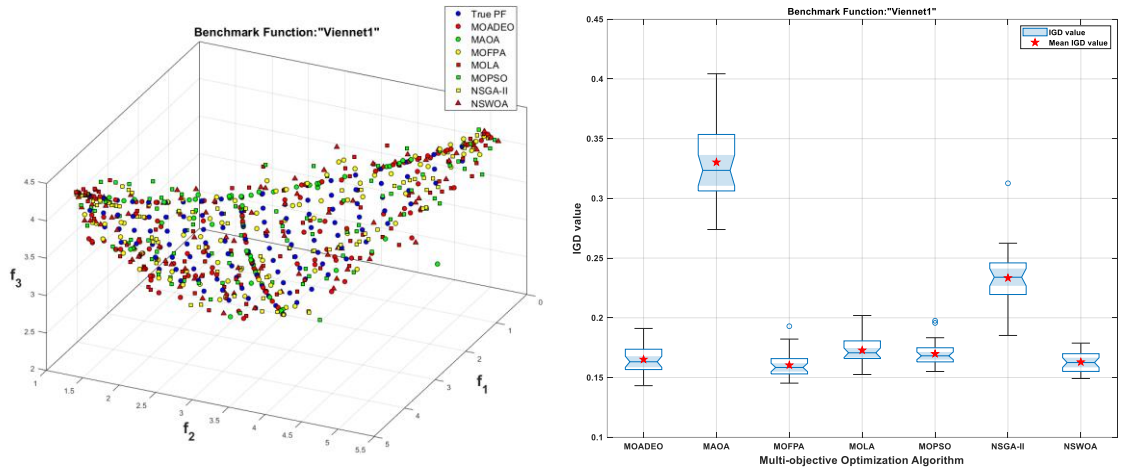

m) Results obtained on the Viennet1 benchmark function.

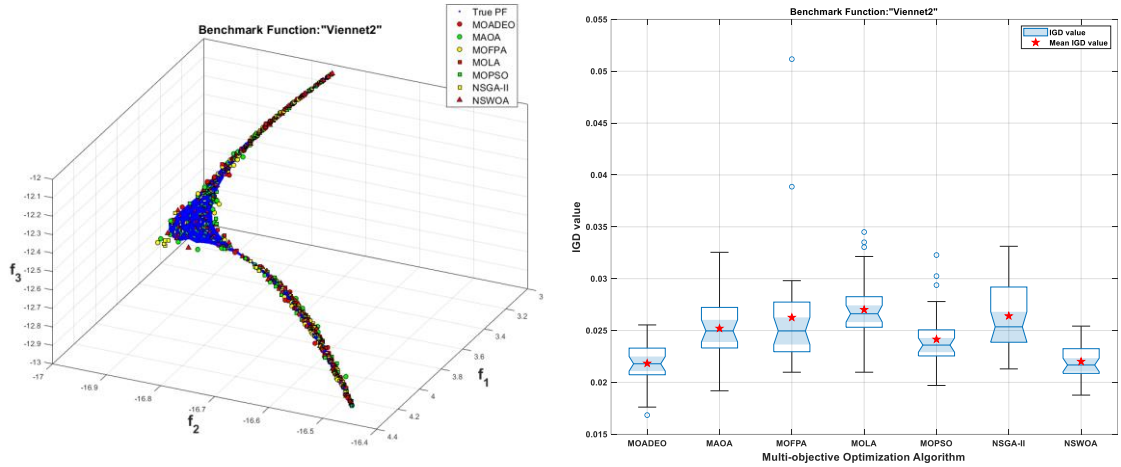

n) Results obtained on the Viennet2 benchmark function.

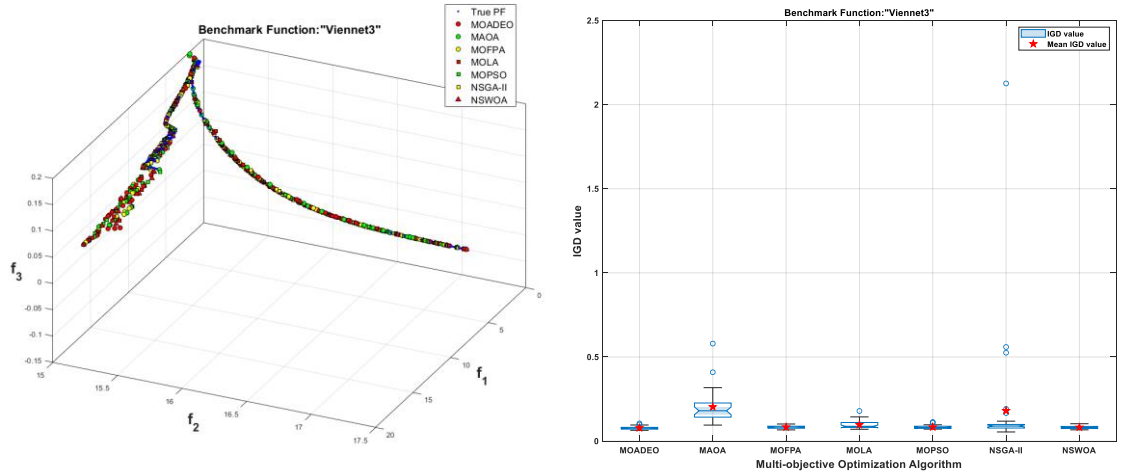

o) Results obtained on the Viennet3 benchmark function.

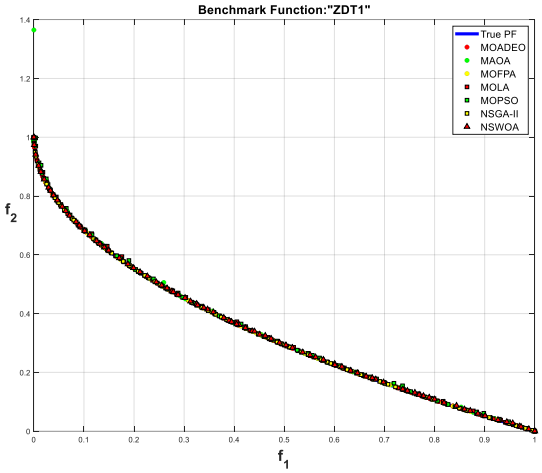

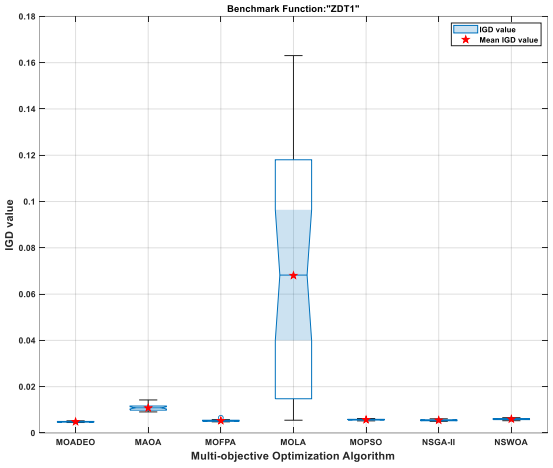

p) Results obtained on the ZDT1 benchmark function.

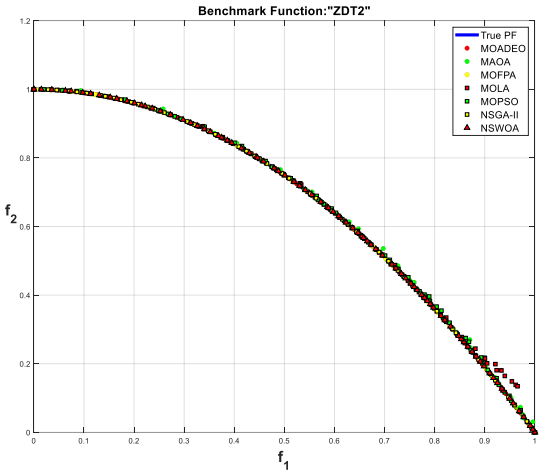

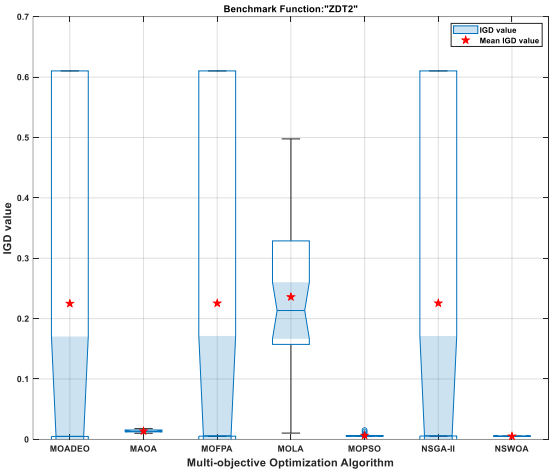

q) Results obtained on the ZDT2 benchmark function.

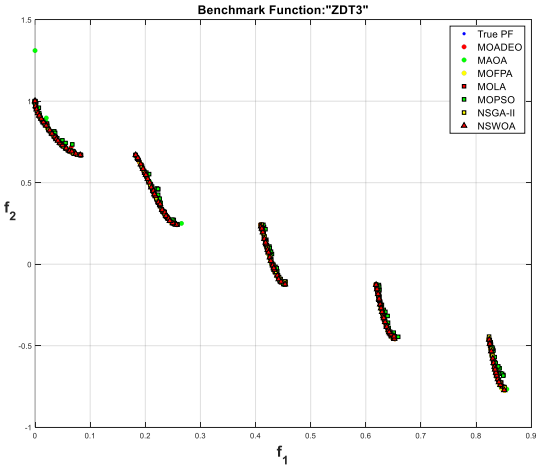

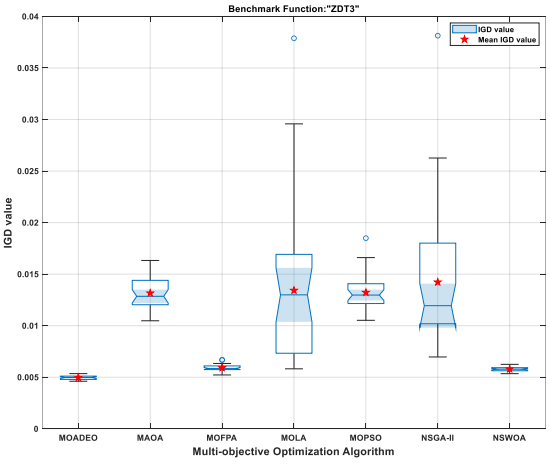

r) Results obtained on the ZDT3 benchmark function.

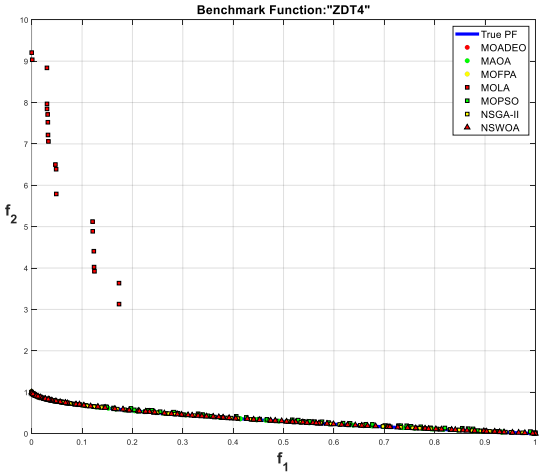

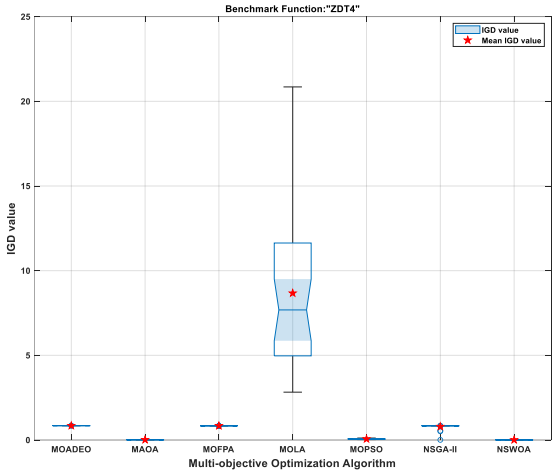

s) Results obtained on the ZDT4 benchmark function.

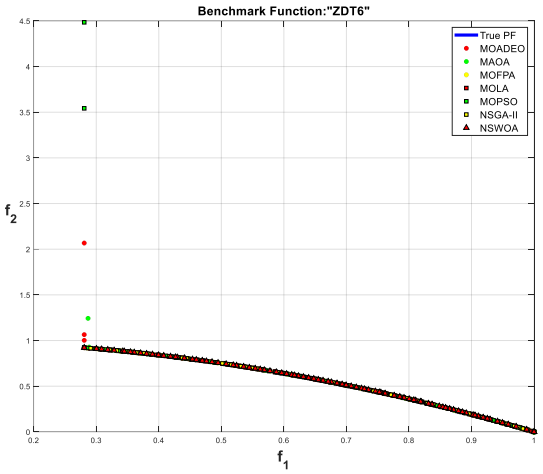

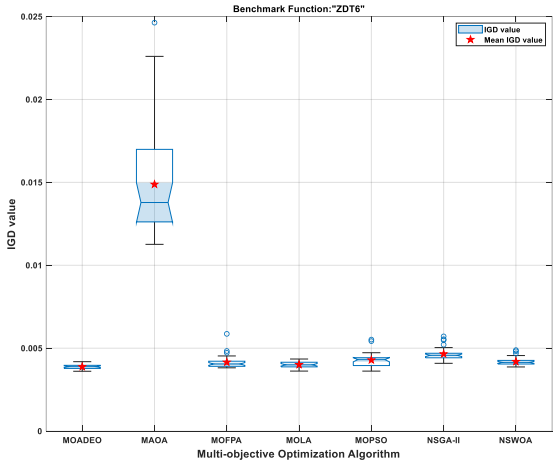

t) Results obtained on the ZDT6 benchmark function.

Figure 4.1 – Results of the simulation obtained by each MOA, on the 20 benchmark functions, for the IGD performance metric.

4.2 Evaluation on Engineering Design Problems

In this section, the performance of the proposed MOADEO algorithm is further investigated and compared through simulations on 4 real-world engineering design problems (EDPs): the welded beam design problem, the gear train design problem, the four-bar truss design problem, and the pressure vessel design problem. These EDPs contain several equality and inequality constraints which the algorithms need to handle, simultaneously, during the optimization process, in order to correctly solve them. To handle the multi-constraints in each MOP, various types of penalty functions can be implemented, such as Static penalty, Dynamic penalty, Annealing penalty, Coevolutionary penalty, and Death penalty [154]. The death penalty function is considered one of the simplest techniques among the different constraint handling function when testing multi-constraint problems [155]. This penalty function awards a big fitness value to the solutions that violate any of the constraints of the problem to easily discard the infeasible solution and does not use the knowledge of those solutions which are helpful to solve the dominated infeasible regions [154], [155]. Due to its low computational demand and its simple implementation, the death penalty was employed in the MOADEO algorithm.

The proposed MOADEO algorithm is compared and simulated with the same six MOAs, mentioned in Section 4.1, and with the same individual control parameters, shown in Table 4.1. The global simulation parameters used in this simulation were the following: the number of maximum iterations (k_{max}) was set to 100; the repository maximum size (rep_{max}) was limited to 90; and the number of candidate solutions / search particles (np) in the multidimensional search space was set to 90; each MOA was run 30 times for each benchmark function, due to the stochastic nature of the optimization. Just like in Section 4.1, for each run, the initial positions of the search particles were the same for all the MOAs. Likewise, the computational tasks were executed in the same Matlab® version and same computational environment.

4.2.1 Welded beam design problem

The welded beam design problem, proposed by [156], consists of the minimization of 2 objectives: the fabrication cost (f_1) and the deflection on the end of the beam (f_2) [157], [158]. This problem contains 4 design variables being: the thickness of the weld (h_{weld}), the length of the part of the beam that is clamped to the wall (l_{beam}), the height of the beam (t_{beam}), and the thickness of the beam (b_{beam}), as shown in Figure

4.2. The 4 design variables h_{weld},l_{beam},t_{beam}, and b_{beam} correspond in the formulation to x_1,x_2,x_3, and x_4, respectively. The mathematical formulation of the welded beam design problem is the following:

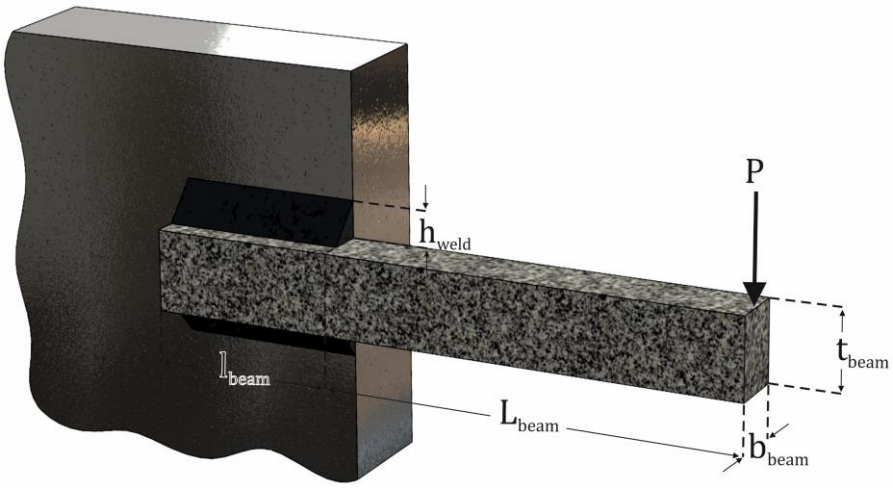

Figure 4.2 – Welded beam design problem.

$$Minimize: \begin{cases} f_1(x) = 1.10471x_1^2x_2 + 0.04811x_3x_4(14.0 + x_2) \\ f_2(x) = \delta(x) \end{cases}$$

$$Subject\ to: \begin{cases} \tau(x) - \tau_{max} \leq 0 \\ \sigma_{beam}(x) - \sigma_{beam_{max}} \leq 0 \\ x_1 - x_4 \leq 10 \\ 0.125 - x_1 \leq 0 \\ P - P_C(x) \leq 0 \end{cases} \tag{4.4}$$

$$Where: \begin{cases} \tau(x) = \sqrt{(\tau')^2 + \dfrac{2\tau'\tau'' x_2}{2R_{beam}} + (\tau'')^2} \\ \tau' = \dfrac{P}{\sqrt{2}x_1 x_2} \\ \tau'' = \dfrac{MR_{beam}}{J} \\ M = P\left(L_{beam} + \dfrac{x_2}{2}\right) \\ R_{beam} = \sqrt{\dfrac{x_2^2}{4} + \left(\dfrac{x_1 + x_3}{2}\right)^2} \\ J = 2\left\{\dfrac{x_1 x_2}{\sqrt{2}}\left[\dfrac{x_2^2}{12} + \left(\dfrac{x_1 + x_3}{2}\right)^2\right]\right\} \\ \sigma_{beam}(x) = \dfrac{6PL_{beam}}{x_4 x_3^2} \\ \delta(x) = \dfrac{4PL_{beam}{}^3}{Ex_4 x_3^3} \\ P_C(x) = \dfrac{4.013\sqrt{\dfrac{EG_{beam}x_3^2 x_4^6}{36}}}{L_{beam}{}^2}\left(1 - \dfrac{x_3}{2L_{beam}}\sqrt{\dfrac{E}{4G_{beam}}}\right) \end{cases} \tag{4.5}$$

Additional considerations: $P = 6000$ lb, $L_{beam} = 14$ in, $\delta_{max} = 0.25$ in, $E = 30 \times 10^6$ psi, $G_{beam} = 12 \times 10^6$ psi, $\tau_{max} = 13600$ psi, $\sigma_{max} = 30000$ psi. Moreover:

$$\begin{cases} 0.125 \leq x_1 \leq 5.0\ in \\ 0.1 \leq x_2 \leq 10.0\ in \\ 0.1 \leq x_3 \leq 10.0\ in \\ 0.125 \leq x_4 \leq 5.0\ in \end{cases} \tag{4.6}$$

4.2.2 Gear train design problem

The gear train design problem, proposed in [159], is a problem involving 4 connected gears and aims to determine the number of teeth and size of each gear. The problem consists of 2 objectives: minimizing the error between the obtained and required gear ratio (f_1), while minimizing the size of the four gears (f_2) [160], [161]. The decision variables are the number of teeth in each gear: Z_d refers to the number of teeth on the driving gear; Z_a is the number of teeth in the driven gear; Z_b indicates the number of teeth of the gear attacked to the driven gear; and Z_f represents the number of teeth in the final gear, as shown in Figure 4.3. The mathematical formulation of the gear train design problem is given below.

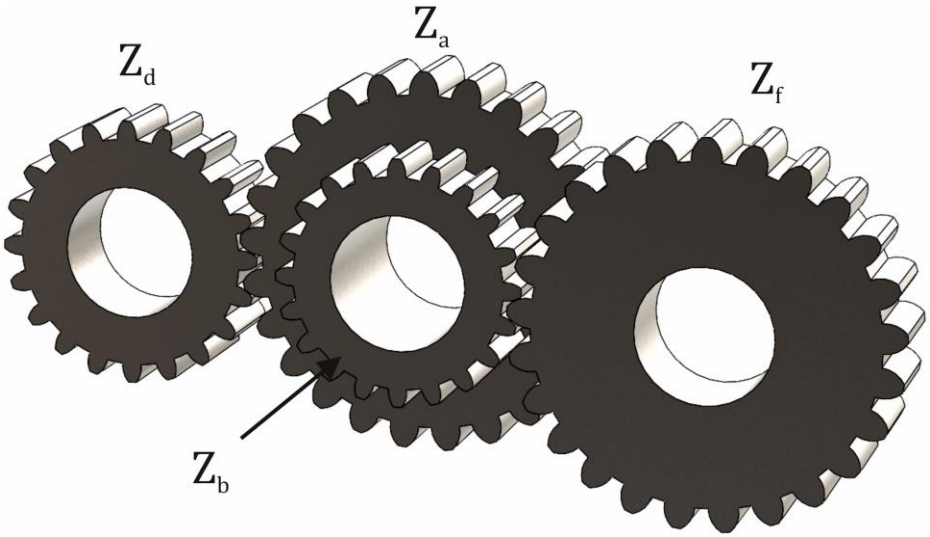

Figure 4.3 – Gear train design problem.

$$Minimize: \begin{cases} f_1(Z) = \left|6.931 - \dfrac{Z_a}{Z_d}\dfrac{Z_f}{Z_b}\right| \\ f_2(Z) = max\left(Z_d, Z_b, Z_a, Z_f\right) \end{cases} \tag{4.7}$$

$$Subject\ to: \frac{f_1(Z)}{6.931} \leq 0.5$$

$$12 \leq Z_d, Z_b, Z_a, Z_f \leq 60, \qquad Z_d, Z_b, Z_a, Z_f \in \mathbb{Z} \tag{4.8}$$

4.2.3 Four-bar truss design problem

The four-bar truss design problem is a multi-objective problem firstly introduced by [162], composed by 4 bars connected to each other by 4 joints, as shown in Figure 4.4. The goal of the problem is to minimize the structural volume (f_1) and minimize the displacement of joint 2 (f_2), when subjected to multiple forces (P), while subjected to stress constraints [163]. The cross-section areas of each bar 1,2,3, and 4 are represented in the formulation as x_1, x_2, x_3, and x_4, respectively. The mathematical formulation of this design problem is given next.

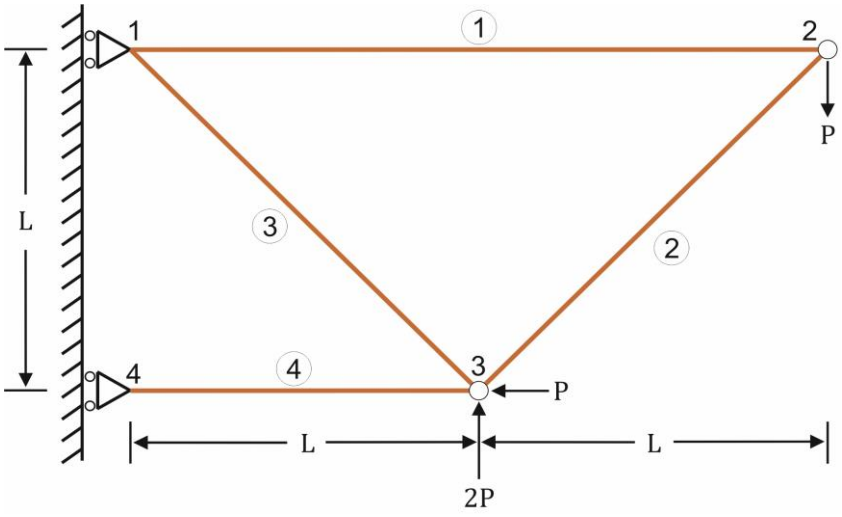

Figure 4.4 – Four-bar truss design problem.

$$Minimize: \begin{cases} f_1(x) = L(2x_1 + \sqrt{2}x_2 + \sqrt{2}x_3 + x_4) \\ f_2(x) = \dfrac{PL}{E}\left(\dfrac{2}{x_1} + \dfrac{2\sqrt{2}}{x_2} - \dfrac{2\sqrt{2}}{x_3} + \dfrac{2}{x_4}\right) \end{cases} \tag{4.9}$$

$$Subject\ to: \begin{cases} \dfrac{P}{\sigma} \leq x_1 \leq \dfrac{3\mathrm{P}}{\sigma} \\ \dfrac{\sqrt{2}P}{\sigma} \leq x_2 \leq \dfrac{3\mathrm{P}}{\sigma} \\ \dfrac{\sqrt{2}P}{\sigma} \leq x_3 \leq \dfrac{3\mathrm{P}}{\sigma} \\ \dfrac{P}{\sigma} \leq x_4 \leq \dfrac{3\mathrm{P}}{\sigma} \end{cases} \tag{4.10}$$

Considering: $P = 10$ kN, $E = 2.00 \times 10^5$ kN/cm2, $L = 200$ cm, and $\sigma = 10$ kN/cm2.

4.2.4 Pressure vessel design problem

The pressure vessel design problem was proposed by [164], is an engineering problem that seeks to minimize the total cost (f_1) including material, forming, and welding costs, and maximize the storage space (f_2) of a cylindrical pressure vessel capped with 2 hemispheres heads in both ends [160], [161]. These 2 objectives are influenced by 4 design variables: the thickness of the shell (T_s), the thickness of the hemisphere head (T_h), the inner radius of the vessel (R), and the length of the cylindrical vessel section (L_{vessel}), as shown in Figure 4.5. The mathematical formulation of the current design problem is the next:

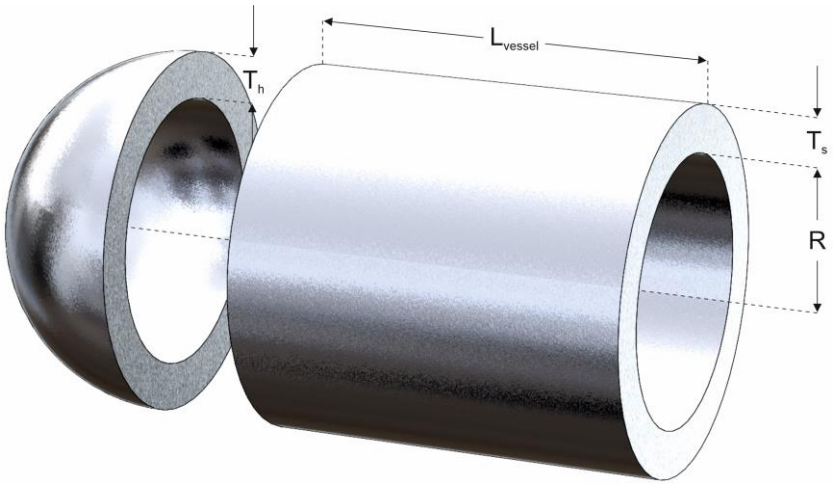

Figure 4.5 – Pressure vessel design problem.

$$Minimize: \begin{cases} f_1(x) = 0.6224T_sL_{vessel}R + 1.7781T_hR^2 + 3.1661T_s^2L_{vessel} + 19.84T_s^2 \\ f_2(x) = -(\pi R^2 L_{vessel} + 1.333\pi R^3) \end{cases} \quad (4.11)$$

$$Subject\ to: \begin{cases} 0.0193R - T_s \leq 0 \\ 0.00954R - T_h \leq 0 \end{cases}$$

$$Where \begin{cases} T_s \geq 0.0625 \\ T_s \leq 5 \\ T_h \geq 0.0625 \\ T_h \leq 5 \\ R \geq 10 \\ R \leq 200 \\ L_{vessel} \geq 10 \\ L_{vessel} \leq 240 \end{cases} \quad (4.12)$$

Among the 4 design variables, x_1 and x_2 are discrete variables: integer numbers, multiples of 0.0625 in; the other 2 variables are continuous variables i.e., x_3 and x_4.

4.2.5 Results and discussion

The results of the simulation of the 4 EDPs are presented in Table 4.5. This time, however, since these are real-world problems, these don't have a theoretical true Pareto optimal Front, and therefore the results of the simulation cannot be compared to a true Pareto Front. Thus, the results obtained by each MOA can only be compared to each other using the SP metric since it does not require the knowledge of the true Pareto Front.

The results obtained by each MOA on the different EDPs are resumed on 3 statistical metrics: the mean value, the standard deviation (STD), and lastly the minimum (Min) value. Similarly to the results on the 20 benchmark function in section 4.1.3: the best results were shaded to emphasize the best algorithm and the respective value; the mean results obtained for each MOA selected from the literature were compared to the proposed MOADEO algorithm through "+","=", and "-" respective whether that algorithm won, tied or lost to the value of the proposed MOADEO algorithm; in the bottom of the table, the evaluations are summarized to show in how many benchmark functions that MOA won, tied or lost to the proposed MOADEO algorithm. The results were considered tied "=" when the mean value of the MOA in question is within 5% of the proposed MOADEO algorithm.

Table 4.5 - Results of the simulation of the 4 EDPs, relative to the SP performance metric.

Benchmark Function/Metric		MOADEO	MAOA		MOFPA		MOLA		MOPSO		NSGA-II		NSWOA	
EDP 1	Mean	0.24231	13.3816	-	3.565977	-	10.58815	-	21.97895	-	3.496549	-	6.017832	-
	STD	0.091561	34.76437		9.545353		33.49958		33.22996		7.273114		16.33383	
	Min	0.159745	0.159481		0.130882		0.154494		0.138557		0.23283		0.12378	
EDP 2	Mean	0.016636	1.902935	-	0.065923	-	0.910693	-	1.384089	-	0.015955	=	0.547691	-
	STD	0.02524	1.808313		0.090954		0.788172		0.921236		0.024453		0.249902	
	Min	0	0.305028		0.001928		0.181835		0.188389		0.000496		0.08376	
EDP 3	Mean	9.270917	15.28113	-	8.073332	+	8.083307	+	7.679697	+	8.439455	+	7.856498	+
	STD	0.965716	1.926882		0.73204		1.632231		0.722782		0.859655		0.727986	
	Min	7.230597	10.88882		6.724864		5.343269		6.516999		6.744559		6.834565	
EDP 4	Mean	185995.7	364033.9	-	330406.6	-	312145.4	-	440951.4	-	294543.9	-	358443.5	-
	STD	243205.8	42013.93		105893.4		53306.62		71830.16		32082.11		77060.09	
	Min	23204.12	279729.4		252141.2		240073.3		322518.2		244370.5		252927.9	
Win			0		1		1		1		1		1	
Tie			0		0		0		0		1		0	
Lose			4		3		3		3		2		3	

As apparent, the proposed MOADEO algorithm obtained the best results for the EDP1 and EDP4, and obtained similar values in the remaining EDPs winning MOA value.

The proposed MOADEO algorithm won 4, 3, 3, 3, 2, and 3 times, respectively, while only losing a maximum of one time to the MOAs selected from the literature. Therefore, the proposed MOADEO algorithm shows a good divergence behavior of the set of optimal solutions, displaying a very evenly spread of optimal solutions in the Pareto Front.

Furthermore, Figure 4.6 exhibits a qualitative and quantitative evaluation of the results presented in Table 4.5. For each EDP, two figures are displayed in similar way with simulation results in 4.1.3: the figures on the left present the true Pareto Front and the Pareto Front of each MOA correspondent to the best SP value (best divergence result), in the given EDP; the figures on the right show the boxplot of the SP results (presented in Table 4.5), for each MOA, exhibiting the minimum, maximum, mean, the percentiles and median value of the results of the 30 repetitions executed, in each EDP. As apparent, the MOAs with a better minimum value present more disperse and coherent Pareto Fronts, with better divergences, whereas MOAs with higher SP minimum values present more inconsistent Pareto Fronts.

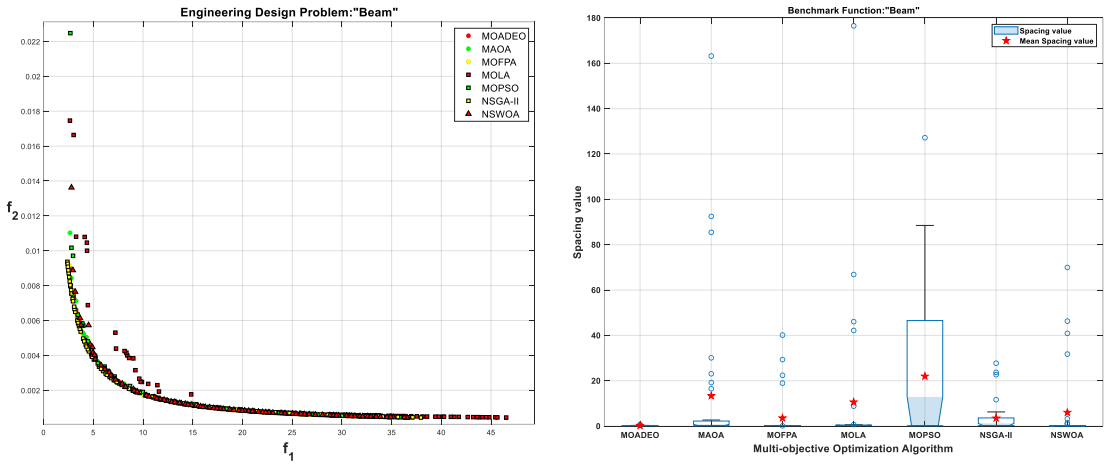

a) Results obtained on the welded beam design problem.

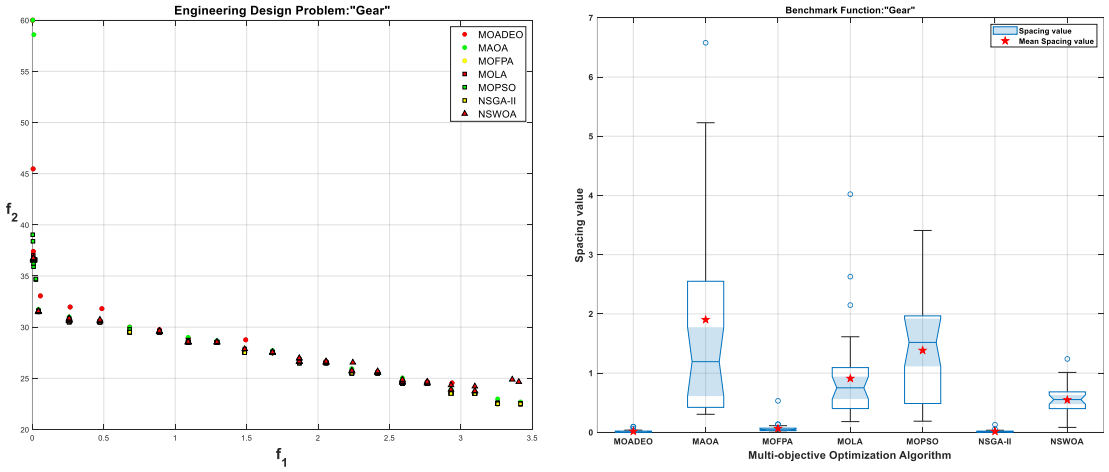

b) Results obtained on the gear train design problem.

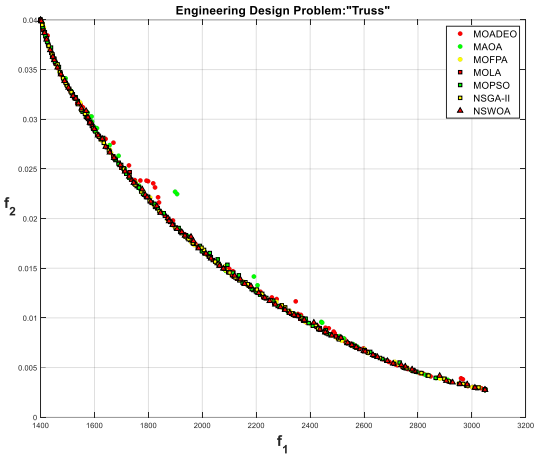

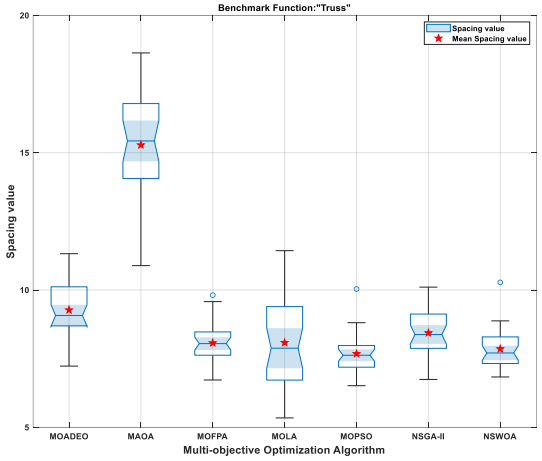

c) Results obtained on the four-bar truss design problem.

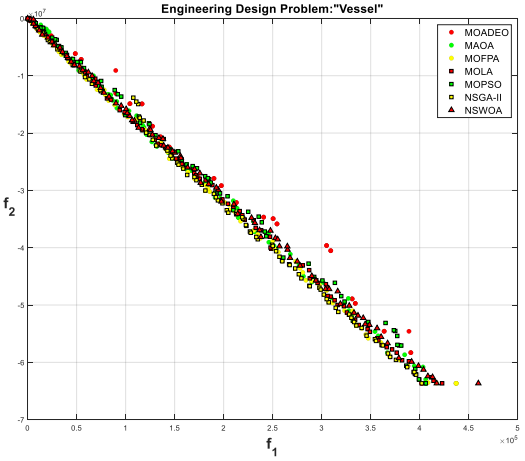

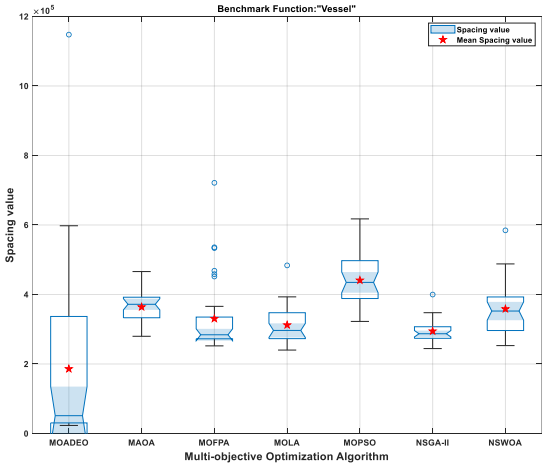

d) Results obtained on the pressure vessel design problem.

Figure 4.6 - Results of the simulation obtained by each MOA, on the 4 EDPs, for the SP performance metric.

CHAPTER 5

Optimal Sizing of the Renewable Energy Community

This chapter initially presents the optimization strategy implemented, regardless of the number of participants of a REC, outlining the required variables relative to the optimization problem. Afterward, an evaluation and performance analysis is conducted in a chosen renewable energy community design, simulated with real dataset profiles, and subsequently, displaying the results obtained from the implemented multi-objective optimization algorithm, for each scenario.

5.1 Optimization Strategy

The optimization technique implemented in this paper combines the specificities of the Multi-Objective Particle Swarm Optimization (MOPSO) algorithm with the use of multiple swarms that cooperate and share information and lived experiences (history) to achieve a set of high-quality solutions. The use of multiple swarms constructs a greater diversity of new solutions and explores the multidimensional search space with greater independence and efficiency. Moreover, the optimization technique used divides the multidimensional search space into smaller subspaces, providing greater independence in the construction of new solutions (exploration of the search space) and minimizing the problem of premature convergence. The number of subspaces and the number of swarms depend on the number of participants in the REC. Each swarm acts in its corresponding subspace, optimizing the sizing of the various energy production and energy storage units inherent to each participant of the REC ($N_{PV_p}, N_{WT_p}, C_{bat_p}$) cooperatively and collaboratively. The multiple swarms use the broadcast strategy to share information and lived experiences (history) with each other, i.e., the social component of each swarm ($gbest$) is transmitted and shared with all the other swarms.

5.1.1 Proposed Optimization Procedure

Figure 5.1 presents the flowchart of the implemented optimization procedure in this paper for an REC with n participants. Initially, all the variables relative to the

optimization problem and all the required variables for the correct use of the MOPSO optimization algorithm are initialized, such as the number of participants in the REC (n); the meteorological variables (temperature, irradiance, wind speed); the load profiles of each participant of the REC; the dimension of the optimization problem (d), the lower (lb) and upper (ub) bounds; the number of particles in the population (np); the maximum capacity of the repository of nondominant solutions; and the number of maximum iterations allowed (k_{max}), among others.

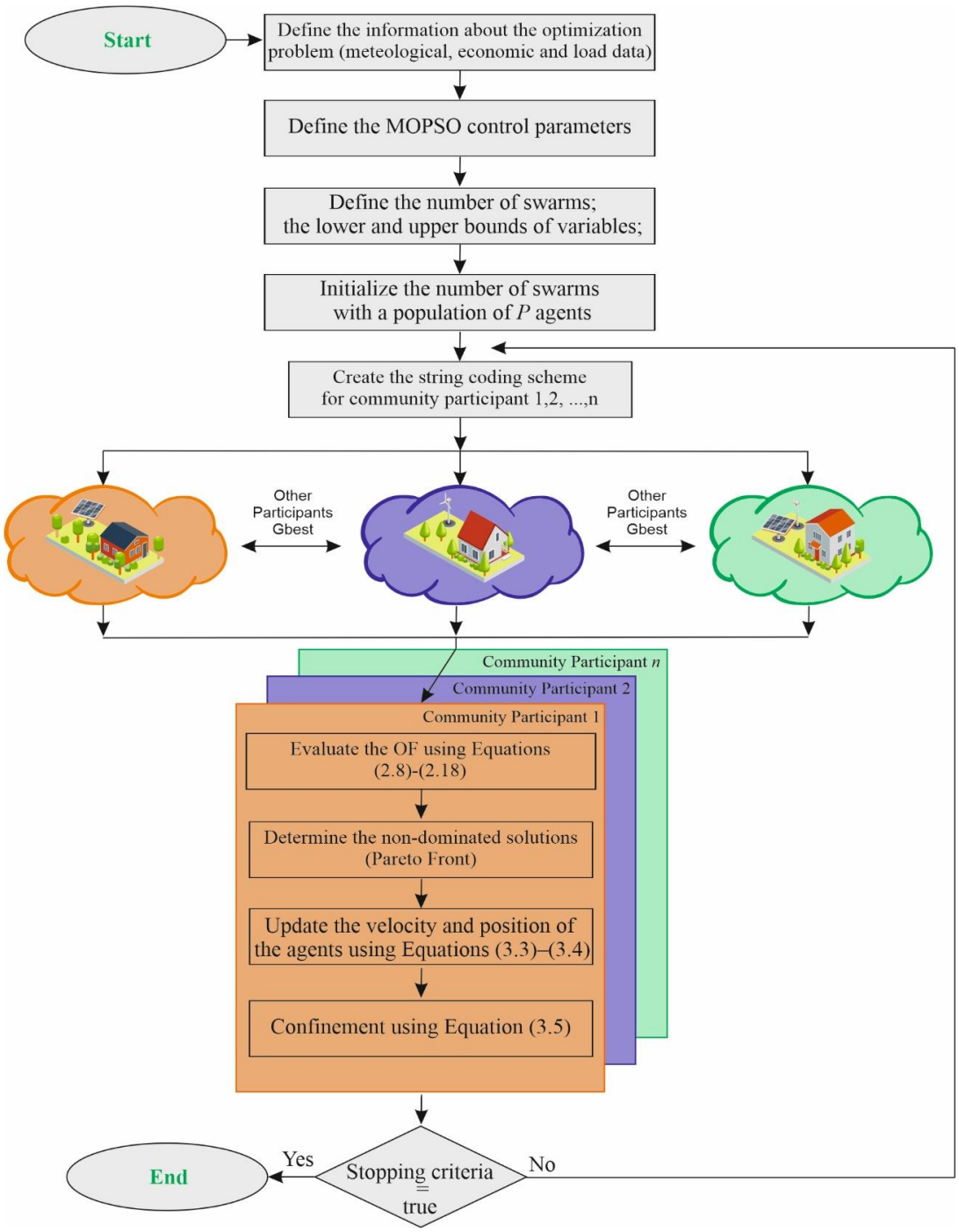

Figure 5.1 - Optimization Strategy Diagram.

After these initializations, the initial positioning of the particles is determined with structure of Equation (5.1):

$$x_i = \overbrace{\underbrace{N_{PV_1}, N_{WT_1}, C_{bat_1}}_{swarm\ 1}, \underbrace{N_{PV_2}, N_{WT_2}, C_{bat_2}}_{swarm\ 2}, \underbrace{N_{PV_3}, N_{WT_3}, C_{bat_3}}_{swarm\ 3}, \dots, \underbrace{N_{PV_n}, N_{WT_n}, C_{bat_n}}_{swarm\ n}}^{Multidimensional\ Search\ Space} \quad (5.1)$$

A random initial position is determined within the multidimensional search space (defined in Equation (2.15)), considering a population of 15 individuals per dimension and a maximum number of allowed interactions (100 iterations per dimension). The population of particles is divided into several swarms with a star topology, i.e., in each swarm, all particles communicate with each other. The various swarms evolve and move independently, while maintaining their own repository of nondominated solutions.

In each iteration, the performance of each particle regarding each swarm was determined using the economic and technical criteria detailed in Section 2.2.2 (Equations (2.8)–(2.18)). However, to evaluate the performance of each particle, a string code scheme was constructed by broadcasting the social component of each swarm (*gbest1,2, 3, …, n*), where n is the number of participants in the REC, as described in Equation (5.2):

$$x_i = \overbrace{N_{PV_1}, N_{WT_1}, C_{bat_1}, gbest_2, gbest_3, \dots, gbest_n}^{Particle\ Position\ for\ swarm_1} \quad (5.2)$$

Subsequently, a repository control mechanism evaluated the individual and collective performance of each particle and, consequently, determined the nondominant solutions inherent to each swarm. As aforementioned, the movement of each particle was determined by Equations (3.3) and (3.4). However, to prevent a new position of the particles outside the multidimensional search space, during the successive iterations, the confinement strategy described by Equation (3.5) was implemented. In this strategy, if any of the limits (lower or upper limit) were exceeded, the particle movement was modified ensuring that the new position was within the search space.

The execution of the various swarms, i.e., the various MOPSO optimization algorithms, ended when the established stopping criterion was reached. The established stopping criterion was within the maximum number of allowed interactions (100 iterations per dimension). Once the optimization process was completed, i.e., when the stopping criterion was reached, an external repository was created with all the

nondominated solutions determined by the various swarms. Through this external repository, a nondominated solution (Final Trade-Off Solution) was selected based on the fuzzy set membership function [165], [166].

5.2 Results Discussion and Analysis

In this section, an evaluation and performance analysis is conducted based on the results obtained from the implemented multi-objective optimization algorithm for each scenario. Firstly, the characteristics of the simulated renewable energy community and the corresponding data profiles will be presented and analyzed. Lastly, all the optimized scenarios obtained from the application of the implemented multi-objective optimization algorithm will be evaluated, discussed, and compared.

5.2.1 Renewable Energy Community

The community under study represents a microcosm of sustainable energy production and consumption, comprising three participants, denoted as (a), (b), and (c) in Figure 5.2. This configuration enables a comprehensive analysis of the interactions and dynamics among participants utilizing different energy sources. Each of the three participants in the community can produce, consume, and potentially store renewable energy under the four energy management scenarios described in Section 2.2.1.

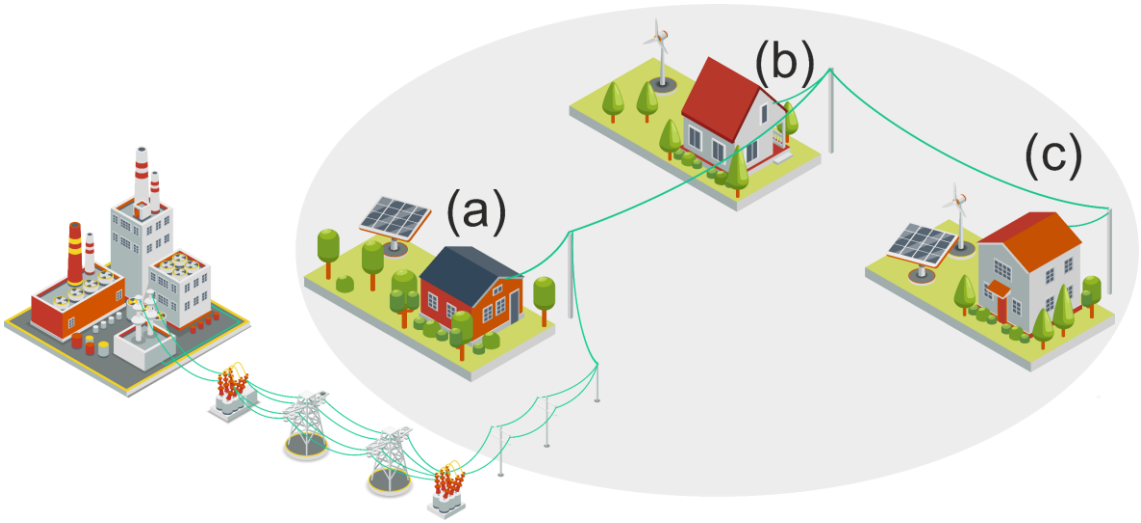

Figure 5.2 - Renewable Energy Community Architecture.

Additionally, when the community's load demand exceeded the local renewable energy production capacity, participants could import additional energy from the electrical grid. This interaction with the grid provides several advantages for the renewable energy community. First, it ensures a reliable power supply, particularly during periods of low renewable energy production or high load demand. Second, it

allows for the integration of intermittent renewable energy sources with the grid's baseload power, ensuring a continuous and stable energy supply. Third, the grid connection enables the community to participate in feed-in tariff programs, incentivizing the production and export of excess renewable energy.

5.2.1.1 Mathematical Models Parameters

This subsection presents a comprehensive overview of the key mathematical model's parameters used in the simulations. These parameters encompass the characteristics of the batteries, PV, and wind turbine models.

Batteries Model Parameters

To accurately replicate the dynamic behavior of a battery within an energy community, it is necessary to adjust certain model parameters values. These parameters enable the model to mimic nuances and interactions that batteries exhibit when integrated into the energy systems of real-world communities, allowing for a more precise representation of their performance [78], [90]. Table 5.1 presents the battery model parameters values used in the simulation.

Table 5.1 - Batteries Model Parameters and Values.

Battery Model Parameter	Value
k_{bat}	0.38
c	0.271

Photovoltaic Model Parameters

The photovoltaic module selected for simulation purposes was the Sharp ND-R250A5, characterized by 60 polycrystalline silicon cells (with 156.5 mm × 156.5 mm) connected in series, divided into three strings, with each string protected by a bypass diode, i.e., a bypass diode for every 20 cells in the PV module [167]. The specifications of the selected PV module are displayed in Table 5.2.

Table 5.2 - Photovoltaic Model Parameters and Values.

PV Model Parameter	Value
μ_{mppt}	95%

P_{STC}	250 W
G_{STC}	1000 Wm^{-2}
α_{VOC}	−0.0044 V $°C^{-1}$
T_{STC}	25 °C
G_{NOCT}	800 Wm^{-2}
$NOCT$	47.5 °C
T_{NOCT}	20 °C

Wind Turbine Generator

The selected wind turbine generator was the Bergey BWC XL-1, a 1 kW three-bladed wind turbine, with horizontal axis and a 2.5 m rotor diameter. It shows remarkable low-wind-speed performances, with intended applications for charging batteries and supply electrical loads in remote power systems or rural electrification programs. The corresponding power curve is displayed in Figure 5.3.

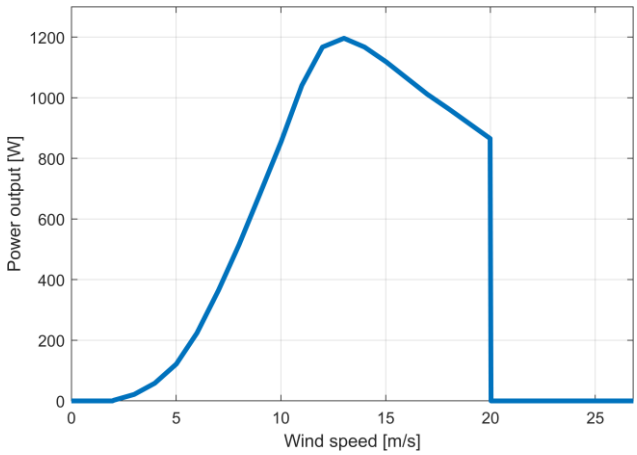

Figure 5.3 - Power curve of the Bergey BWC XL-1 Wind Turbine.

To complete the wind component modeling, the power law exponent (α_{Wind}) must be addressed for the simulation site characteristics. The power law exponent or friction coefficient value depends on numerous factors like terrain roughness, altitude, exposed site level, temperature, and season of site [168]. The value normally used for this parameter in open land areas is 0.142 [169]. However, this value does not take into consideration various terrain roughness characteristics and atmospheric stability classes, leading to large discrepancies in wind speed value prediction and huge errors in energy estimation [170]. Given this fact, the value chosen for this parameter was 0.4, a fair value considering a location with high surface roughness, with a high stability atmosphere [170], [171], [172].

The parameters provided by the manufacturer of the selected wind turbine generator, as well as the power law exponent and the remaining model parameters required to complete the formulation i.e. the hub heights chosen, and the corresponding values, are displayed in Table 5.3.

Table 5.3 - Wind Turbine Model Parameters and Values.

Wind Turbine Model Parameter	Value
Rated Power	1.000 W
Maximum output power	1.200 W
Rated wind speed	11.0 m/s
Cut-in wind speed	2.5 m/s
Furling wind speed	13.0 m/s
Cut-out wind speed	20.0 m/s
h_h	20 m
h_a	10 m
α_{Wind}	0.4

5.2.1.2 Economic Parameters

In order to quote the LCOE ratio and rate the economic criteria in the simulation, 2 economic parameters must be quantified, and are shown in Table 5.4: the nominal interest rate (int) and the project lifetime (N).

Table 5.4 - Economic Criteria Parameters and Values.

Parameter	Value
Nominal interest rate (int) [%]	0.05
Project lifetime (N) [years]	20

5.2.2 Data Profiles

The data profiles used in this paper were obtained from the U.S. Department of Energy's (DOE) Open Energy Data Initiative (OEDI) [173], a large and centralized repository of datasets containing weather data of all the Typical Meteorological Year version 3 (TMY3) locations, as well as dataset simulations of the residential and commercial prototype model load profiles for these locations. TMY3 is the most recent version of the Typical Meteorological Year (TMY), a group of selected weather data measured in more than a thousand different locations across the US for at least 15 years

[174], fused and shortened into a single year, representing hypothetically typical weather data in each different location, with one year of values with one-hour resolution (8760 h time series data) based on real-life values.

Load data: Three different location datasets were selected from the TMY3 residential load datasets with different time-series statistical values and shape profiles.

Weather data: The weather data profiles were made by scaling the TMY3 weather data of one of the locations (base location), proportionally to the other two locations, including a ± 20% deviation to induce additional variability [175]. These weather datasets contain multiple parameters, three of which are required to simulate the energy community using the mathematical models described in Section 2.1: air temperature, solar irradiance, and wind speed.

Box and whisker diagrams were used to visualize and understand in greater detail the dataset profiles used to simulate the REC. The dataset profiles for each REC participant are presented with two different resolutions: hourly and monthly. Thus, one can visualize the behavior and evolution of each dataset profile during the 24 h of the day, but also visualize throughout the 12 months of the year. Figure 5.4 shows the hourly resolution box and whisker diagrams of the three load data profiles: Load 1 in diagram (a), Load 2 in diagram (b), and Load 3 in diagram (c); and the three weather data variables of the base location (simulation location of load 2): air temperature in diagram (d), irradiance in diagram (e), and wind speed in diagram (f). Figure 5.5 shows the same datasets but in a monthly resolution box and whisker diagrams, with the same disposition and identification.

Table 5.5 presents the time-series statistical analysis for each dataset profile, including the mean, median, standard deviation, and statistics related to the shape of the dataset profiles, such as skewness and kurtosis. As can be seen, load profiles 1 and 2 exhibited very similar mean values. However, they differed significantly in terms of their standard deviation: Load Profile 1 had a high standard deviation of 66%, while Load Profile 2 had a standard deviation of only 42%. Moreover, these two load profiles displayed distinct skewness values: Load Profile 1 had a positively skewed distribution, while Load Profile 2 showed an approximately symmetric distribution. On the other hand, Load Profile 3 featured a lower mean and median values, with a lower standard deviation compared to the other two loads, as intended.

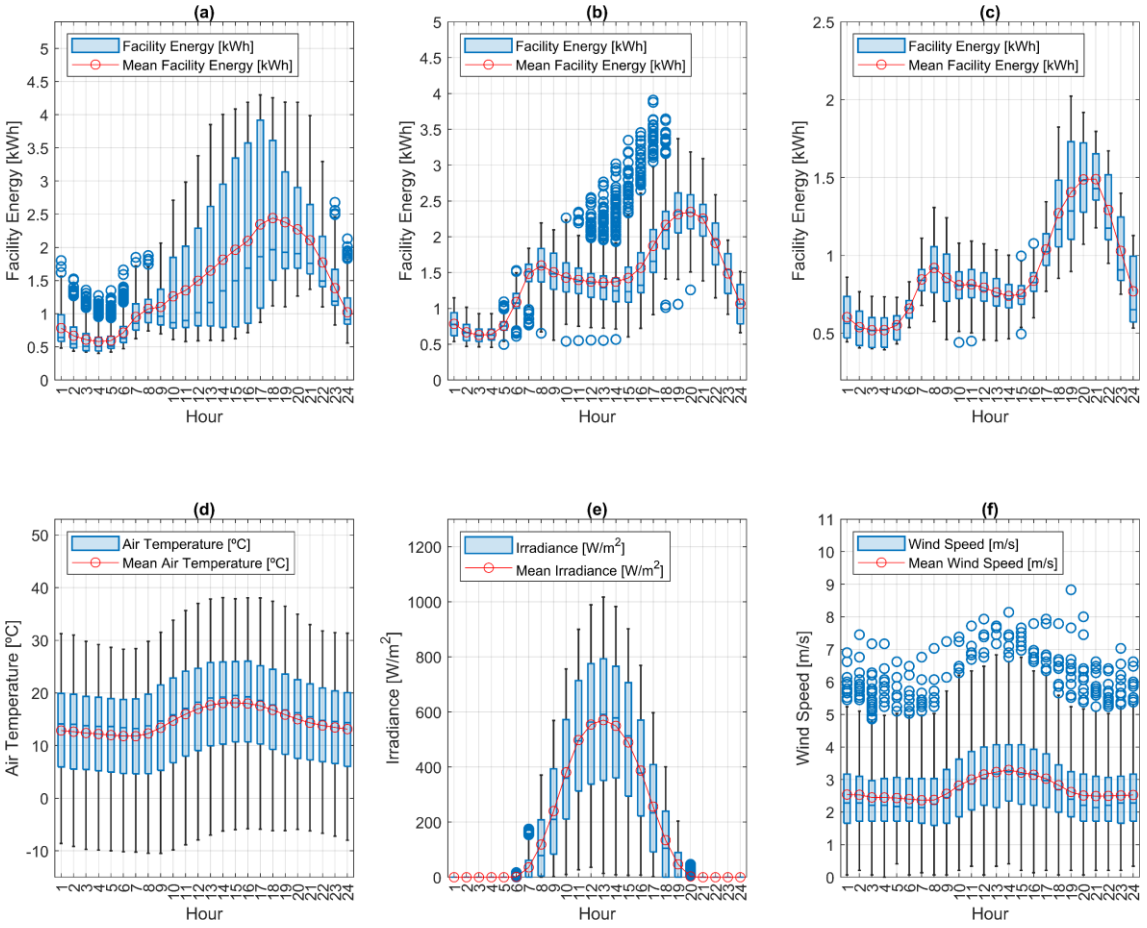

Figure 5.4 - Box-and-whisker diagrams with an hourly resolution for each dataset profile. (a) Participant a). (b) Participant b). (c) Participant c). (d) Air temperature. (e) Solar Irradiance. (f) Wind speed.

However, its shape metrics were similar to Load Profile 1. The air temperature revealed a very symmetric shape distribution, also demonstrated by the proximity between the mean and median values, despite a high standard deviation value. Inevitably, the irradiance showed very dispersed values, demonstrated by the high value of standard deviation in contrast with the null median value.

Table 5.6 provides detailed information on the maximum and minimum values of each dataset profile, including the corresponding month, day, and hour when these values occurred. As expected, the maximum energy demand of the load profiles occurred during the evening, and the minimum energy demand of the load profiles happened during the night. Similarly, the air temperature showed expected results, registering the highest temperature during the afternoon of summer times, in harmony with the irradiance, and reaching the minimum air temperature value in the winter.

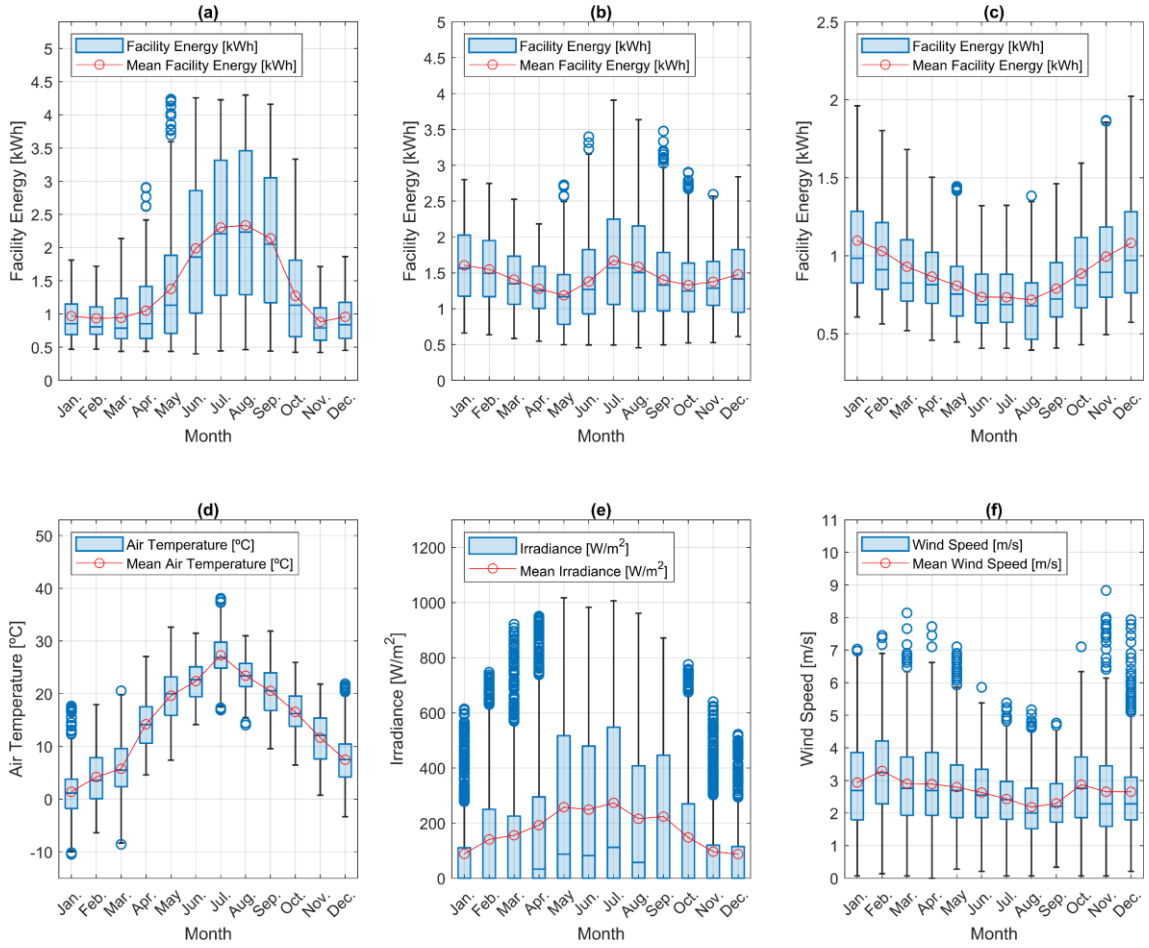

Figure 5.5 - Box-and-whisker diagrams with a monthly resolution for each dataset profile. (a) Participant a). (b) Participant b). (c) Participant c). (d) Air temperature. (e) Solar Irradiance. (f) Wind speed.

Table 5.5 - Time-Series Analysis of Dataset Profiles: Statistical Values.

Parameter	**Mean**	**Median**	**St. Dev.**	**Skewness**	**Kurtosis**
Load 1 [kWh]	1.4347	1.0874	0.95063	1.2517	3.6939
Load 2 [kWh]	1.4373	1.3567	0.60812	0.56598	2.849
Load 3 [kWh]	0.88781	0.80909	0.33569	0.99622	3.5528
Air Temperature [°C]	14.6192	15.4	9.306	−0.20139	2.1832
Irradiance [Wm^{-2}]	177.8128	0	261.7154	1.3709	3.6711
Wind Speed [ms^{-1}]	2.7075	2.48	1.2744	0.80935	3.7417

Table 5.6 - Time-Series Analysis of Dataset Profiles: Maximum and Minimum Values and Corresponding Dates.

Parameter	Max.	Hour of the Day	Month of the Year	Min.	Hour of the Day	Month of the Year
Load 1 [kWh]	4.2977	17	8 (Aug.)	0.40097	4	6 (Jun.)
Load 2 [kWh]	3.9086	17	7 (Jul.)	0.45593	4	8 (Aug.)
Load 3 [kWh]	2.0233	19	12 (Dec.)	0.39432	4	8 (Aug.)
Air Temperature [°C]	38.09	14	7 (Jul.)	−10.46	9	1 (Jan.)
Irradiance [Wm^{-2}]	1017	13	5 (May)	0	*	*
Wind Speed [ms^{-1}]	8.83	19	11 (Nov.)	0	*	*

* Multiple results.

Finally, Table 5.7 details the highest and lowest mean dataset values of each profile, with the respective hour and month they occurred. In the hour resolution diagrams, all load profiles show a similar shape with a slight peak during early morning hours and reaching daily peaks during the end of the evening/beginning of the night. Monthly, all the load profiles have completely different behaviors: Load Profile 1 had a substantial increase in values during the summer months, while Load Profile 3 displayed the opposite scenario, and Load Profile 2 had no significant changes during the months of the year.

Table 5.7 - Time-Series Analysis of Dataset Profiles: Mean value details of each dataset profile.

		Hourly Resolution Profiles		Monthly Resolution Profiles	
Parameter	**Evaluation**	**Value**	**Hour**	**Value**	**Month**
Load 1 [kWh]	Highest mean value	2.4427	18	2.3372	8 (Aug.)
	Lowest mean value	0.58	4	0.88195	11 (Nov.)
Load 2 [kWh]	Highest mean value	2.3471	20	1.6732	7 (Jul.)
	Lowest mean value	0.6279	3	1.1867	5 (May)
Load 3 [kWh]	Highest mean value	1.4899	21	1.0971	1 (Jan.)
	Lowest mean value	0.51981	3	0.7179	8 (Aug.)
Air Temperature [°C]	Highest mean value	18.1138	15	27.3003	7 (Jul.)
	Lowest mean value	11.787	7	1.3899	1 (Jan.)
Irradiance [Wm^{-2}]	Highest mean value	570.8571	13	273.5148	7 (Jul.)
	Lowest mean value	0	*	87.5972	12 (Dec.)
Wind Speed [ms^{-1}]	Highest mean value	3.2959	14	3.2932	2 (Feb.)
	Lowest mean value	2.3648	7	2.1831	8 (Aug.)

* Multiple results.

Relative to the air temperature data profile, as expected, the temperature rose with sun exposure, but with very little variation, increasing hourly after sunrise and dropping during the evening, and throughout the night. Monthly, the temperature increased gradually until the summer months and decreased substantially during the autumn and winter months. The hour of the day with the highest mean air temperature was the 15th hour (18.1138 ℃), while the hour with the lowest mean air temperature (11.787 ℃) was the 7th hour. The month of July had the highest mean air temperature (27.3003 ℃), while January had the lowest mean air temperature (1.3899 ℃).

Regarding solar irradiance, the location is not very privileged, reaching the monthly highest mean value (273.5148 Wm^{-2}) in the month of June and the lowest monthly mean irradiance (87.5972 Wm^{-2}) in December. The hour with the highest mean irradiance (570.8571 Wm^{-2}) was the 13th hour of the day.

The wind speed at the location was relatively slow and revealed consistent wind speeds throughout the day and the year, with the highest monthly mean value (3.2932 ms^{-1}) in February, approximately the same as the highest hourly mean value, while the lowest monthly mean value (2.1831 ms^{-1}) was in August.

5.2.3 Performance Evaluation and Results Discussion

This section presents and analyzes the results obtained with the implemented multi-objective optimization algorithm discussed in the previous sections. To ensure the reliability of the results, the implemented optimization algorithm underwent 15 simulations. Figure 5.6 provides a representation of the statistical distribution and variability of the objective functions' fitness values.

As can be seen, Scenario 1 presents a low standard deviation for LCOE, indicating relatively consistent operational costs. The mean LCOE value is 0.0609, while the median LCOE is slightly lower at 0.0604. The SSR and SCR present relatively high mean values, with 0.8154 and 0.6676 respectively. In Scenario 2, the LCOE exhibits a higher mean value of 0.0435 and a slightly higher median value of 0.0429. The SSR and SCR values are also valuable, with SSR at 0.6805 and SCR at 0.6451. This suggests that, despite higher operational costs, the community maintains a high degree of self-sufficiency and self-consumption.

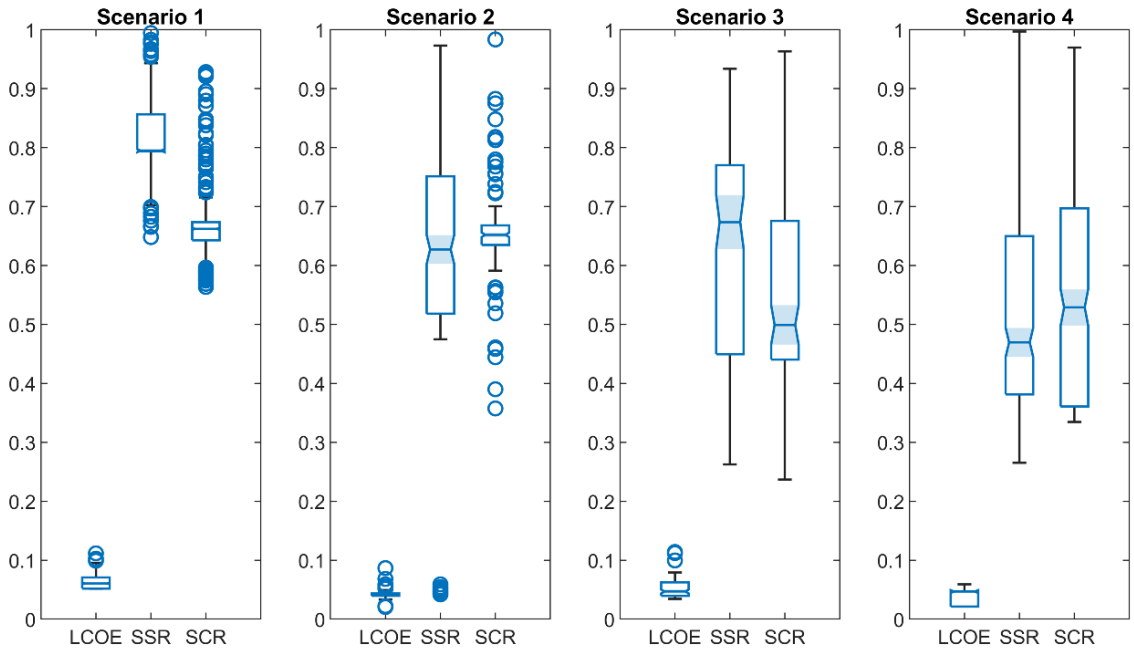

Figure 5.6 - Statistical distribution of the objective functions' fitness values.

Scenario 3 presents the highest LCOE among the scenarios, with a mean value of 0.0523 and a median of 0.0468. The SSR and SCR values are lower in this scenario, indicating a focus on community independence over cost-efficiency. Lastly, Scenario 4 demonstrates a lower mean LCOE of 0.0371 and a median of 0.0468, making it the most cost-effective scenario. The SSR and SCR values are also advantageous, with SSR at 0.5082 and SCR at 0.5524, suggesting a balanced approach between cost efficiency and community independence.

Table 5.8 displays the sizing ratio for each participant's optimal battery capacity and the optimal installed renewable capacity in each scenario. This ratio is calculated by dividing the installed capacity of the storage systems or the renewable energy sources for each participant by their load's maximum value. This ratio ensures a more reliable assessment of each element's optimal sizing within the renewable energy community.

In the following subsections, the performance analysis of each scenario is discussed, considering the optimal sizing of each element within the renewable energy community. This analysis provides a comprehensive understanding of the strengths and weaknesses of each scenario, aiding in the selection of the most suitable approach for a sustainable and efficient renewable energy community.

Table 5.8 - Sizing Ratio for Renewable Energy Community Scenarios.

	Participant 1		Participant 2		Participant 3	
Scenarios	**Storage Systems Ratio**	**Renewable Energy Systems Ratio**	**Storage Systems Ratio**	**Renewable Energy Systems Ratio**	**Storage Systems Ratio**	**Renewable Energy Systems Ratio**
Scenario 1	7.9079	2.5955	4.8611	1.9828	3.7229	2.1523
Scenario 2	6.4251	1.4827	1.7909	2.6864	2.3268	2.0941
Scenario 3	2.4712	0.7426	2.0468	2.3666	2.3268	2.0941
Scenario 4	0.9885	2.2241	0.7675	2.0468	2.5595	2.9085

5.2.3.1 Scenario 1

This scenario provides a baseline comparison for the other scenarios where each participant adopts an individualist position within the community. Scenario 1 resembles a conventional microgrid where there are no energy transactions between the participants. Participants rely on their own individual renewable production and batteries to meet their load demand, exchanging required or surplus energy only with the electrical grid. Figure 5.7 shows the hourly average values of PV production, battery discharge and charge, imported and exported energy from/to the grid, and the average load of each participant. These diagrams offer a concise visual representation of the energy dynamics and transactions of the community, allowing for a comprehensive understanding of the participants' renewable production, battery usage, grid interaction, and overall energy flow throughout the course of a typical day.

In this scenario, the energy storage systems are exclusively used for individual energy storage, with no coordination or collaboration among community participants to maximize the community's energy independence. As indicated in Table 5.8, all participants exhibit a similar renewable production ratio of approximately two. However, they present considerable differences in their Storage Systems Ratio.

As Figure 5.7 illustrates, this lack of energy-sharing mechanisms within the community result in surplus energy being exported to the electrical grid without benefiting other REC members. Consequently, most of the available renewable energy in the RECs is exported to the main grid.

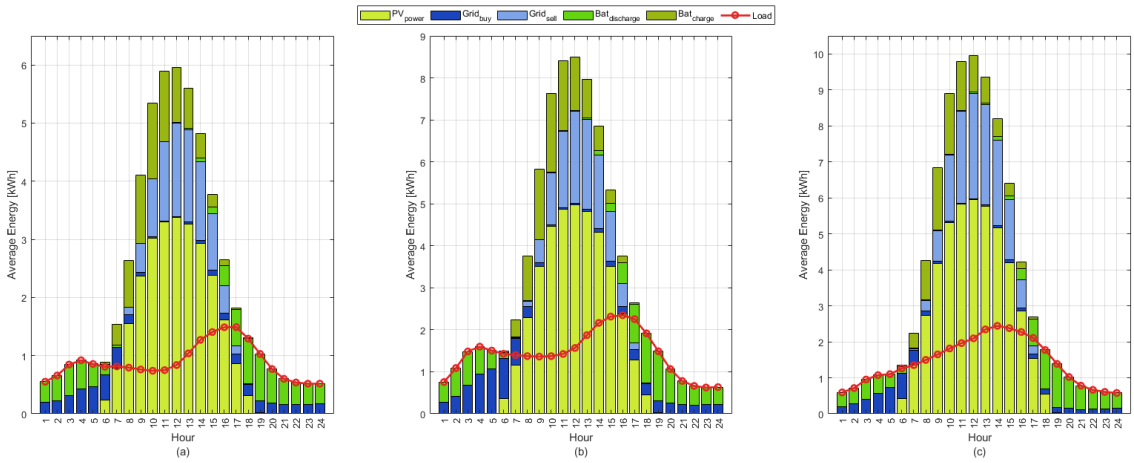

Figure 5.7 - Scenario 1: hourly energy contributions. (a) Participant a). (b) Participant b). (c). Participant c).

Importantly, all participants rely solely on solar energy production systems, with each participant achieving their maximum PV production at 12:00 PM: Participant (a) achieved a maximum PV production of 5.82 kWh, Participant (b) reached 8.34 kWh, and Participant (c) achieved 10.26 kWh. Therefore, during periods of low solar irradiation, the community becomes dependent on the electrical grid to supply its load demand. Similarly, when renewable energy production is insufficient to satisfy the participant's load demand and the energy storage systems present a reduced SOC, the community relies exclusively on the electrical grid for energy supply. On average, each participant imports 0.19 kWh of energy from the electrical grid per hour to satisfy their demand. This reliance is evident in the increased energy importation from the grid throughout the night hours. As a result, the use of the energy storage systems during these hours decreases in correlation with the respective SOC levels.

To perform a broader analysis of the community operation in Scenario 1, Figure 5.8 depicts a diagram that illustrates the monthly cumulative energy values of PV production, energy storage systems, imported and exported energy from/to the grid, and the load for all the community's participants. This diagram provides a comprehensive overview of the community's energy dynamics over the course of a year. By showcasing the cumulative values, this analysis allows a macro-level understanding of the participants' renewable energy production, storage, grid interaction, and overall energy consumption patterns over the year.

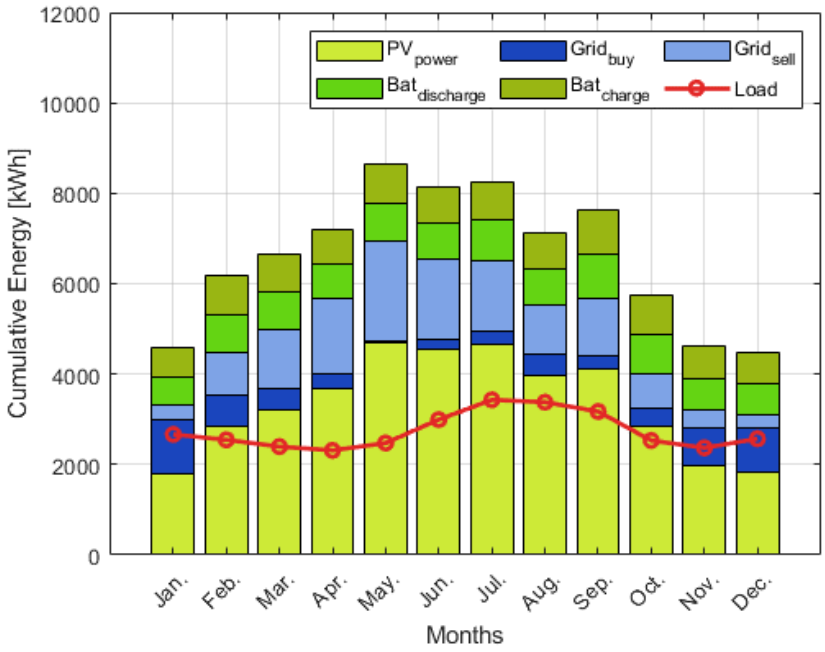

Figure 5.8 - Scenario 1: monthly energy contributions.

As seen in Figure 5.8, the community's overall PV production varies in solar energy production throughout the year, reaching maximum production in May and a mean monthly production of 4677.43 kWh.

During the summer months, there is a significant rise in load demand, which decreases during the spring and autumn months. However, there is a slight increase in load demand during the peak winter months (November, December, and January). Notably, during these months, the total renewable production cannot satisfy the REC's total load demand. As a result, there is a substantial increase in energy importation from the electrical grid, surpassing the amount of exported energy. Conversely, in other months, particularly during the spring and summer, renewable production greatly exceeds the load demand. This creates an evident disparity in energy flow, with higher energy exportation to the grid.

The energy storage systems usage remains relatively consistent throughout the year, which indicates a consistent reliance on the energy storage systems to meet the community's load demand regardless of seasonal variations in load demand and renewable production.

5.2.3.2 Scenario 2

In contrast to the individualist position in Scenario 1, where participants rely solely on their renewable production and batteries, Scenario 2 promotes a collaborative approach. In this scenario, participants prioritize meeting their load demand, and any surplus or deficit power is exchanged among other participants within the community. This enables efficient utilization of available energy resources within the community and reduces reliance on the electrical grid. As Table 5.8 suggests, in this scenario, participant (a) has a storage system ratio much higher than the other participants but, however, presents a lower renewable production ratio. As for participants (b) and (c), they present very similar ratios in terms of production and storage. Figure 5.9 presents the hourly average values for each participant in Scenario 2.

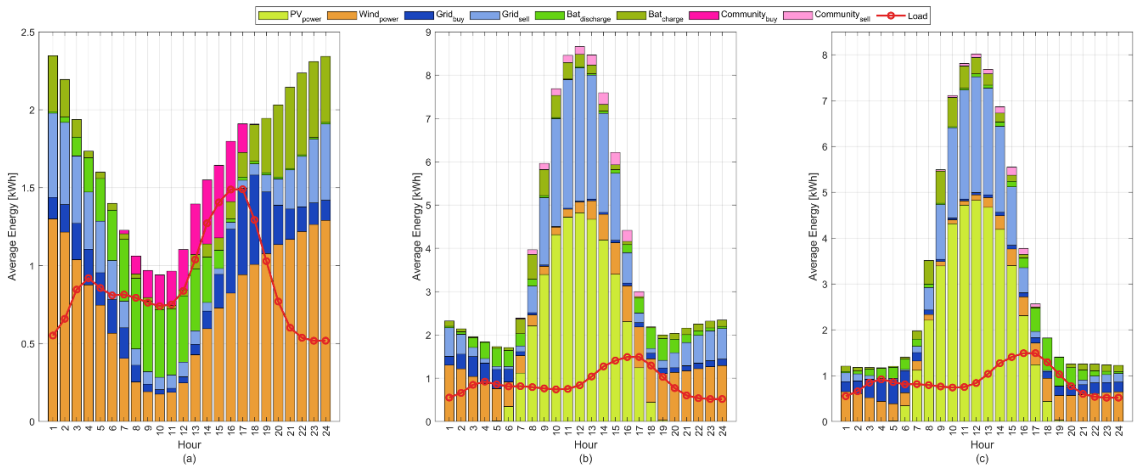

Figure 5.9 - Scenario 2: hourly energy contributions. (a) Participant a). (b) Participant b). (c). Participant c).

As depicted in Figure 5.9, Participant (a) exhibits a notable load demand during the day. To meet this demand, Participant (a) relies on the electrical grid, individual energy storage systems, or intra-community energy transactions with other participants, especially during the afternoon. These transactions become necessary during hours of low wind energy production, when the capacity of the individual storage systems is insufficient to meet the load demand and other participants have surplus energy due to high PV production. Although only two participants had solar production systems, this type of production significantly contributed to the community's renewable energy supply, producing, on average, approximately 1.03 kWh of electricity per hour. Conversely, Participant (a) benefits from significant surplus energy during the night due

to the wind energy production systems. This surplus energy facilitates the charging of Participant (a)'s energy storage systems, thereby reducing the reliance on other transactions. In contrast, Participant (b) experiences significant energy surpluses during hours of high solar irradiation, due to the PV production systems. This surplus energy is mainly used to charge the energy storage systems and fulfill the load demand of other participants. Additionally, Participant (b) typically experiences an energy production surplus throughout the entire day, benefiting from the advantageous complementarity between PV and wind production. Consequently, Participant (b) became the community's top exporter, with an hourly average intra-community transaction of 0.081 kWh and an average energy sale to the electrical grid of 0.96 kWh per hour. Figure 5.10 depicts the monthly cumulative energy contributions that resume the RES operation in Scenario 2.

As shown in Figure 5.10, grid interactions exhibit a significant pattern throughout the year. Initially, during the early months, grid interactions are primarily characterized by energy exportation to the electrical grid, indicating a surplus of energy within the community. However, as we transition into the summer months, the balance shifts and grid interactions predominantly involve energy importations. This shift can be attributed to the reduced production of wind power during this period, resulting in a deficit of renewable production to meet the total load demand.

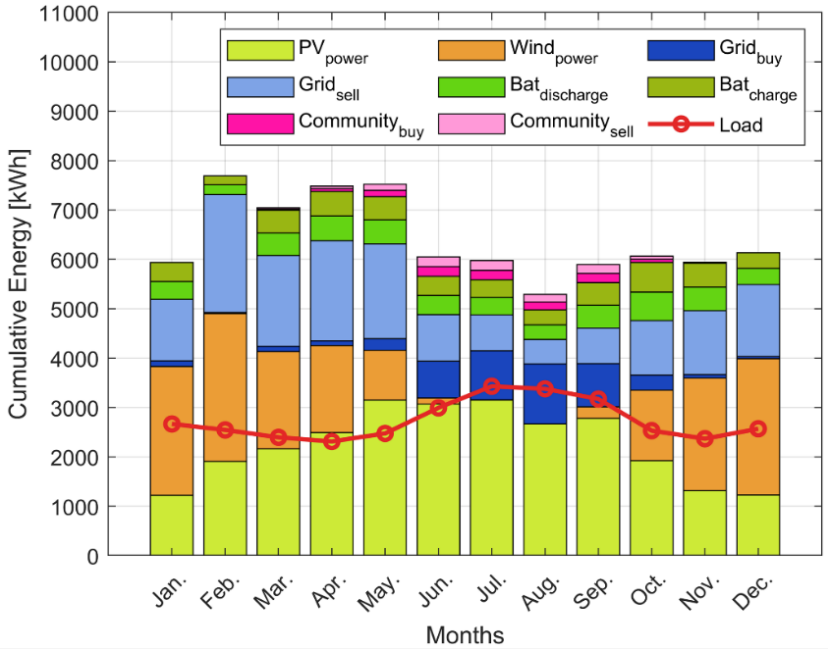

Figure 5.10 - Scenario 2: monthly energy contributions.

5.2.3.3 Scenario 3

In Scenario 3, community participants share their surplus renewable energy directly to fulfill the load demand of other participants before relying on their batteries for charging. This collaborative approach ensures an efficient utilization of excess renewable energy to effectively supply the energy needs of the community, reducing the utilization of the individual storage systems and, therefore, improving their lifespan. As can be seen in Table 5.8, both participants have similar installed capacity ratio, but, on the other hand, participant (a) present a distinct renewable production ratio when compared to the other participants. Figure 5.11 illustrates the hourly average energy for each participant in Scenario 3.

As can be observed in Figure 5.11, Participant (a) exhibits a distinct load demand pattern, particularly during daylight hours, when there is a decrease in energy consumption. To supply its energy needs during daylight hours, Participant (a) mostly relies on intra-community energy exchanges and grid importation. On average, Participant (a) imports 0.255 kWh of electricity per hour from the community and 0.253 kWh from the grid, reflecting its low renewable energy production during daylight hours. In contrast, Participants (b) and (c) demonstrate significant surplus renewable generation, primarily due to their PV generation systems. During the night hours, both Participant (a) and Participant (b) experience a substantial surplus in wind energy production. Figure 5.12 illustrates a monthly cumulative energy diagram for Scenario 3.

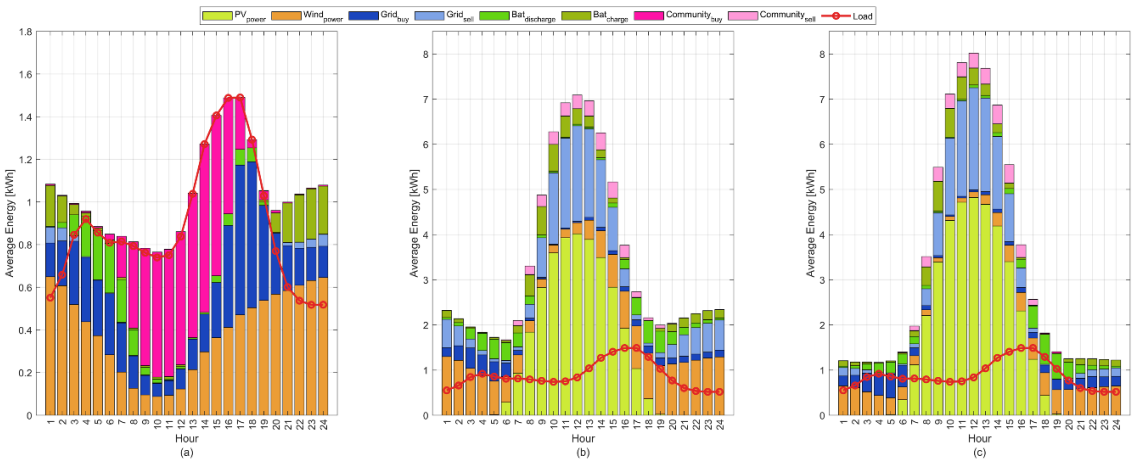

Figure 5.11 - Scenario 3: hourly energy contributions. (a) Participant a). (b) Participant b). (c). Participant c).

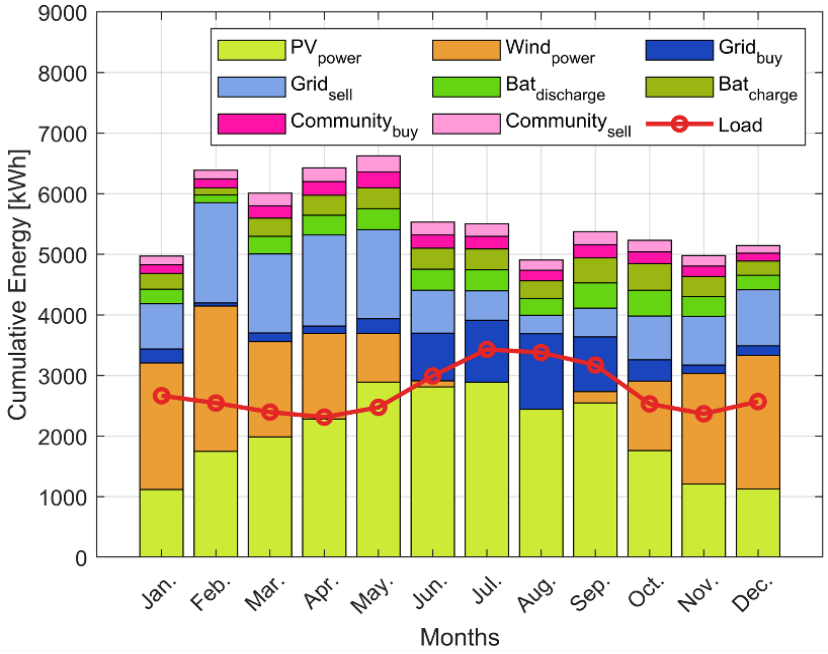

Figure 5.12 - Scenario 3: monthly energy contributions.

Figure 5.12 exhibits a similar behavior to Scenario 2 but with a notable increase in inner-community transactions. During the early months, the renewable energy production matrix is largely dominated by wind energy and, as the peak summer months approach, gradually decreases and is partially replaced by PV production. However, during these peak months, renewable energy production becomes insufficient to meet the high load demand, mainly due to the decrease in wind energy production. As a result, the grid interactions, which were predominantly energy exportation, shift towards energy importation to satisfy the load demand. Moreover, community transactions account for a significant portion of the energy flow, reaching an average of 191 kWh per month.

5.2.3.4 Scenario 4

In Scenario 4, all renewable energy sources and storage systems are shared among the participants. When one participant has surplus energy, it can be used to meet the load demand of others. Firstly, they charge their own batteries to SOCmax and then proceed to charge other peers' batteries sequentially. Conversely, if a participant faces an energy deficit, they can use the energy surplus from others, discharge their battery to the lower limit of SOCmin, and even discharge other peers' batteries if necessary. As can be seen in Table 5.8, both participants present similar renewable production ratio, but with a diversified production mix. Specifically, participant (a) presents a production mix

consisting only of wind production, participant (b) a mix of photovoltaic and wind production and, on the other hand, participant (c) only has photovoltaic production. Figure 5.13 presents the hourly average energy for each participant in Scenario 4.

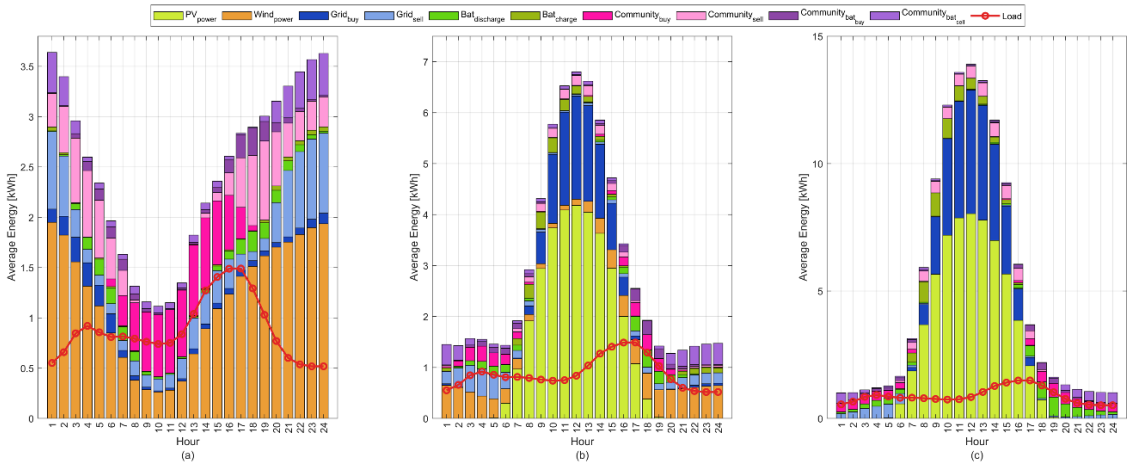

Figure 5.13 - Scenario 4: hourly energy contributions. (a) Participant a). (b) Participant b). (c). Participant c).

As shown, Participant (a) experiences frequent energy deficits during the day, relying on intra-community energy exchanges, occasional grid transactions, and even energy exchanges with other participants to fulfill its energy needs. These deficits are primarily due to the limited wind energy production, while the other participants have significant surplus energy, especially during peak PV production in the afternoon. However, during the night, Participant (a) benefits from excessive energy production, enabling the charge of their individual batteries. In contrast, Participant (b) has substantial surplus energy during the day, due to their PV production, complemented by considerable wind energy production during the night. On the other hand, Participant (c) consistently faces energy deficits during the first and last hours of the day, as no renewable energy production is available in that period. Nevertheless, Participant (c) has substantial surplus energy from PV sources during daylight hours. Like Participant (b), Participant (c) also capitalizes on the high PV production during energy deficit hours to charge its storage systems. Figure 5.14 presents a monthly cumulative energy diagram that summarizes the RES operation in Scenario 4.

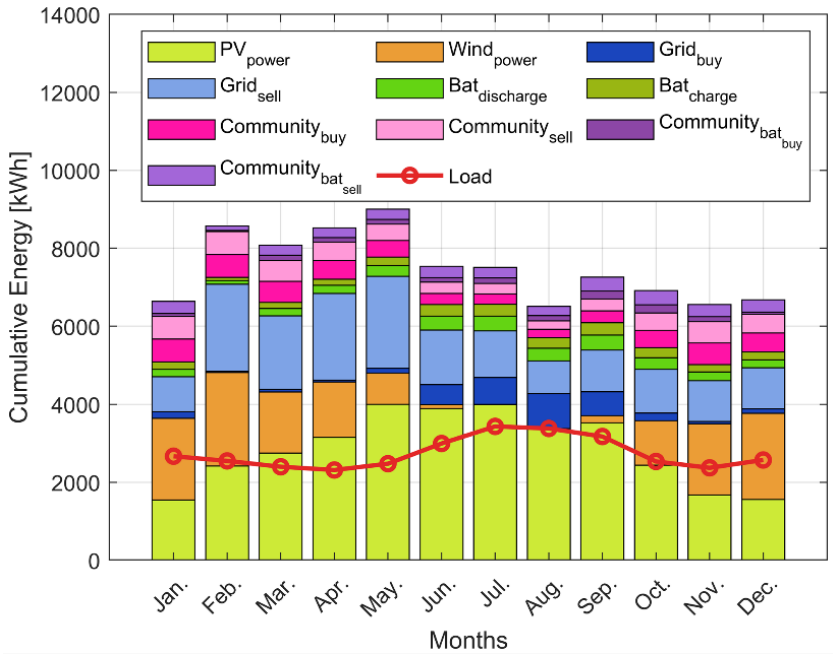

Figure 5.14 - Scenario 4: monthly energy contributions.

Unlike the previous scenarios, in Scenario 4, the total renewable energy production consistently exceeds the total load demand every month of the year, even during peak summer months when wind production is negligible. This indicates a more efficient and optimized energy system. In the winter and autumn period, grid transactions are primarily energy exportations, and the community heavily relies on inner-community exchanges and battery exchanges. However, individual battery reserves are not frequently needed. On the other hand, in the spring and summer periods, grid transactions gradually shift towards grid importation. Moreover, energy storage system reserves increase in this period, while community and battery exchanges have a relatively lower impact on the overall community operation.

5.2.4 Overall Results and Analysis of Renewable Energy Scenarios

The following section presents and discusses the overall results of each scenario, including an analysis of the energy dynamics, performance metrics, and the impact of collaborative approaches on renewable energy integration. Examining the outcomes of each scenario one can evaluate the effectiveness of different energy management strategies and their implications for achieving greater energy independence, optimizing renewable resource utilization, and minimizing reliance on the electrical grid within the renewable energy community.

As seen in Figure 5.15, Scenario 1 exhibits a high percentage of grid exchanges (33%), which can be attributed to the individualist approach adopted by the community participants. With no energy transactions among participants, the participants' surplus energy is exported to the grid, resulting in a higher percentage of exports (22.4%) compared to importations (10.4%). In this scenario, all the renewable energy generation (67%) comes exclusively from PV production, with no wind power production.

In Scenario 2, grid transactions constitute 31.2% of the total energy usage, where 24.0% are grid exportations and 7.2% are grid importations. Community transactions accounted for 3% of the energy usage, while renewable energy sources (RES) contributed 65.8% of the energy supply. Within the renewable energy generation category, PV generation accounts for 40.3%, and wind power generation contributes 25.5%.

In Scenario 3, grid transactions represent 27.6% of the total energy in the renewable energy community (where grid importations represent 9% and exports 18.6%). By prioritizing the use of excess energy to meet the load demand of other participants before charging their individual batteries, the need for grid interactions is reduced.

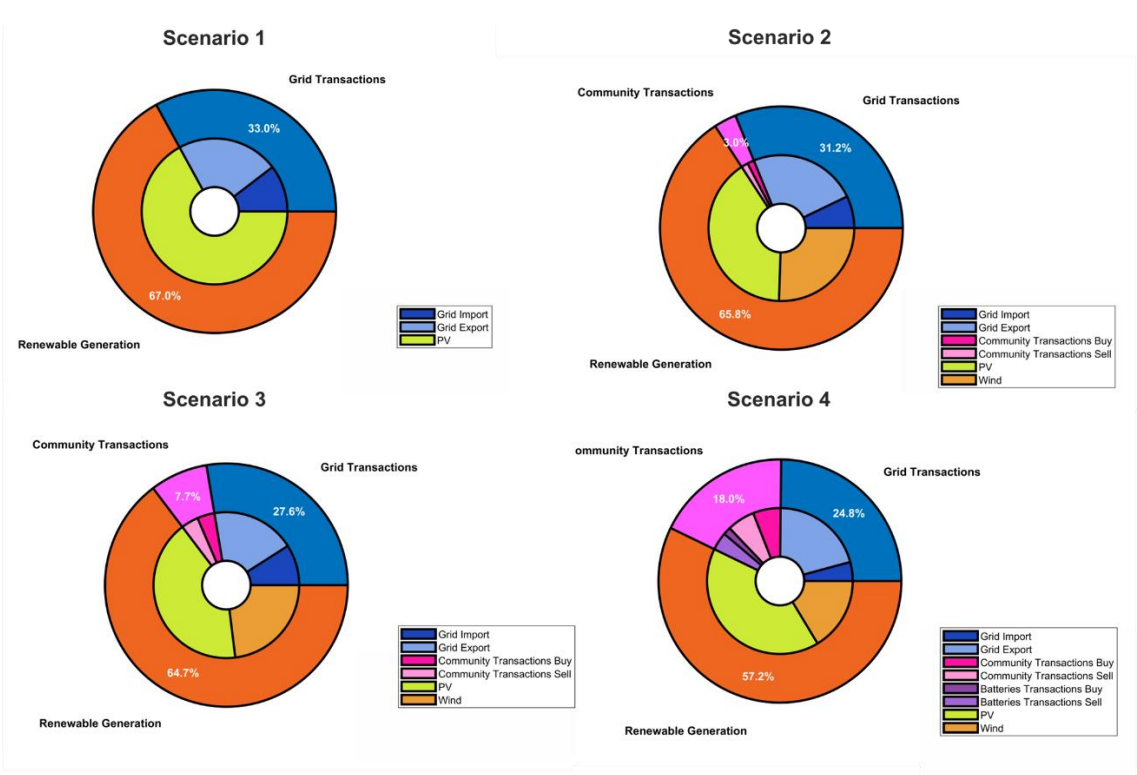

Figure 5.15 - Percentage of transacted energy in each scenario.

This balanced distribution between exports and imports from the grid reflects a more efficient use of renewable energy resources, which reached a percentage of 64.7%, of which 41.6% resulted from solar origin and the remaining 23.1% from wind production.

In Scenario 4, the decrease in overall grid interactions (24.8%, where 20.6% were grid exportations and 4.2% were importations) can be attributed to the collaborative approach adopted by the community participants. By sharing batteries and renewable energy sources, surplus energy can be used to meet the load demand of other community participants, resulting in a higher percentage of community transactions (12.3%). Notably, most of the battery transactions were selling transactions (70%), indicating the community's proactive use of surplus energy to reduce dependence on external sources.

Overall, the variations in the percentage of grid transactions and community transactions in each scenario reflect the different energy management strategies employed. The collaboration and sharing of resources within the community leads to a more efficient utilization of renewable energy and a reduction in dependence on the electrical grid.

Table 5.9 presents several performance metrics that summarize the renewable energy community's operations in each scenario.

Table 5.9 - Performance Metrics for Renewable Energy Community Scenarios.

Scenario	**Initial Investment Cost (Euro)**	**Annual Energy Cost (Euro)**	**Annual Exported Energy (kWh)**	**Annual Imported Energy (kWh)**	**Annual Community Transactions (kWh)**	**Annual Community Battery Transactions (kWh)**	**Annual Greenhouse Gas (kgCO2)**
Scenario 1	55,930	1371.3	13,536	6233	0	0	72,908
Scenario 2	51,700	1054.7	16,176	4794	2021.3	0	73,750
Scenario 3	41,750	1185.5	11,090	5388.6	4584.7	0	57,879
Scenario 4	39,720	777.53	17,329	3534.2	10,318	4793	72,037

The Initial Investment column represents the amount of money required to initially implement each scenario. This parameter is calculated based on the initial investment required to build each REC, assuming costs of 170 Euros per solar panel, 3500 Euros per wind turbine, and 800 Euros per kW of battery. The Annual Cost of Energy indicates the annual energy cost associated with the community's operation

under each scenario. This parameter is calculated based on the total energy imported and exported by the REC during the simulated year, assuming a cost of 0.22 Euros per kWh for importing and 0.06 Euros per kWh for exporting to the grid.

The Annual Exported Energy and Annual Imported Energy columns show the amount of energy exported to and imported from the electrical grid, respectively. The Annual Intra-Community Transactions and Annual Community Battery Transactions columns represent the amount of energy exchanged within the community and through battery transactions, respectively. Lastly, Annual Greenhouse Gas Emissions quantifies the amount of greenhouse gases emitted during the year under each scenario. The reference values used for the calculations was 0.373 kg CO_2 per kWh, which corresponds to the United States electrical grid average Greenhouse Gas Emissions in 2021. Additionally, the specific values for greenhouse gas emissions factors were as follows: 0.028 kg CO_2 per kWh for the energy storage system, 0.225 kg CO_2 per kWh for the PV modules and 0.008 kg CO_2 per kWh for the Wind Turbine [176].

As shown in Table 5.9, Scenario 4 emerges as the most favorable option in terms of economic factors, with a relatively lower Initial Investment compared to other scenarios, indicating a more cost-effective implementation. Additionally, this scenario demonstrates a significantly lower Annual Energy Cost, highlighting its efficiency and cost-effectiveness in long-term operations. Scenarios 2 and 3 show a balanced Initial Investment Cost with a relatively low Annual Energy Cost. In contrast, Scenario 1 exhibits a higher Initial Investment Cost and Annual Energy Costs.

In terms of energy independence and grid interaction, Scenarios 2 and 4 exhibit the highest Annual Exported Energy, suggesting a higher surplus of energy. Additionally, Scenario 4 has a relatively lower Annual Imported Energy, indicating reduced reliance on the electrical grid. This scenario also shows the highest Annual Community Transactions and Annual Community Battery Transactions, highlighting active collaboration and battery energy sharing among community participants. In terms of environmental impact, Scenario 2 has the lowest Annual Greenhouse Gas Emissions, indicating a more sustainable energy operation.

Based on these performance metrics, Scenario 4 stands out as the most favorable option, offering a lower Initial Investment, which contributes to cost savings in the implementation phase. Additionally, it demonstrates reduced energy costs, ensuring long-term affordability and sustainability. Scenario 4 also presents higher energy independence, with a significant amount of exported energy and a lower reliance on

imports from the grid. Moreover, this scenario exhibits a reasonably low rate of greenhouse gas emissions, reflecting its environmentally friendly approach. Nonetheless, Scenarios 2 and 3 also display promising characteristics, demonstrating active community engagement and a well-balanced energy operation. While they do not outperform Scenario 4 in all aspects, they present valuable alternatives that foster collaboration and contribute to the community's energy sustainability.

CHAPTER 6

Conclusions

In conclusion, this paper presented a comprehensive analysis of a renewable energy community, examining four different scenarios with varying degrees of collaboration and energy management strategies. To address the issue of optimal sizing in a multi-objective optimization approach, this paper implements a novel Multi-Objective Optimization Algorithm named Multi-Objective Arithmetic & Differential Evolution Optimization (MOADEO). This algorithm was evaluated and compared to a set of algorithms present in the literature, where it proved to have a robust performance. The sizing of the various energy production and storage units inherent to each participant of the renewable energy community was, however, carried out using a multi-swarm MOPSO considering economical and technical criteria, namely the levelized cost of energy (LCOE), self-consumption ratio (SCR) and self-sufficiency ratio (SSR).

The results revealed valuable insights into the performance and effectiveness of each scenario. Scenario 4 emerged as the most beneficial option, showing a lower initial investment, reduced energy costs, higher energy independence, and a reasonable greenhouse gas emission. This collaborative approach, where surplus power is shared among participants and individual storage systems are utilized as a last resort, demonstrated improved renewable energy integration and a decreased reliance on the electrical grid. Additionally, Scenarios 2 and 3 also displayed promising characteristics, emphasizing active community engagement and balanced energy operations.

Overall, the findings from this research contribute to advancing our understanding of renewable energy integration in community settings and offer valuable guidance for enhancing the resilience and sustainability of future energy systems. As renewable energy adoption continues to grow, collaborative approaches like those explored in these scenarios will play a vital role in building more sustainable and self-reliant communities.

6.1 Future Works

The research presented in this study provides valuable insights into the optimization of renewable energy communities. However, several avenues for future research and exploration can further enhance our understanding and practical implementation of collaborative energy sharing and optimization strategies:

- Scalability Assessment: Exploring the scalability of the proposed optimization approach is crucial. Investigating its applicability to larger and more complex renewable energy community settings can help determine its robustness and efficiency in a broader range of scenarios [177].
- Geographical Variability: Examining how different geographical locations and climates impact the effectiveness of energy management strategies is important. Understanding how environmental factors influence energy sharing and distribution can lead to region-specific optimization models [178].
- Regulatory and Policy Implications: Research into potential regulatory and policy implications for the successful implementation of collaborative renewable energy sharing in communities. This includes exploring legal frameworks and policy changes necessary to support and incentivize energy sharing initiatives at various levels [179].
- Practical Case Studies: Implement pilot RES or collaborate with real-world stakeholders and implement the proposed optimization strategies in pilot projects to validate theoretical models and provide practical insights [180].
- Integration of Emerging Technologies: Evaluate the integration of emerging renewable energy technologies, including blockchain, into the optimization framework. Assess the efficiency gains, economic benefits, and potential for enhancing trust and transparency in energy sharing and management [181], [182].

Relatively to the proposed MOADEO algorithm, the efficiency and the effectiveness of this novel MOA can be significantly improved by implementing algorithm enhancements like dynamic mechanisms to adjust the algorithm parameters throughout iterations, or by perhaps refining the operators and parameters to improve the balance between the diversity and convergence mechanisms, preventing premature convergence of the optimal solutions regardless of the optimization problem, among others.

Bibliography

[1] O. Azeem *et al.*, "A Comprehensive Review on Integration Challenges, Optimization Techniques and Control Strategies of Hybrid AC/DC Microgrid," *Applied Sciences 2021, Vol. 11, Page 6242*, vol. 11, no. 14, p. 6242, Jul. 2021, doi: 10.3390/APP11146242.

[2] A. Chauhan and R. P. Saini, "A review on Integrated Renewable Energy System based power generation for stand-alone applications: Configurations, storage options, sizing methodologies and control," *Renewable and Sustainable Energy Reviews*, vol. 38, pp. 99–120, Oct. 2014, doi: 10.1016/J.RSER.2014.05.079.

[3] K. Shivarama Krishna and K. Sathish Kumar, "A review on hybrid renewable energy systems," *Renewable and Sustainable Energy Reviews*, vol. 52, pp. 907–916, Dec. 2015, doi: 10.1016/J.RSER.2015.07.187.

[4] L. Olatomiwa, S. Mekhilef, M. S. Ismail, and M. Moghavvemi, "Energy management strategies in hybrid renewable energy systems: A review," *Renewable and Sustainable Energy Reviews*, vol. 62, pp. 821–835, Sep. 2016, doi: 10.1016/J.RSER.2016.05.040.

[5] "THE PARIS AGREEMENT," 2016, Accessed: Jan. 13, 2024. [Online]. Available: https://treaties.un.org/Pages/ViewDetails.aspx?src=TREATY&mtdsg_no=XXVII-7-

[6] "Global climate action - European Commission." Accessed: Jan. 13, 2024. [Online]. Available: https://climate.ec.europa.eu/eu-action/international-action-climate-change/global-climate-action_en

[7] "ROTEIRO PARA A NEUTRALIDADE CARBÓNICA 2050 (RNC2050) ESTRATÉGIA DE LONGO PRAZO PARA A NEUTRALIDADE CARBÓNICA DA ECONOMIA PORTUGUESA EM 2050 PT Ambiente".

[8] "Clean energy for all Europeans package." Accessed: Jan. 13, 2024. [Online]. Available: https://energy.ec.europa.eu/topics/energy-strategy/clean-energy-all-europeans-package_en

[9] "2030 climate & energy framework - European Commission." Accessed: Jan. 13, 2024. [Online]. Available: https://climate.ec.europa.eu/eu-action/climate-strategies-targets/2030-climate-energy-framework_en

[10] "Directive - 2018/2001 - EN - EUR-Lex." Accessed: Jan. 13, 2024. [Online]. Available: https://eur-lex.europa.eu/legal-content/EN/TXT/?uri=celex%3A32018L2001

[11] "Directive - 2018/844 - EN - EUR-Lex." Accessed: Jan. 13, 2024. [Online]. Available: https://eur-lex.europa.eu/legal-content/EN/ALL/?uri=CELEX%3A32018L0844

[12] "Decreto-Lei n.º 162/2019 | DR." Accessed: Jan. 13, 2024. [Online]. Available: https://diariodarepublica.pt/dr/detalhe/decreto-lei/162-2019-125692189

[13] "Regulation - 2018/1999 - EN - EUR-Lex." Accessed: Jan. 13, 2024. [Online]. Available: https://eur-lex.europa.eu/legal-content/EN/TXT/?uri=uriserv%3AOJ.L_.2018.328.01.0001.01.ENG

[14] "Decreto-Lei n.º 15/2022 | DR." Accessed: Jan. 13, 2024. [Online]. Available: https://diariodarepublica.pt/dr/detalhe/decreto-lei/15-2022-177634016

[15] “Resolução do Conselho de Ministros n.º 107/2019 | DR.” Accessed: Jan. 13, 2024. [Online]. Available: https://diariodarepublica.pt/dr/detalhe/resolucao-conselho-ministros/107-2019-122777644
[16] “PLANO NACIONAL ENERGIA E CLIMA 2021-2030 (PNEC 2030)”.
[17] “Directive - 2019/944 - EN - EUR-Lex.” Accessed: Jan. 13, 2024. [Online]. Available: https://eur-lex.europa.eu/legal-content/EN/TXT/?uri=celex%3A32019L0944
[18] “Energy communities.” Accessed: Jan. 22, 2024. [Online]. Available: https://energy.ec.europa.eu/topics/markets-and-consumers/energy-communities_en
[19] D. J. de C. G. M. Santana, “Estudo para a Implementação de uma Comunidade de Energia Renovável,” 2022, Accessed: Jan. 22, 2024. [Online]. Available: https://comum.rcaap.pt/handle/10400.26/43317
[20] “O que é uma comunidade de energia?” Accessed: Jan. 13, 2024. [Online]. Available: https://www.dgeg.gov.pt/pt/areas-setoriais/energia/energias-renovaveis-e-sustentabilidade/comunidades-de-energia/o-que-e-uma-comunidade-de-energia/
[21] “What is an energy community? - European Commission.” Accessed: Jan. 23, 2024. [Online]. Available: https://rural-energy-community-hub.ec.europa.eu/energy-communities/what-energy-community_en
[22] R. Lazdins, A. Mutule, D. Zalostiba, V. Efthymiou, C. N. Papadimitriou, and E.-C. Cho, “PV Energy Communities—Challenges and Barriers from a Consumer Perspective: A Literature Review,” *Energies 2021, Vol. 14, Page 4873*, vol. 14, no. 16, p. 4873, Aug. 2021, doi: 10.3390/EN14164873.
[23] S. Sen and S. Ganguly, “Opportunities, barriers and issues with renewable energy development – A discussion,” *Renewable and Sustainable Energy Reviews*, vol. 69, pp. 1170–1181, Mar. 2017, doi: 10.1016/J.RSER.2016.09.137.
[24] G. Yiasoumas *et al.*, “Key Aspects and Challenges in the Implementation of Energy Communities,” *Energies 2023, Vol. 16, Page 4703*, vol. 16, no. 12, p. 4703, Jun. 2023, doi: 10.3390/EN16124703.
[25] A. Nic Aoidh Údarás na Gaeltachta Christina Hülsken *et al.*, “PESTLE ANALYSIS of Barriers to Community Energy Development CONTRIBUTING AUTHORS AND INSTITUTIONS IN ALPHABETICAL ORDER”.
[26] A. S. Aziz, M. F. N. Tajuddin, T. E. K. Zidane, C. L. Su, A. J. K. Alrubaie, and M. J. Alwazzan, “Techno-economic and environmental evaluation of PV/diesel/battery hybrid energy system using improved dispatch strategy,” *Energy Reports*, vol. 8, pp. 6794–6814, Nov. 2022, doi: 10.1016/J.EGYR.2022.05.021.
[27] A. Ahmadifar, M. Ginocchi, M. S. Golla, F. Ponci, and A. Monti, “Development of an Energy Management System for a Renewable Energy Community and Performance Analysis via Global Sensitivity Analysis,” *IEEE Access*, vol. 11, pp. 4131–4154, 2023, doi: 10.1109/ACCESS.2023.3235590.
[28] T. F. Agajie *et al.*, “A Comprehensive Review on Techno-Economic Analysis and Optimal Sizing of Hybrid Renewable Energy Sources with Energy Storage Systems,” *Energies 2023, Vol. 16, Page 642*, vol. 16, no. 2, p. 642, Jan. 2023, doi: 10.3390/EN16020642.
[29] J. Lowitzsch, C. E. Hoicka, and F. J. van Tulder, “Renewable energy communities under the 2019 European Clean Energy Package – Governance model for the

energy clusters of the future?," *Renewable and Sustainable Energy Reviews*, vol. 122, p. 109489, Apr. 2020, doi: 10.1016/J.RSER.2019.109489.

[30] Y. Li, F. Qian, W. Gao, H. Fukuda, and Y. Wang, "Techno-economic performance of battery energy storage system in an energy sharing community," *J Energy Storage*, vol. 50, p. 104247, Jun. 2022, doi: 10.1016/J.EST.2022.104247.

[31] N. Salehi, H. Martinez-Garcia, G. Velasco-Quesada, and J. M. Guerrero, "A Comprehensive Review of Control Strategies and Optimization Methods for Individual and Community Microgrids," *IEEE Access*, vol. 10, pp. 15935–15955, 2022, doi: 10.1109/ACCESS.2022.3142810.

[32] D. Sadeghi, A. Hesami Naghshbandy, and S. Bahramara, "Optimal sizing of hybrid renewable energy systems in presence of electric vehicles using multi-objective particle swarm optimization," *Energy*, vol. 209, p. 118471, Oct. 2020, doi: 10.1016/J.ENERGY.2020.118471.

[33] J. L. Duchaud, G. Notton, C. Darras, and C. Voyant, "Multi-Objective Particle Swarm optimal sizing of a renewable hybrid power plant with storage," *Renew Energy*, vol. 131, pp. 1156–1167, Feb. 2019, doi: 10.1016/J.RENENE.2018.08.058.

[34] S. H. Park, Y. S. Jang, and E. J. Kim, "Multi-objective optimization for sizing multi-source renewable energy systems in the community center of a residential apartment complex," *Energy Convers Manag*, vol. 244, Sep. 2021, doi: 10.1016/J.ENCONMAN.2021.114446.

[35] H. G. G. Nunes, J. P. A. Portugal, J. A. N. Pombo, S. J. P. S. Mariano, and M. R. A. Calado, "Parameter Estimation of Per-Unit Photovoltaic Models Using Optimization Algorithms: Comparative Study," *Studies in Systems, Decision and Control*, vol. 212, pp. 157–195, 2022, doi: 10.1007/978-3-031-07512-4_6/COVER.

[36] T. Easwarakhanthan, J. Bottin, I. Bouhouch, and C. Boutrit, "Nonlinear Minimization Algorithm for Determining the Solar Cell Parameters with Microcomputers," *International Journal of Solar Energy*, vol. 4, no. 1, pp. 1–12, 1986, doi: 10.1080/01425918608909835.

[37] A. K. Tossa, Y. M. Soro, Y. Azoumah, and D. Yamegueu, "A new approach to estimate the performance and energy productivity of photovoltaic modules in real operating conditions," *Solar Energy*, vol. 110, pp. 543–560, Dec. 2014, doi: 10.1016/J.SOLENER.2014.09.043.

[38] L. Wu *et al.*, "Parameter extraction of photovoltaic models from measured I-V characteristics curves using a hybrid trust-region reflective algorithm," *Appl Energy*, vol. 232, pp. 36–53, Dec. 2018, doi: 10.1016/j.apenergy.2018.09.161.

[39] H. G. G. Nunes, J. A. N. Pombo, P. M. R. Bento, S. J. P. S. Mariano, and M. R. A. Calado, "Collaborative swarm intelligence to estimate PV parameters," *Energy Convers Manag*, vol. 185, pp. 866–890, Apr. 2019, doi: 10.1016/J.ENCONMAN.2019.02.003.

[40] J. Zhang, M. Xiao, L. Gao, and Q. Pan, "Queuing search algorithm: A novel metaheuristic algorithm for solving engineering optimization problems," *Appl Math Model*, vol. 63, pp. 464–490, Nov. 2018, doi: 10.1016/J.APM.2018.06.036.

[41] W. Zhao, C. Du, and S. Jiang, "An adaptive multiscale approach for identifying multiple flaws based on XFEM and a discrete artificial fish swarm algorithm," *Comput Methods Appl Mech Eng*, vol. 339, pp. 341–357, Sep. 2018, doi: 10.1016/J.CMA.2018.04.037.

[42] N. Khodadadi, L. Abualigah, E. S. M. El-Kenawy, V. Snasel, and S. Mirjalili, “An Archive-Based Multi-Objective Arithmetic Optimization Algorithm for Solving Industrial Engineering Problems,” *IEEE Access*, vol. 10, pp. 106673–106698, 2022, doi: 10.1109/ACCESS.2022.3212081.
[43] C. Blum and A. Roli, “Metaheuristics in combinatorial optimization,” *ACM Computing Surveys (CSUR)*, vol. 35, no. 3, pp. 268–308, Sep. 2003, doi: 10.1145/937503.937505.
[44] M. Abdel-Basset, L. Abdel-Fatah, and A. K. Sangaiah, “Metaheuristic Algorithms: A Comprehensive Review,” *Computational Intelligence for Multimedia Big Data on the Cloud with Engineering Applications*, pp. 185–231, Jan. 2018, doi: 10.1016/B978-0-12-813314-9.00010-4.
[45] H. G. G. Nunes, P. N. C. Silva, J. A. N. Pombo, S. J. P. S. Mariano, and M. R. A. Calado, “Multiswarm spiral leader particle swarm optimisation algorithm for PV parameter identification,” *Energy Convers Manag*, vol. 225, p. 113388, Dec. 2020, doi: 10.1016/J.ENCONMAN.2020.113388.
[46] C. Voudouris and E. Tsang, “Guided local search and its application to the traveling salesman problem,” *Eur J Oper Res*, vol. 113, no. 2, pp. 469–499, Mar. 1999, doi: 10.1016/S0377-2217(98)00099-X.
[47] J. Kennedy and R. Eberhart, “Particle swarm optimization,” *Proceedings of ICNN’95 - International Conference on Neural Networks*, vol. 4, pp. 1942–1948, doi: 10.1109/ICNN.1995.488968.
[48] A. U. Rehman *et al.*, “An Optimal Power Usage Scheduling in Smart Grid Integrated with Renewable Energy Sources for Energy Management,” *IEEE Access*, vol. 9, pp. 84619–84638, 2021, doi: 10.1109/ACCESS.2021.3087321.
[49] J. Faria, J. Pombo, M. Do Rosário Calado, and S. Mariano, “Current Control Optimization for Grid-tied Inverters Using Cuckoo Search Algorithm,” *KnE Engineering*, Jun. 2020, doi: 10.18502/KEG.V5I6.7099.
[50] N. S. Jayalakshmi, V. K. Jadoun, D. N. Gaonkar, A. Shrivastava, N. Kanwar, and K. K. Nandini, “Optimal operation of multi-source electric vehicle connected microgrid using metaheuristic algorithm,” *J Energy Storage*, vol. 52, p. 105067, Aug. 2022, doi: 10.1016/J.EST.2022.105067.
[51] O. Laayati, A. Elmaghraoui, H. El Hadraoui, Y. Ledmaoui, M. Bouzi, and A. Chebak, “Tabu Search Optimization for Energy Management in Microgrids: A Solution to Grid-Connected and Standalone Operation Modes,” *Proceedings - 2023 IEEE 5th Global Power, Energy and Communication Conference, GPECOM 2023*, pp. 401–406, 2023, doi: 10.1109/GPECOM58364.2023.10175809.
[52] J. Faria, J. Fermeiro, J. Pombo, M. Calado, and S. Mariano, “Proportional Resonant Current Control and Output-Filter Design Optimization for Grid-Tied Inverters Using Grey Wolf Optimizer,” *Energies 2020, Vol. 13, Page 1923*, vol. 13, no. 8, p. 1923, Apr. 2020, doi: 10.3390/EN13081923.
[53] A. R. Singh, L. Ding, D. K. Raju, R. S. Kumar, and L. P. Raghav, “Demand response of grid-connected microgrid based on metaheuristic optimization algorithm,” *Energy Sources, Part A: Recovery, Utilization, and Environmental Effects*, Oct. 2021, doi: 10.1080/15567036.2021.1985654.
[54] R. Somakumar, P. Kasinathan, G. Monicka, A. Rajagopalan, V. K. Ramachandaramurthy, and U. Subramaniam, “Optimization of emission cost and economic analysis for microgrid by considering a metaheuristic algorithm-

assisted dispatch model," *International Journal of Numerical Modelling: Electronic Networks, Devices and Fields*, vol. 35, no. 4, p. e2993, Jul. 2022, doi: 10.1002/JNM.2993.

[55] V. Suresh, P. Janik, M. Jasinski, J. M. Guerrero, and Z. Leonowicz, "Microgrid energy management using metaheuristic optimization algorithms," *Appl Soft Comput*, vol. 134, p. 109981, Feb. 2023, doi: 10.1016/J.ASOC.2022.109981.

[56] M. Rizvi, B. Pratap, and S. B. Singh, "Demand-side management in microgrid using novel hybrid metaheuristic algorithm," *Electrical Engineering*, vol. 105, no. 3, pp. 1867–1881, Jun. 2023, doi: 10.1007/S00202-023-01778-7/METRICS.

[57] R. Faia, J. Soares, T. Pinto, F. Lezama, Z. Vale, and J. M. Corchado, "Optimal Model for Local Energy Community Scheduling Considering Peer to Peer Electricity Transactions," *IEEE Access*, vol. 9, pp. 12420–12430, 2021, doi: 10.1109/ACCESS.2021.3051004.

[58] A. Overview *et al.*, "Optimal Scheduling of Controllable Resources in Energy Communities: An Overview of the Optimization Approaches," *Energies 2023, Vol. 16, Page 101*, vol. 16, no. 1, p. 101, Dec. 2022, doi: 10.3390/EN16010101.

[59] M. S. Simoiu, I. Fagarasan, S. Ploix, and V. Calofir, "Sizing and Management of an Energy System for a Metropolitan Station with Storage and Related District Energy Community," *Energies 2021, Vol. 14, Page 5997*, vol. 14, no. 18, p. 5997, Sep. 2021, doi: 10.3390/EN14185997.

[60] G. Talluri, G. M. Lozito, F. Grasso, C. Iturrino Garcia, and A. Luchetta, "Optimal Battery Energy Storage System Scheduling within Renewable Energy Communities," *Energies 2021, Vol. 14, Page 8480*, vol. 14, no. 24, p. 8480, Dec. 2021, doi: 10.3390/EN14248480.

[61] R. Trevisan, E. Ghiani, S. Ruggeri, S. Mocci, G. Pisano, and F. Pilo, "Optimal sizing of PV and Storage for a Port Renewable Energy Community," *SyNERGY MED 2022 - 2nd International Conference on Energy Transition in the Mediterranean Area, Proceedings*, 2022, doi: 10.1109/SYNERGYMED55767.2022.9941383.

[62] A. Cosic, M. Stadler, M. Mansoor, and M. Zellinger, "Mixed-integer linear programming based optimization strategies for renewable energy communities," *Energy*, vol. 237, p. 121559, Dec. 2021, doi: 10.1016/J.ENERGY.2021.121559.

[63] E. Cutore, R. Volpe, R. Sgroi, and A. Fichera, "Energy management and sustainability assessment of renewable energy communities: The Italian context," *Energy Convers Manag*, vol. 278, p. 116713, Feb. 2023, doi: 10.1016/J.ENCONMAN.2023.116713.

[64] F. Foiadelli, S. Nocerino, M. Di Somma, and G. Graditi, "Optimal Design of der for Economic/Environmental Sustainability of Local Energy Communities," *Proceedings - 2018 IEEE International Conference on Environment and Electrical Engineering and 2018 IEEE Industrial and Commercial Power Systems Europe, EEEIC/I and CPS Europe 2018*, Oct. 2018, doi: 10.1109/EEEIC.2018.8493898.

[65] M. Secchi, G. Barchi, D. Macii, D. Moser, and D. Petri, "Multi-objective battery sizing optimisation for renewable energy communities with distribution-level constraints: A prosumer-driven perspective," *Appl Energy*, vol. 297, p. 117171, Sep. 2021, doi: 10.1016/J.APENERGY.2021.117171.

[66] S. A. El-Batawy and W. G. Morsi, “Optimal design of community battery energy storage systems with prosumers owning electric vehicles,” *IEEE Trans Industr Inform*, vol. 14, no. 5, pp. 1920–1931, May 2018, doi: 10.1109/TII.2017.2752464.
[67] D. Fioriti, A. Frangioni, and D. Poli, “Optimal sizing of energy communities with fair revenue sharing and exit clauses: Value, role and business model of aggregators and users,” *Appl Energy*, vol. 299, p. 117328, Oct. 2021, doi: 10.1016/J.APENERGY.2021.117328.
[68] D. L. Rodrigues, X. Ye, X. Xia, and B. Zhu, “Battery energy storage sizing optimisation for different ownership structures in a peer-to-peer energy sharing community,” *Appl Energy*, vol. 262, p. 114498, Mar. 2020, doi: 10.1016/J.APENERGY.2020.114498.
[69] C. Avilés A., S. Oliva H., and D. Watts, “Single-dwelling and community renewable microgrids: Optimal sizing and energy management for new business models,” *Appl Energy*, vol. 254, p. 113665, Nov. 2019, doi: 10.1016/J.APENERGY.2019.113665.
[70] J. Sousa *et al.*, “Renewable energy communities optimal design supported by an optimization model for investment in PV/wind capacity and renewable electricity sharing,” *Energy*, vol. 283, p. 128464, Nov. 2023, doi: 10.1016/J.ENERGY.2023.128464.
[71] F. Hafiz, A. Rodrigo de Queiroz, P. Fajri, and I. Husain, “Energy management and optimal storage sizing for a shared community: A multi-stage stochastic programming approach,” *Appl Energy*, vol. 236, pp. 42–54, Feb. 2019, doi: 10.1016/J.APENERGY.2018.11.080.
[72] M. Bohringer, S. Choudhury, S. Weck, and J. Hanson, “Sizing and Placement of Community Energy Storage Systems using Multi-Period Optimal Power Flow,” *2021 IEEE Madrid PowerTech, PowerTech 2021 - Conference Proceedings*, Jun. 2021, doi: 10.1109/POWERTECH46648.2021.9494820.
[73] M. Geraedts, J. Alpizar-Castillo, L. Ramirez-Elizondo, and P. Bauer, “Optimal Sizing of a Community Level Thermal Energy Storage System,” *MELECON 2022 - IEEE Mediterranean Electrotechnical Conference, Proceedings*, pp. 52–57, 2022, doi: 10.1109/MELECON53508.2022.9842945.
[74] A. Yaldız, T. Gökçek, İ. Şengör, and O. Erdinç, “Optimal sizing and economic analysis of Photovoltaic distributed generation with Battery Energy Storage System considering peer-to-peer energy trading,” *Sustainable Energy, Grids and Networks*, vol. 28, p. 100540, Dec. 2021, doi: 10.1016/J.SEGAN.2021.100540.
[75] B. Bhandari, K. T. Lee, G. Y. Lee, Y. M. Cho, and S. H. Ahn, “Optimization of hybrid renewable energy power systems: A review,” *International Journal of Precision Engineering and Manufacturing - Green Technology*, vol. 2, no. 1, pp. 99–112, Jan. 2015, doi: 10.1007/S40684-015-0013-Z/METRICS.
[76] H. M. Ridha, C. Gomes, H. Hizam, M. Ahmadipour, A. A. Heidari, and H. Chen, “Multi-objective optimization and multi-criteria decision-making methods for optimal design of standalone photovoltaic system: A comprehensive review,” *Renewable and Sustainable Energy Reviews*, vol. 135, p. 110202, Jan. 2021, doi: 10.1016/J.RSER.2020.110202.
[77] P. Bento, H. Nunes, J. Pombo, M. do Rosário Calado, and S. Mariano, “Daily Operation Optimization of a Hybrid Energy System Considering a Short-Term

Electricity Price Forecast Scheme," *Energies 2019, Vol. 12, Page 924*, vol. 12, no. 5, p. 924, Mar. 2019, doi: 10.3390/EN12050924.

[78] J. F. Manwell and J. G. McGowan, "Lead acid battery storage model for hybrid energy systems," *Solar Energy*, vol. 50, no. 5, pp. 399–405, May 1993, doi: 10.1016/0038-092X(93)90060-2.

[79] A. Mahesh and K. S. Sandhu, "Optimal Sizing of a Grid-Connected PV/Wind/Battery System Using Particle Swarm Optimization," *Iranian Journal of Science and Technology - Transactions of Electrical Engineering*, vol. 43, no. 1, pp. 107–121, Mar. 2019, doi: 10.1007/S40998-018-0083-3/METRICS.

[80] L. M. Rodrigues, N. L. Bitencourt, L. Rech, C. Montez, and R. Moraes, "An analytical model to estimate the state of charge and lifetime for batteries with energy harvesting capabilities," *Int J Energy Res*, vol. 44, no. 7, pp. 5243–5258, Jun. 2020, doi: 10.1002/ER.5269.

[81] S. Mandelli, C. Brivio, E. Colombo, and M. Merlo, "A sizing methodology based on Levelized Cost of Supplied and Lost Energy for off-grid rural electrification systems," *Renew Energy*, vol. 89, pp. 475–488, Apr. 2016, doi: 10.1016/J.RENENE.2015.12.032.

[82] D. Yousri, H. E. Z. Farag, H. Zeineldin, and E. F. El-Saadany, "Integrated model for optimal energy management and demand response of microgrids considering hybrid hydrogen-battery storage systems," *Energy Convers Manag*, vol. 280, p. 116809, Mar. 2023, doi: 10.1016/J.ENCONMAN.2023.116809.

[83] A. Mahesh and K. S. Sandhu, "A genetic algorithm based improved optimal sizing strategy for solar-wind-battery hybrid system using energy filter algorithm," *Frontiers in Energy*, vol. 14, no. 1, pp. 139–151, Mar. 2020, doi: 10.1007/S11708-017-0484-4/METRICS.

[84] C. O. Okoye and O. Solyalı, "Optimal sizing of stand-alone photovoltaic systems in residential buildings," *Energy*, vol. 126, pp. 573–584, May 2017, doi: 10.1016/J.ENERGY.2017.03.032.

[85] C. G. Justus, "Wind energy statistics for large arrays of wind turbines (New England and Central U.S. Regions)," *Solar Energy*, vol. 20, no. 5, pp. 379–386, Jan. 1978, doi: 10.1016/0038-092X(78)90153-6.

[86] W. M. Hamanah, M. A. Abido, and L. M. Alhems, "Optimum Sizing of Hybrid PV, Wind, Battery and Diesel System Using Lightning Search Algorithm," *Arab J Sci Eng*, vol. 45, no. 3, pp. 1871–1883, Mar. 2020, doi: 10.1007/S13369-019-04292-W/METRICS.

[87] S. Zheng, G. Huang, and A. C. Lai, "Techno-economic performance analysis of synergistic energy sharing strategies for grid-connected prosumers with distributed battery storages," *Renew Energy*, vol. 178, pp. 1261–1278, Nov. 2021, doi: 10.1016/J.RENENE.2021.06.100.

[88] A. S. Aziz, M. F. N. Tajuddin, T. E. K. Zidane, C. L. Su, A. J. K. Alrubaie, and M. J. Alwazzan, "Techno-economic and environmental evaluation of PV/diesel/battery hybrid energy system using improved dispatch strategy," *Energy Reports*, vol. 8, pp. 6794–6814, Nov. 2022, doi: 10.1016/J.EGYR.2022.05.021.

[89] B. K. Das, R. Hassan, M. S. Islam, and M. Rezaei, "Influence of energy management strategies and storage devices on the techno-enviro-economic optimization of hybrid energy systems: A case study in Western Australia," *J Energy Storage*, vol. 51, p. 104239, Jul. 2022, doi: 10.1016/J.EST.2022.104239.

[90] S. Mandal, B. K. Das, and N. Hoque, “Optimum sizing of a stand-alone hybrid energy system for rural electrification in Bangladesh,” *J Clean Prod*, vol. 200, pp. 12–27, Nov. 2018, doi: 10.1016/J.JCLEPRO.2018.07.257.
[91] M. S. Simoiu, I. Fagarasan, S. Ploix, and V. Calofir, “Sizing and Management of an Energy System for a Metropolitan Station with Storage and Related District Energy Community,” *Energies 2021, Vol. 14, Page 5997*, vol. 14, no. 18, p. 5997, Sep. 2021, doi: 10.3390/EN14185997.
[92] P. Venet *et al.*, “Overview and Comparative Study of Energy Management Strategies for Residential PV Systems with Battery Storage,” *Batteries 2022, Vol. 8, Page 279*, vol. 8, no. 12, p. 279, Dec. 2022, doi: 10.3390/BATTERIES8120279.
[93] Y. Li, H. Liu, K. Xie, and X. Yu, “A method for distributing reference points uniformly along the Pareto front of DTLZ test functions in many-objective evolutionary optimization,” *2015 5th International Conference on Information Science and Technology, ICIST 2015*, pp. 541–546, Oct. 2015, doi: 10.1109/ICIST.2015.7289031.
[94] H. Ishibuchi, N. Tsukamoto, and Y. Nojima, “Evolutionary many-objective optimization: A short review,” *2008 IEEE Congress on Evolutionary Computation, CEC 2008*, pp. 2419–2426, 2008, doi: 10.1109/CEC.2008.4631121.
[95] P. Ngatchou, A. Zarei, and M. A. El-Sharkawi, “Pareto multi objective optimization,” *Proceedings of the 13th International Conference on Intelligent Systems Application to Power Systems, ISAP’05*, vol. 2005, pp. 84–91, 2005, doi: 10.1109/ISAP.2005.1599245.
[96] H. Tamaki, H. Kita, and S. Kobayashi, “Multi-objective optimization by genetic algorithms: a review,” *Proceedings of the IEEE Conference on Evolutionary Computation*, pp. 517–522, 1996, doi: 10.1109/ICEC.1996.542653.
[97] “Research on Evolutionary Multi-Objective Optimization Algorithms,” *Journal of Software*, pp. 271–289, doi: 10.0000/1000-9825-3483.
[98] A. Konak, D. W. Coit, and A. E. Smith, “Multi-objective optimization using genetic algorithms: A tutorial,” *Reliab Eng Syst Saf*, vol. 91, no. 9, pp. 992–1007, Sep. 2006, doi: 10.1016/J.RESS.2005.11.018.
[99] S. Mirjalili, P. Jangir, and S. Saremi, “Multi-objective ant lion optimizer: a multi-objective optimization algorithm for solving engineering problems,” *Applied Intelligence*, vol. 46, no. 1, pp. 79–95, Jan. 2017, doi: 10.1007/S10489-016-0825-8/METRICS.
[100] S. Mirjalili, S. Saremi, S. M. Mirjalili, and L. D. S. Coelho, “Multi-objective grey wolf optimizer: A novel algorithm for multi-criterion optimization,” *Expert Syst Appl*, vol. 47, pp. 106–119, Apr. 2016, doi: 10.1016/J.ESWA.2015.10.039.
[101] Y. Cui, Z. Geng, Q. Zhu, and Y. Han, “Review: Multi-objective optimization methods and application in energy saving,” *Energy*, vol. 125, pp. 681–704, Apr. 2017, doi: 10.1016/J.ENERGY.2017.02.174.
[102] H. R. Baghaee, M. Mirsalim, and G. B. Gharehpetian, “Multi-objective optimal power management and sizing of a reliable wind/PV microgrid with hydrogen energy storage using MOPSO,” *Journal of Intelligent & Fuzzy Systems*, vol. 32, no. 3, pp. 1753–1773, Jan. 2017, doi: 10.3233/JIFS-152372.
[103] S. Z. Mirjalili, S. Mirjalili, S. Saremi, H. Faris, and I. Aljarah, “Grasshopper optimization algorithm for multi-objective optimization problems,” *Applied*

Intelligence, vol. 48, no. 4, pp. 805–820, Apr. 2018, doi: 10.1007/S10489-017-1019-8/TABLES/9.

[104] F. Y. Edgeworth and P. Newman, "F.Y. Edgeworth : mathematical psychics and further papers on political economy," p. 653, 2003, Accessed: Nov. 03, 2023. [Online]. Available: https://global.oup.com/academic/product/f-y-edgeworths-mathematical-psychics-and-further-papers-on-political-economy-9780198287124

[105] V. Pareto, "Cours d'économie politique," *Cours d'économie politique*, 1964, doi: 10.3917/DROZ.PARET.1964.01.

[106] C. A. Coello Coello, "Evolutionary multi-objective optimization: Some current research trends and topics that remain to be explored," *Front Comput Sci China*, vol. 3, no. 1, pp. 18–30, Mar. 2009, doi: 10.1007/S11704-009-0005-7/METRICS.

[107] L. Abualigah, A. Diabat, S. Mirjalili, M. Abd Elaziz, and A. H. Gandomi, "The Arithmetic Optimization Algorithm," *Comput Methods Appl Mech Eng*, vol. 376, p. 113609, Apr. 2021, doi: 10.1016/J.CMA.2020.113609.

[108] F. Glover, "Future paths for integer programming and links to artificial intelligence," *Comput Oper Res*, vol. 13, no. 5, pp. 533–549, Jan. 1986, doi: 10.1016/0305-0548(86)90048-1.

[109] Y. J. Zhang, Y. X. Yan, J. Zhao, and Z. M. Gao, "AOAAO: The Hybrid Algorithm of Arithmetic Optimization Algorithm With Aquila Optimizer," *IEEE Access*, vol. 10, pp. 10907–10933, 2022, doi: 10.1109/ACCESS.2022.3144431.

[110] J. Kennedy and R. Eberhart, "Particle swarm optimization," *Proceedings of ICNN'95 - International Conference on Neural Networks*, vol. 4, pp. 1942–1948, doi: 10.1109/ICNN.1995.488968.

[111] S. Mirjalili, S. M. Mirjalili, and A. Lewis, "Grey Wolf Optimizer," *Advances in Engineering Software*, vol. 69, pp. 46–61, Mar. 2014, doi: 10.1016/J.ADVENGSOFT.2013.12.007.

[112] S. Mirjalili and A. Lewis, "The Whale Optimization Algorithm," *Advances in Engineering Software*, vol. 95, pp. 51–67, May 2016, doi: 10.1016/J.ADVENGSOFT.2016.01.008.

[113] R. Storn and K. Price, "Differential Evolution - A Simple and Efficient Heuristic for Global Optimization over Continuous Spaces," *Journal of Global Optimization*, vol. 11, no. 4, pp. 341–359, 1997, doi: 10.1023/A:1008202821328/METRICS.

[114] S. Mirjalili, "The Ant Lion Optimizer," *Advances in Engineering Software*, vol. 83, pp. 80–98, May 2015, doi: 10.1016/J.ADVENGSOFT.2015.01.010.

[115] E. Bonabeau, M. Dorigo, and G. Theraulaz, "Swarm Intelligence: From Natural to Artificial Systems," Oct. 1999, doi: 10.1093/OSO/9780195131581.001.0001.

[116] X. S. Yang, M. Karamanoglu, and X. He, "Flower pollination algorithm: A novel approach for multiobjective optimization," *Engineering Optimization*, vol. 46, no. 9, pp. 1222–1237, Sep. 2014, doi: 10.1080/0305215X.2013.832237.

[117] L. Abualigah, A. Diabat, S. Mirjalili, M. Abd Elaziz, and A. H. Gandomi, "The Arithmetic Optimization Algorithm," *Comput Methods Appl Mech Eng*, vol. 376, p. 113609, Apr. 2021, doi: 10.1016/J.CMA.2020.113609.

[118] C. A. Coello Coello and M. S. Lechuga, "MOPSO: A proposal for multiple objective particle swarm optimization," *Proceedings of the 2002 Congress on Evolutionary Computation, CEC 2002*, vol. 2, pp. 1051–1056, 2002, doi: 10.1109/CEC.2002.1004388.

[119] G. Hu, J. Zhong, B. Du, and G. Wei, “An enhanced hybrid arithmetic optimization algorithm for engineering applications,” *Comput Methods Appl Mech Eng*, vol. 394, p. 114901, May 2022, doi: 10.1016/J.CMA.2022.114901.
[120] K. G. Dhal, B. Sasmal, A. Das, S. Ray, and R. Rai, “A Comprehensive Survey on Arithmetic Optimization Algorithm,” *Archives of Computational Methods in Engineering 2023 30:5*, vol. 30, no. 5, pp. 3379–3404, Mar. 2023, doi: 10.1007/S11831-023-09902-3.
[121] N. Khodadadi, V. Snasel, and S. Mirjalili, “Dynamic Arithmetic Optimization Algorithm for Truss Optimization under Natural Frequency Constraints,” *IEEE Access*, vol. 10, pp. 16188–16208, 2022, doi: 10.1109/ACCESS.2022.3146374.
[122] K. G. Dhal, B. Sasmal, A. Das, S. Ray, and R. Rai, “A Comprehensive Survey on Arithmetic Optimization Algorithm,” *Archives of Computational Methods in Engineering 2023 30:5*, vol. 30, no. 5, pp. 3379–3404, Mar. 2023, doi: 10.1007/S11831-023-09902-3.
[123] R. Storn and K. Price, “Differential Evolution - A Simple and Efficient Heuristic for Global Optimization over Continuous Spaces,” *Journal of Global Optimization*, vol. 11, no. 4, pp. 341–359, 1997, doi: 10.1023/A:1008202821328/METRICS.
[124] M. Georgioudakis and V. Plevris, “A Comparative Study of Differential Evolution Variants in Constrained Structural Optimization,” *Front Built Environ*, vol. 6, p. 552667, Jul. 2020, doi: 10.3389/FBUIL.2020.00102/BIBTEX.
[125] A. A. Ewees, M. Abd Elaziz, and D. Oliva, “A new multi-objective optimization algorithm combined with opposition-based learning,” *Expert Syst Appl*, vol. 165, p. 113844, Mar. 2021, doi: 10.1016/J.ESWA.2020.113844.
[126] A. Konak, D. W. Coit, and A. E. Smith, “Multi-objective optimization using genetic algorithms: A tutorial,” *Reliab Eng Syst Saf*, vol. 91, no. 9, pp. 992–1007, Sep. 2006, doi: 10.1016/J.RESS.2005.11.018.
[127] W. Gong *et al.*, “Multiobjective adaptive surrogate modeling-based optimization for parameter estimation of large, complex geophysical models,” *Water Resour Res*, vol. 52, no. 3, pp. 1984–2008, Mar. 2016, doi: 10.1002/2015WR018230.
[128] C. A. Coello Coello, A. H. Aguirre, and E. Zitzler, “Evolutionary multi-objective optimization,” *Eur J Oper Res*, vol. 181, no. 3, pp. 1617–1619, Sep. 2007, doi: 10.1016/J.EJOR.2006.08.003.
[129] C. R. Raquel and P. C. Naval, “An effective use of crowding distance in multiobjective particle swarm optimization,” *GECCO 2005 - Genetic and Evolutionary Computation Conference*, pp. 257–264, 2005, doi: 10.1145/1068009.1068047.
[130] X. S. Yang, M. Karamanoglu, and X. He, “Flower pollination algorithm: A novel approach for multiobjective optimization,” *Engineering Optimization*, vol. 46, no. 9, pp. 1222–1237, Sep. 2014, doi: 10.1080/0305215X.2013.832237.
[131] J. Luiz Junho Pereira, G. Antônio Oliver, M. Brendon Francisco, S. Simões Cunha, and G. Ferreira Gomes, “Multi-objective lichtenberg algorithm: A hybrid physics-based meta-heuristic for solving engineering problems,” *Expert Syst Appl*, vol. 187, p. 115939, Jan. 2022, doi: 10.1016/J.ESWA.2021.115939.
[132] C. A. Coello Coello and M. S. Lechuga, “MOPSO: A proposal for multiple objective particle swarm optimization,” *Proceedings of the 2002 Congress on Evolutionary Computation, CEC 2002*, vol. 2, pp. 1051–1056, 2002, doi: 10.1109/CEC.2002.1004388.

[133] K. Deb, A. Pratap, S. Agarwal, and T. Meyarivan, “A fast and elitist multiobjective genetic algorithm: NSGA-II,” *IEEE Transactions on Evolutionary Computation*, vol. 6, no. 2, pp. 182–197, Apr. 2002, doi: 10.1109/4235.996017.
[134] Dr. P. Jangir and N. Jangir, “Non-Dominated Sorting Whale Optimization Algorithm (NSWOA): A Multi-Objective Optimization algorithm for Solving Engineering Design Problems,” *Global Journals of Research in Engineering*, vol. 17, no. F4, pp. 15–42, Mar. 2017, Accessed: Nov. 14, 2023. [Online]. Available: https://engineeringresearch.org/index.php/GJRE/article/view/1643/3-Non-Dominated-Sorting-Whale_html
[135] K. Deb, L. Thiele, M. Laumanns, and E. Zitzler, “Scalable Test Problems for Evolutionary Multiobjective Optimization,” *Evolutionary Multiobjective Optimization*, pp. 105–145, Sep. 2005, doi: 10.1007/1-84628-137-7_6.
[136] C. M. Fonseca and P. J. Fleming, “An Overview of Evolutionary Algorithms in Multiobjective Optimization,” *Evol Comput*, vol. 3, no. 1, pp. 1–16, Mar. 1995, doi: 10.1162/EVCO.1995.3.1.1.
[137] F. Kursawe, “A variant of evolution strategies for vector optimization,” *Lecture Notes in Computer Science (including subseries Lecture Notes in Artificial Intelligence and Lecture Notes in Bioinformatics)*, vol. 496 LNCS, pp. 193–197, 1991, doi: 10.1007/BFB0029752/COVER.
[138] “(PDF) Hybrid GA for multi objective aerodynamic shape optimization.” Accessed: Nov. 14, 2023. [Online]. Available: https://www.researchgate.net/publication/243686783_Hybrid_GA_for_multi_objective_aerodynamic_shape_optimization
[139] “(PDF) Some Experiments in Machine Learning Using Vector Evaluated Genetic Algorithms.” Accessed: Nov. 14, 2023. [Online]. Available: https://www.researchgate.net/publication/236443691_Some_Experiments_in_Machine_Learning_Using_Vector_Evaluated_Genetic_Algorithms
[140] R. Viennet, C. Fonteix, and I. Marc, “Multicriteria optimization using a genetic algorithm for determining a Pareto set,” *Int J Syst Sci*, vol. 27, no. 2, pp. 255–260, 1996, doi: 10.1080/00207729608929211.
[141] E. Zitzler, K. Deb, and L. Thiele, “Comparison of multiobjective evolutionary algorithms: empirical results.,” *Evol Comput*, vol. 8, no. 2, pp. 173–195, 2000, doi: 10.1162/106365600568202.
[142] S. Reddy and G. S. Dulikravich, “A self-adapting algorithm for many-objective optimization,” *Appl Soft Comput*, vol. 129, p. 109484, Nov. 2022, doi: 10.1016/J.ASOC.2022.109484.
[143] “GitHub - fillipe-gsm/dtlz-test-functions: Set of files to run the DTLZ scalable multi-objective test suite.” Accessed: Dec. 11, 2023. [Online]. Available: https://github.com/fillipe-gsm/dtlz-test-functions
[144] “Test functions for optimization - Wikipedia.” Accessed: Dec. 11, 2023. [Online]. Available: https://en.wikipedia.org/wiki/Test_functions_for_optimization
[145] “Benchmark Problems - mathlayer®.” Accessed: Dec. 11, 2023. [Online]. Available: http://www.mathlayer.com/support/benchmark-problems.html
[146] “Alroomi Website - Unconstrained List.” Accessed: Dec. 11, 2023. [Online]. Available: https://www.al-roomi.org/benchmarks/multi-objective/unconstrained-list

[147] “Release Multiobjective Optimization Test Environment · pat2017b/Multiobjective-Optimization-Test-Environment · GitHub.” Accessed: Dec. 11, 2023. [Online]. Available: https://github.com/pat2017b/Multiobjective-Optimization-Test-Environment/releases/tag/v1.0
[148] “File Exchange - MATLAB Central.” Accessed: Dec. 11, 2023. [Online]. Available: https://www.mathworks.com/matlabcentral/fileexchange/
[149] Y. Tian, R. Cheng, X. Zhang, and Y. Jin, “PlatEMO: A MATLAB Platform for Evolutionary Multi-Objective Optimization [Educational Forum],” *IEEE Comput Intell Mag*, vol. 12, no. 4, pp. 73–87, Nov. 2017, doi: 10.1109/MCI.2017.2742868.
[150] S. Reddy and G. S. Dulikravich, “A self-adapting algorithm for many-objective optimization,” *Appl Soft Comput*, vol. 129, p. 109484, Nov. 2022, doi: 10.1016/J.ASOC.2022.109484.
[151] C. A. C. Coello and M. R. Sierra, “A study of the parallelization of a coevolutionary multi-objective evolutionary algorithm,” *Lecture Notes in Artificial Intelligence (Subseries of Lecture Notes in Computer Science)*, vol. 2972, pp. 688–697, 2004, doi: 10.1007/978-3-540-24694-7_71/COVER.
[152] C. K. Goh and K. C. Tan, “An investigation on noisy environments in evolutionary multiobjective optimization,” *IEEE Transactions on Evolutionary Computation*, vol. 11, no. 3, pp. 354–381, Jun. 2007, doi: 10.1109/TEVC.2006.882428.
[153] E. Zitzler, K. Deb, and L. Thiele, “Comparison of multiobjective evolutionary algorithms: empirical results.,” *Evol Comput*, vol. 8, no. 2, pp. 173–195, 2000, doi: 10.1162/106365600568202.
[154] C. A. Coello Coello, “Theoretical and numerical constraint-handling techniques used with evolutionary algorithms: a survey of the state of the art,” *Comput Methods Appl Mech Eng*, vol. 191, no. 11–12, pp. 1245–1287, Jan. 2002, doi: 10.1016/S0045-7825(01)00323-1.
[155] M. H. Nadimi-Shahraki, S. Taghian, and S. Mirjalili, “An improved grey wolf optimizer for solving engineering problems,” *Expert Syst Appl*, vol. 166, p. 113917, Mar. 2021, doi: 10.1016/J.ESWA.2020.113917.
[156] T. Ray and K. M. Liew, “A Swarm Metaphor for Multiobjective Design Optimization,” *Engineering Optimization*, vol. 34, no. 2, pp. 141–153, Mar. 2002, doi: 10.1080/03052150210915.
[157] H. Kaur, A. Rai, S. S. Bhatia, and G. Dhiman, “MOEPO: A novel Multi-objective Emperor Penguin Optimizer for global optimization: Special application in ranking of cloud service providers,” *Eng Appl Artif Intell*, vol. 96, p. 104008, Nov. 2020, doi: 10.1016/J.ENGAPPAI.2020.104008.
[158] S. Mirjalili, P. Jangir, and S. Saremi, “Multi-objective ant lion optimizer: a multi-objective optimization algorithm for solving engineering problems,” *Applied Intelligence*, vol. 46, no. 1, pp. 79–95, Jan. 2017, doi: 10.1007/S10489-016-0825-8/METRICS.
[159] G. Dhiman and V. Kumar, “Multi-objective spotted hyena optimizer: A Multi-objective optimization algorithm for engineering problems,” *Knowl Based Syst*, vol. 150, pp. 175–197, Jun. 2018, doi: 10.1016/J.KNOSYS.2018.03.011.
[160] G. Dhiman and V. Kumar, “Multi-objective spotted hyena optimizer: A Multi-objective optimization algorithm for engineering problems,” *Knowl Based Syst*, vol. 150, pp. 175–197, Jun. 2018, doi: 10.1016/J.KNOSYS.2018.03.011.

[161] G. Dhiman *et al.*, "MOSOA: A new multi-objective seagull optimization algorithm," *Expert Syst Appl*, vol. 167, p. 114150, Apr. 2021, doi: 10.1016/J.ESWA.2020.114150.
[162] "Multicriteria Optimization In Engineering: A Tutorial And Survey," *Structural Optimization: Status And Promise*, pp. 209–249, Jan. 1993, doi: 10.2514/5.9781600866234.0209.0249.
[163] T. Ray and K. M. Liew, "A Swarm Metaphor for Multiobjective Design Optimization," *Engineering Optimization*, vol. 34, no. 2, pp. 141–153, Mar. 2002, doi: 10.1080/03052150210915.
[164] B. K. Kannan and S. N. Kramer, "An Augmented Lagrange Multiplier Based Method for Mixed Integer Discrete Continuous Optimization and Its Applications to Mechanical Design," *Journal of Mechanical Design*, vol. 116, no. 2, pp. 405–411, Jun. 1994, doi: 10.1115/1.2919393.
[165] Q. Zhang, J. Ding, W. Shen, J. Ma, and G. Li, "Multiobjective Particle Swarm Optimization for Microgrids Pareto Optimization Dispatch," *Math Probl Eng*, vol. 2020, 2020, doi: 10.1155/2020/5695917.
[166] G. Chen, L. Liu, P. Song, and Y. Du, "Chaotic improved PSO-based multi-objective optimization for minimization of power losses and L index in power systems," *Energy Convers Manag*, vol. 86, pp. 548–560, Oct. 2014, doi: 10.1016/J.ENCONMAN.2014.06.003.
[167] H. G. G. Nunes, F. A. L. Morais, J. A. N. Pombo, S. J. P. S. Mariano, and M. R. A. Calado, "Bypass diode effect and photovoltaic parameter estimation under partial shading using a hill climbing neural network algorithm," *Front Energy Res*, vol. 10, p. 837540, Aug. 2022, doi: 10.3389/FENRG.2022.837540/BIBTEX.
[168] T. Ma and M. S. Javed, "Integrated sizing of hybrid PV-wind-battery system for remote island considering the saturation of each renewable energy resource," *Energy Convers Manag*, vol. 182, pp. 178–190, Feb. 2019, doi: 10.1016/J.ENCONMAN.2018.12.059.
[169] R. C. Bansal, T. S. Bhatti, and D. P. Kothari, "On some of the design aspects of wind energy conversion systems," *Energy Convers Manag*, vol. 43, no. 16, pp. 2175–2187, Nov. 2002, doi: 10.1016/S0196-8904(01)00166-2.
[170] A. Albani and M. Z. Ibrahim, "Wind Energy Potential and Power Law Indexes Assessment for Selected Near-Coastal Sites in Malaysia," *Energies 2017, Vol. 10, Page 307*, vol. 10, no. 3, p. 307, Mar. 2017, doi: 10.3390/EN10030307.
[171] J. S. Touma, "Dependence of the Wind Profile Power Law on Stability for Various Locations," *J Air Pollut Control Assoc*, vol. 27, no. 9, pp. 863–866, 1977, doi: 10.1080/00022470.1977.10470503.
[172] M. Ikhwan, "Investigation of flow and pressure characteristics around pyramidal buildings," 2005, doi: 10.5445/KSP/1000003455.
[173] "OEDI: Commercial and Residential Hourly Load Profiles for all TMY3 Locations in the United States." Accessed: Nov. 01, 2023. [Online]. Available: https://data.openei.org/submissions/153
[174] S. Wilcox and W. Marion, "Users Manual for TMY3 Data Sets (Revised)," May 2008, doi: 10.2172/928611.
[175] J. Lin, M. Pipattanasomporn, and S. Rahman, "Comparative analysis of auction mechanisms and bidding strategies for P2P solar transactive energy markets," *Appl Energy*, vol. 255, p. 113687, Dec. 2019, doi: 10.1016/J.APENERGY.2019.113687.

[176] “National Inventory Submissions 2021 | UNFCCC.” Accessed: Dec. 06, 2023. [Online]. Available: https://unfccc.int/ghg-inventories-annex-i-parties/2021
[177] Y. T. Aklilu and J. Ding, “Survey on Blockchain for Smart Grid Management, Control, and Operation,” *Energies 2022, Vol. 15, Page 193*, vol. 15, no. 1, p. 193, Dec. 2021, doi: 10.3390/EN15010193.
[178] M. M. Kamal, I. Ashraf, and E. Fernandez, “Planning and optimization of microgrid for rural electrification with integration of renewable energy resources,” *J Energy Storage*, vol. 52, p. 104782, Aug. 2022, doi: 10.1016/J.EST.2022.104782.
[179] J. Lowitzsch, C. E. Hoicka, and F. J. van Tulder, “Renewable energy communities under the 2019 European Clean Energy Package – Governance model for the energy clusters of the future?,” *Renewable and Sustainable Energy Reviews*, vol. 122, p. 109489, Apr. 2020, doi: 10.1016/J.RSER.2019.109489.
[180] K. Sperling, “How does a pioneer community energy project succeed in practice? The case of the Samsø Renewable Energy Island,” *Renewable and Sustainable Energy Reviews*, vol. 71, pp. 884–897, May 2017, doi: 10.1016/J.RSER.2016.12.116.
[181] V. K. Mololoth, S. Saguna, and C. Åhlund, “Blockchain and Machine Learning for Future Smart Grids: A Review,” *Energies 2023, Vol. 16, Page 528*, vol. 16, no. 1, p. 528, Jan. 2023, doi: 10.3390/EN16010528.
[182] M. Mureddu, E. Ghiani, and F. Pilo, “Smart grid optimization with blockchain based decentralized genetic Algorithm,” *IEEE Power and Energy Society General Meeting*, vol. 2020-August, Aug. 2020, doi: 10.1109/PESGM41954.2020.9281759.

Appendixes

A. Formulations and settings of the 20 benchmark functions used in the evaluation of the proposed MOADEO algorithm.

No.	Benchmark Function	Mathematical Formulation	Number of objectives (o)	Dim (d)	Boundaries $[lb, ub]$	Comments
1	**DTLZ1**	$f_1(x) = (1 + g(X_o)) \times \frac{1}{2}\prod_{i=1}^{o-1} x_i$ $f_2(x) = (1 + g(X_o))(1 - x_{o-1})\frac{1}{2}\prod_{i=1}^{o-2} x_i$ ⋮ $f_o(x) = (1 + g(X_o))\frac{1}{2}(1 - x_1)$ $g(X_o) = 100\left[\lvert X_o\rvert + \sum_{x_i \in X_o}[(x_i - 0.5)^2 - \cos(20\pi(x_i - 0.5))]\right]$	3	7	[0,1]	$d = o - 1 + v$. For DTLZ1, $v = 5$
2	**DTLZ2**	$f_1(x) = (1 + g(X_o))\prod_{i=1}^{o-1}\cos\left(\frac{x_i\pi}{2}\right)$ $f_2(x) = (1 + g(X_o))\sin\left(\frac{x_{o-1}\pi}{2}\right)\prod_{i=1}^{o-2}\cos\left(\frac{x_i\pi}{2}\right)$ ⋮ $f_o(x) = \left(1 + g(X_o)\right)\sin\left(\frac{x_1\pi}{2}\right)$ $g(X_o) = \sum_{x_i \in \ _o}(x_i - 0.5)^2$	3	12	[0,1]	$d = o - 1 + v$. For DTLZ2, $v = 10$
3	**DTLZ3**	As **DTLZ2,** except that g is replaced with the one from **DTLZ1**	3	12	[0,1]	$d = o - 1 + v$. For DTLZ3, $v = 10$
4	**DTLZ4**	As **DTLZ2,** except all $x_i \in X$ are replaced by x_i^{α}, where $\alpha > 0$	3	12	[0,1]	$d = o - 1 + v$. For DTLZ4, $v = 10$
5	**DTLZ5**	As **DTLZ2,** except all $x_2, \ldots, x_{M-1} \in X$ are replaced by $\frac{1+2gx_i}{2(1+g)}$	3	12	[0,1]	$d = o - 1 + v$. For DTLZ5, $v = 10$
6	**DTLZ6**	As **DTLZ5,** except the equation for $g(X_M)$ is replaced by $g(X_M) = \sum_{i=1}^{k} z_i^{0.1}$.	3	12	[0,1]	$d = o - 1 + v$. For DTLZ6, $v = 10$
7	**DTLZ7**	$f_1(x) = x_1$ $f_2(x) = x_2$	3	22	[0,1]	$d = o - 1 + v$.

		$\vdots$ $f_o(x) = \big(1 + g(x_o)\big)h(f_1, f_2, \dots, f_{o-1}, g)$ $g(x_o) = 1 + \frac{9}{\lvert x_o \rvert}\sum_{x_i \in X_o} x_i$ $h(f_1, f_2, \dots, f_{o-1}, g) = o - \sum_{i=1}^{o-1} \frac{f_i}{1+g}(1 + \sin 3\pi f_i)$			For DTLZ7, $v = 20$
8	**Fonseca-Fleming**	$f_1(x) = 1 - \exp\left[-\sum_{i=1}^{d}\left(x_i - \frac{1}{\sqrt{d}}\right)^2\right]$ $f_2(x) = 1 - \exp\left[-\sum_{i=1}^{d}\left(x_i - \frac{1}{\sqrt{d}}\right)^2\right]$	2	3	[-4,4]
9	**Kursawe**	$f_1(x) = \sum_{i=1}^{2}\left[-10\ exp\left(-0.2\sqrt{x_i^2 + x_{i+1}^2}\right)\right]$ $f_2(x) = \sum_{i=1}^{3}\left[\lvert x_i \rvert^{0.8} + 5\sin\left(x_i^3\right)\right]$	2	3	[-5,5]
10	**Poloni**	$f_1(x,y) = \left[1 + \big(A_1 - B_1(x,y)\big)^2 + \big(A_2 - B_2(x,y)\big)^2\right]$ $f_2(x,y) = (x-3)^2 + (y+1)^2$ $A_1 = 0.5\sin(1) - 2\cos(1) + \sin(2) - 1.5\cos(2)$ $A_2 = 1.5\sin(1) - \cos(1) + 2\sin(2) - 0.5\cos(2)$ $B_1(x,y) = 0.5\sin(x) - 2\cos(x) + \sin(y) - 1.5\cos(y)$ $B_2(x,y) = 1.5\sin(x) - \cos(x) + 2\sin(y) - 0.5\cos(y)$	2	2	$[-\pi, \pi]$
11	**Schaffer 1**	$f_1(x) = x^2$ $f_2(x) = (x-2)^2$	2	3	[-500,500]
12	**Schaffer 2**	$f_1(x) = \begin{cases} -x, & if\ x \le 1 \\ x-2, & if\ 1 < x < 3 \\ 4-x, & if\ 3 < x < 4 \\ x-4, & if\ x > 4 \end{cases}$ $f_2(x) = (x-5)^2$	2	1	[-5,10]
13	**Viennet 1**	$f_1(x) = x^2 + (y-1)^2$ $f_2(x) = x^2 + (y-1)^2 + 1$ $f_3(x) = (x-1)^2 + y^2 + 2$	3	2	[-2,2]
14	**Viennet 2**	$f_1(x) = \frac{(x-2)^2}{2} + \frac{(y+1)^2}{13} + 3$ $f_2(x) = \frac{(x+y-3)^2}{36} + \frac{(-x+y+2)^2}{8} - 17$	3	2	[-3,3]

		$f_3(x) = \frac{(x+2y-1)^2}{175} + \frac{(2y-x)^2}{17} - 13$			
15	**Viennet 3**	$f_1(x) = 0.5(x^2+y^2) + \sin(x^2+y^2)$ $f_2(x) = \frac{(3x-2y+4)^2}{8} + \frac{(x-y+1)^2}{27} + 15$ $f_3(x) = \frac{1}{x^2+\quad^2+1} - 1.1\,exp(-(x^2+y^2))$	3	2	[-4,4]
16	**ZDT1**	$f_1(x) = x_1$ $f_2(x) = g(x) \times h(f_1(x), g(x))$ $g(x) = 1 + \frac{9}{d-1}\sum_{i=2}^{d} x_i$ $h(f_1(x), g(x)) = 1 - \sqrt{\frac{f_1(x)}{g(x)}}$	2	30	[0,1]
17	**ZDT2**	As **ZDT1**, except the equation for h is replaced by $h(f_1(x), g(x)) = 1 - \left(\frac{f_1(x)}{g(x)}\right)^2$	2	30	[0,1]
18	**ZDT3**	As **ZDT1**, except the equation for h is replaced by $h(f_1(x), g(x)) = 1 - \sqrt{\frac{f_1(x)}{g(x)}} - \left(\frac{f_1(x)}{g(x)}\right)\sin 10\pi f_1(x)$	2	30	[0,1]
19	**ZDT4**	As **ZDT1**, except the equation for g is replaced by $g(x) = 1 + 10(d-1) + \sum_{i=2}^{d}[x_i^2 - 10\cos(4\pi x_i)]$	2	10	$x_1 \in [0,1]$; $x_i \in [-5,5]$, $i = 2, \ldots, n$
20	**ZDT6**	$f_1(x) = 1 - e^{-4f_1(x)} \times \sin^6(6\pi f_1(x))$ $f_2(x) = g(x) \times h(f_1(x), g(x))$ $g(x) = 1 + 9\left[\frac{\sum_{i=2}^{d} x_i}{d-1}\right]$ $h(f_1(x), g(x)) = 1 - \left(\frac{f_1(x)}{g(x)}\right)^2$	2	10	[0,1]

Annexes

A. Scientific Publications.

Optimal Sizing of Renewable Energy Communities: A Multiple Swarms Multi-Objective Particle Swarm Optimization Approach

João Faria[1,2], Carlos Marques[2], José Pombo[1,2], Sílvio Mariano[1,2], Maria do Rosário Calado[1,2]

[1] IT—Instituto de Telecomunicações, Faculty of Engineering, Calçada Fonte do Lameiro, 6201-001 Covilhã, Portugal

[2] Department of Electromechanical Engineering, Faculty of Engineering, University of Beira Interior, Calçada Fonte do Lameiro, 6201-001 Covilhã, Portugal

Abstract

Renewable energy communities have gained popularity as a means of reducing carbon emissions and enhancing energy independence. However, determining the optimal sizing for each production and storage unit within these communities poses challenges due to conflicting objectives, such as minimizing costs while maximizing energy production. To address this issue, this paper employs a Multi-Objective Particle Swarm Optimization (MOPSO) algorithm with multiple swarms. This approach aims to foster a broader diversity of solutions while concurrently ensuring a good plurality of nondominant solutions that define a Pareto frontier. To evaluate the effectiveness and reliability of this approach, four case studies with different energy management strategies focused on real-world operations were evaluated, aiming to replicate the practical challenges encountered in actual renewable energy communities. The results demonstrate the effectiveness of the proposed approach in determining the optimal size of production and storage units within renewable energy communities, while simultaneously addressing multiple conflicting objectives, including economic viability and flexibility, specifically Levelized Cost of Energy (LCOE), Self-Consumption Ratio (SCR) and Self-Sufficiency Ratio (SSR). The findings also provide valuable insights that clarify which energy management strategies are most suitable for this type of community.

Keywords

renewable energy community (REC); energy management strategies; multi-objective optimization algorithm; multi-swarm MOPSO; energy storage systems; energy storage sharing